

**Stemness status in differentiated
and undifferentiated glioma cells**

By

Zarine Khan

A thesis submitted in partial fulfilment for the requirements for the degree of PhD in
Molecular and Cellular Biology at the University of Central Lancashire

May 2011

Declaration

I declare that while registered as a candidate for this degree I have not been registered as a candidate for any other award from an academic institution. The work present in this thesis, except where otherwise stated, is based on my own research and has not been submitted previously for any other award in this or any other University.

Signed

Zarine Khan

Abstract

Undifferentiated cancer stem cells (CSCs) with their unique potential of self-renewal and multi-lineage differentiation fuel tumour growth and relapse. Efficacy of glioma therapy can be considerably improved if the target is focused towards successful identification and elimination of CSCs. The aim of this research lies in defining specific and selective marker(s) to isolate glioma stem cells, to explore the differentiation state of brain tumour cells and to determine the protein profile changes that assist tumour cells to sustain stem cell-like characteristics. The three stem cell-related protein (CD133, Oct4-A and BMP3) expressions were investigated in control, hypoxic and serum-deprived U87-MG cells in order to shed light on the influence the micro-environment has in generating stem cells. Hypoxia offered a rapid state of undifferentiation as compared to serum deprivation by expressing a basal level of CD133 protein, a designated stem cell marker. Subsequent measurements of chemosensitivity and cell cycle analysis under undifferentiation conditions added to the cytotoxic potential of Taxol and showed an enhanced sensitivity of serum-deprived cells towards chemotherapeutic drugs.

Moreover, proteomic analysis produced a wide dataset, depicting the changes that occur at the proteomic level in the differentiated and undifferentiated U87-MG cells. With ingenuity pathway analysis (IPA), human protein research database (HPRD) and the literature review, several proteins were proposed to be tested as potential biomarkers. They included Uracil DNA glycosylase (UDG), Phosphoglycerate kinase 1 (PGK1), Heterogeneous nuclear riboprotein K (HNRNPK) and moesin that can be used as differentiated markers for glioma cells. Vimentin, Eukaryotic translation initiation factor 4e (EIF4e), Casein kinase II alpha 1 (CSNK2A1) should be further investigated to study their precise role in gliomagenesis. Laminin binding protein associated with Integrin $\alpha 6\beta 1$ and BMP2 should also be explored as a potential biomarker for isolation of glioma stem cells.

This novel study envelops diverse aspects related to CSCs such as biomarkers, stem cell niche, chemoresistance, cell cycle and proteomics and also suggests the existence of two sub-types of CSCs within glioma population. It can be concluded that the finding thus obtained may be a step in the right direction in helping treat brain tumours.

To My Loving Family

Contents

Declaration	2
Abstract	3
Contents	5
List of Figures	8
List of Tables	10
Acknowledgements	11
Abbreviations	13
CHAPTER 1 Introduction	17
1.1 Glioma.....	18
1.2 Cancer stem cells (CSCs)	19
1.3 Stem cell markers	22
1.3.1 CD133.....	22
1.3.2 Oct4-A	25
1.3.3 BMP2.....	28
1.4 Undifferentiation	29
1.4.1 i) Serum deprivation	30
1.4.1 ii) Hypoxia.....	31
1.5 Focus of current research.....	33
1.5.1 Chemosensitivity.....	33
1.5.2 Cell cycle analysis.....	36
1.5.3 Proteomics	36
1.6 Previous studies	38
1.7 U87-MG cell line to evaluate stemness.....	40
1.8 Questions to be addressed concerning the investigation	41
1.8.1 Aims	41
1.8.2 Novelty of the current research project	41
CHAPTER 2 Materials and Methods	42
2.1 Cell Culture	43
2.1.1 Cell lines	44

2.1.2 Media and reagents	45
2.1.3 Resuscitation of frozen cells.....	47
2.1.4 Subculture and cell treatment.	48
2.1.5 Cryopreservation.....	49
2.1.6 Cell library maintenance	50
2.1.7 Quantification of cells and cell viability	50
2.2 Messenger RNA (mRNA) isolation and quantification	51
2.2.1 mRNA isolation.....	53
2.2.2 mRNA quantification	55
2.3 Bioinformatics.	56
2.3.1 Gene sequence and location.....	56
2.3.2 Primer design	57
2.4 Complementary (cDNA) synthesis.....	63
2.4.1 cDNA synthesis protocol	65
2.5 Quantitative Real Time Polymerase Chain Reaction (qRT-PCR).....	65
2.5.1 Primer Preparation.....	67
2.5.2 PCR protocol.....	69
2.5.3 Analysis of qRT-PCR product	70
2.5.4 Agarose gel electrophoresis.....	71
2.5.5 Quantification analysis of qRT-PCR	72
2.6 Chemosensitivity Assay	74
2.6.1 Chemosensitivity.....	74
2.6.2 Cell viability	75
2.7 Cell cycle analysis.....	76
2.8 Flow cytometry.....	77
2.8.1 Sample preparation.....	78
2.8.2 Data analysis.....	79
2.9 Immunofluorescence (IF).....	81
2.9.1 Cell culture IF	82
2.10 Proteomics.....	83
2.10.1 Protein extraction	85
2.10.2 Protein quantification	85
2.10.3 Over view of work carried out by Applied Biomics (U.S.A).....	86
2.11 Statistical analysis.....	89

CHAPTER 3 Results	90
3.1 mRNA, cDNA and qRT-PCR.....	92
3.2 Expression of candidate proteins level in the control glioma cell lines.....	93
3.2.1 Oct4-A protein levels in the control glioma cells using IF.....	94
3.2.2 Candidate protein expression in the control cells (1321-N1, GOS-3 and U87-MG) using flow cytometry.....	95
3.3 Protein expression profile in the undifferentiated U87-MG cell line.....	99
3.3.1 i) Morphological changes observed in U87-MG cell line subjected to micro-environmental changes.....	100
3.3.1 ii) Qualitative protein expression by immunofluorescent staining	101
3.3.2 Analysis of CD133, Oct4-A and BMP2 protein expression in the U87-MG control cells.....	102
3.3.3 Analysis of CD133, Oct4-A and BMP2 protein expression in the U87-MG after 30 min treatment with hypoxia (followed by 24 hr of incubation).....	103
3.3.4 Analysis of CD133, Oct4-A and BMP2 protein expression in the U87-MG after serum deprivation (5 days).....	104
3.4 Chemosensitivity and Cell viability.....	106
3.4.1 Cell viability assay for the U87-MG cells treated with Taxol.....	107
3.4.2 Cell viability assay for the U87-MG cells treated with TMZ.....	108
3.5 Cell cycle analysis.....	110
3.5.1 Cell cycle analysis of the control, hypoxic and serum-deprived U87-MG cells.....	111
3.5.2 Cell cycle analysis of the U87-MG cells treated with Taxol.....	112
3.5.3 Cell cycle analysis of the U87-MG cells treated with TMZ.....	113
3.6 Proteomic analysis.....	118
3.6.1 Differential protein expression profile obtained using Mass spectrophotometric analysis.....	120
3.6.2 Bioinformatic analysis.....	128
CHAPTER 4 Discussion	135
CHAPTER 5 References	160
Appendix	183

List of Figures

Figure 1.1 Cancer stem cell hypotheses	19
Figure 1.2 Cancer therapies	20
Figure 1.3 CD133, transmembrane glycoprotein	22
Figure 1.4 Pluripotency pathways.	26
Figure 1.5 Gene Regulatory Network of Transcription Factor family Oct4 in human.	27
Figure 1.6 Glioma cell undifferentiation.....	29
Figure 1.7 Functions of HIF induced gene products.	31
Figure 1.8 Generation of stem cell induced by HIFs under hypoxic conditions.	32
Figure 1.9 Mechanism of action of TMZ	34
Figure 1.10 Stabilization of microtubules by Taxol in order to bring about mitotic arrest.....	35
Figure 1.11 Differentiation and undifferentiation of cells.....	39
Figure 2.1 Schematic representation of the principle of mRNA isolation	52
Figure 2.2 Bioinformatic data generated for prominin 1 (<i>CD133</i>).	59
Figure 2.3 Bioinformatic data generated for Octamer 4 (<i>Oct4-A</i>).....	60
Figure 2.4 Bioinformatic data generated for Bone morphogenetic protein 2 (<i>BMP2</i>).....	61
Figure 2.5 Bioinformatic data generated for glyceraldehyde-3-phosphate dehydrogenase (<i>GAPDH</i>)..	62
Figure 2.6 Principle of Reverse transcription of mRNA to cDNA	63
Figure 2.7 Steps involved in a PCR	66
Figure 2.8 Standards to calculate the copy number of the targeted gene.....	72,73
Figure 2.9 An example of a histogram plot of a cell viability assay	76
Figure 2.10 An illustration of flow cytometry.....	78
Figure 2.11 A histogram graph demonstrating flow cytometric data... ..	80
Figure 2.12 Indirect Immunofluorescent staining	81
Figure 2.13 An overview of proteomic strategies.....	84
Figure 2.14 Workflow of 2D-DIGE via DeCyder.....	88

Figure 3.1 Gene expression of <i>GAPDH</i> , <i>CD133</i> , <i>OCT4-A</i> and <i>BMP2</i> in all the three glioma cell lines.....	92
Figure 3.2 Nucleolus Oct4-A protein in different grades of glioma cell lines.....	94
Figure 3.3 Expression profile of CD133, Oct4-A and BMP2 protein in 1321-N1.....	95
Figure 3.4 Quantitative protein expression profile of CD133, Oct4-A and BMP2 proteins in the GOS-3 cell line.....	96
Figure 3.5 Percentage of cells positive for CD133, Oct4-A and BMP2 proteins in the U87-MG cells.....	97
Figure 3.6 Morphological changes in U87-MG cells due to micro-environmental changes ...	100
Figure 3.7 Display of CD133 and Oct4-A proteins in the hypoxic U87-MG cells.....	101
Figure 3.8 Percentage of cells positive for CD133, Oct4-A and BMP2 proteins in the U87-MG control cells.....	102
Figure 3.9 Analysis of the protein expression profile followed by hypoxia treatment	103
Figure 3.10 Proteins detected in serum-deprived U87-MG cells.....	104
Figure 3.11 Cell viability assay results of U87-MG cells treated with Taxol.....	107
Figure 3.12 Corresponds to the percentage of dead U87-MG cells on treatment with TMZ..	108
Figure 3.13 Cell cycle analysis of U87-MG cells.....	111
Figure 3.14 Cell cycle analysis of U87-MG cells treated with Taxol.....	112
Figure 3.15 Cell cycle analysis of U87-MG cells treated with TMZ.....	113
Figure 3.16 Cell cycle phases of control, hypoxic and serum-deprived U87-MG cells.	115
Figure 3.17 Cell cycle phases of control, hypoxic and serum-deprived U87-MG cells treated with Taxol.....	116
Figure 3.18 Cell cycle phases of control, hypoxic and serum-deprived U87-MG cells treated with TMZ.....	117
Figure 3.19 Representation of 2D-DIGE protein expression profile.....	119
Figure 3.20 Function distribution graph of the identified proteins using HPRD database.....	127
Figure 3.21 Functional network analysis by IPA.....	131
Figure 3.22 Network generated by IPA path designer overlaid with cancer biomarkers from ingenuity knowledge database.....	134

List of Tables

Table 2.1 Cell lines used and their media formulation.....	44
Table 2.2 Media, reagents, supplements and storage conditions.	46
Table 2.3 Table reagents used for mRNA isolation	54
Table 2.4 Reagents used for cDNA synthesis.....	64
Table 2.5 Reagents provided in the PCR kit (Roche, UK) and volume of reagents required to make PCR master mix... ..	67
Table 2.6 Primer sequence and the annealing temperature of the targeted genes....	68
Table 2.7 Default conditions for all amplifications for a qrt-PCR	70
Table 2.8 Reagents used for agarose gel electrophoresis.....	71
Table 2.9 Genomic DNA correspondence to its average Ct values and equivalent copy number.....	74
Table 2.10 Drug preparation	74
Table 2.11 Reagents used for cell cycle analysis.....	77
Table 2.12 Antibodies used in this study with the recommended dilution factor as recommended by the supplier.....	80
Table 3.1 Quantitative expression of proteins CD133, Oct4-A and BMP2 in the control glioma cell lines 1321-N1, GOS-3 and U87-MG.	98
Table 3.2 Quantitative expression of proteins CD133, Oct4-A and BMP2 in the U87-MG glioma cell line when subjected to treatment of hypoxia and serum deprivation	105
Table 3.3 Cell viability results of the chemosensitivity assay using flow cytometry... ..	109
Table 3.4 Percentages of differentiated and undifferentiated U87-MG cells in diverse phases of cell cycle and on treatment with cytotoxic drugs Taxol and TMZ	114
Table 3.5 Differential protein expression profile obtained using mass spectrophotometric analysis.....	121
Table 3.6 Molecular class, molecular function and biological function of proteins identified by mass spectrophotometry using Human Protein Research Database	124
Table 3.7 Top bio functions as generated by IPA	130
Table 3.8 Representing the 17 potential biomarkers in cancer from the protein dataset using IPA analysis.	132

Acknowledgements

First and foremost I would like to offer my sincere gratitude towards Almighty Allah and Prophet Muhammad (P.B.U.H) for giving me an opportunity to attain one of the highest levels of education. I thank you for answering my prayers and providing me with immense knowledge and strength to fulfil my dream. May your name be exalted, honoured, and glorified.

My eternal gratitude goes to Dr. Amal Shervington whose constant guidance and supervision from the preliminary to the concluding level enabled me to develop an understanding of the subject. I appreciate her constructive criticism and advice throughout this research project. I am grateful to her for being my mentor and sharing the insights of her admirable knowledge with me. I heartily express thanks to Dr. Amal Shervington for having faith in me and being the guiding light in every step taken to complete this extraordinary journey of my PhD.

My special thanks to Dr. Leroy Shervington for his kind support and patience during the countless revisions of this thesis. I would also like to acknowledge Dr. Nadia Chuzhanova and Prof. Jai Paul Singh for rendering their help in completing this research. I take the opportunity to thank Dr. Rahima Patel and Dr. Julie Shorrocks who spent their valuable time in sharing their knowledge and helping me to complete my thesis with the best possible results.

I appreciate the contribution of my lab colleagues Dr. Dipti Thakkar, Chinmay Munje, Adi Mehta and Glenda Melling in helping me during my experiments and also maintaining a lively environment throughout the research. Particular thanks to

Mohammad Mudasar, Mohammad Saleem and K.W. foods for being extremely caring and supportive and encouraging me to give my best towards my education.

Big thanks to my friends Syed Munawar, Mohammed Yaseen Shareef, Sriharsha Puranik, Atul Gadhave, Chinmay Munje, Pooja Babar, Seema Jaiswal, Nehala Parkar, Sukhmander Kaur, Shweta Kamble, Shantaram Muthaye, Shahid Shaikh, Mohammed Ibraheem and Fahim Hussain who have offered an immense love, care and support all these years and especially during my thesis write-up.

I owe my deepest gratitude to my mum Mrs. Shahjahan Khan for being there with me at every moment and inspiring me at every step. I value her belief in me and thank her for giving me the best of the things I could have ever imagined. I cannot end without thanking my brothers Sayeed and Shahdad Khan and my sister Reshma, my sister-in-law Nahid and my little niece Ayesha for their endless love, support, and encouragement throughout my educational life.

Lastly, I offer my regards to all the people in my life who have made this research possible by supporting me in different ways. From the deepest of my heart, I would like to thank all of you.

Abbreviations

2D-DIGE	2D Fluorescence Difference gel electrophoresis
2D-PAGE	Two-Dimensional Polyacrylamide Gel Electrophoresis
ACDP	Advisory Committee on Dangerous Pathogens
ACL	ATP citrate lyase
AMF	Autocrine motility factor
ANG-2	Angiopoietin-2
aNSC	Adult neural stem cell
ANXA2	Annexin A2
Ap₄A	Dinucleotide poly phosphate
ATCC	American Type Culture Collection
Atg5	Autophagy protein 5
Bcl2	B-cell lymphoma 2
Bcl-x_L	Anti-apoptotic protein
BER	Base excision repair
bFGF	basic Fibroblast growth factor
BMP (2,4)	Bone morphogenetic proteins (2,4)
BNIP3	Bcl-2/adenovirus E1B 19 kDa-interacting Protein 3
BNIP3L	Bcl-2/adenovirus E1B 19 kDa-interacting protein 3 like
BSA	Bovine serum albumin
CA IX, XII	Carbonic anhydrase
CD133	Prominin-1
CD44	Extracellular matrix receptor III gene
CD74	Cluster of Differentiation 74
CGB	Chorionic gonadotropin beta
c-IAP2	Cellular inhibitor of apoptosis-1
c-myc	Avian myelocytomatosis virus oncogene cellular homolog
COL11A	Collagen alpha-1(XI)
COL2A1	Collagen type II alpha 1
CSCs	Cancer Stem Cells
CSNK2A1	Casein kinase II alpha 1
CSTB	Cathepsin B
CXCR4	Cytokine (C-X-C motif) Receptor 4

Cy-5	Cyanine 5
DDC	Dopamine Decarboxylase
DMEM	Dulbecco's modified eagle's medium
DMSO	dimethyl sulphoxide
DNA	Deoxyribonucleic acid
ECACC	European Collection of Cell Cultures
ECS	Embryonic stem cell
EGFRvIII	Epidermal growth factor receptor vIII
EIF4e	Eukaryotic translation initiation factor 4e
EMEM	Eagle's minimum essential medium
FBS	Foetal bovine serum
FGF4	Fibroblast growth factor-4
FLI1	Friend leukaemia virus integration 1
FLIP	FLICE-inhibitory protein
fNSC	Foetal neural stem cell
FOXD3	Forkhead box D3
FRAP	FKBP12/rapamycin associated protein
GADD45 alpha	Growth arrest and DNA-damage-inducible protein alpha
GAPDH	Glyceraldehyde-3-phosphate dehydrogenase
GBM	Glioblastoma multiforme
GFPT2	Glutamine-fructose-6-phosphate transaminase 2
GLUT1	Glucose transporter 1
GTP	Guanosine triphosphate
hAR	Human aldose reductase
hEGF	human Epidermal growth factor
HIF2α	Hypoxia induced factor 2 α
HMGB1	High-mobility group protein B1
HMGB2	High-mobility group protein B2
HNRPK	Heterogenous nuclear riboprotein K
HOXA10	Homeobox protein-A10
HPRD	Human protein research database
Hsp90β	Heat shock protein 90kDa beta
IEF	Isoelectric focusing
IF	Immunofluorescence
IFNE1	Interferon epsilon 1

IgG	Immunoglobulin
IPA	Ingenuity pathway analysis
LC3	Light chain 3
LDH-A	Lactate dehydrogenase-A
LON	A mitochondrial protease
LOX	Lysyl oxidase
MALDI-TOF	Matrix-assisted laser desorption/ionization-time of flight
MCT1, 4	Monocarboxylate transporter
MDR1	Multi-drug resistant gene product 1
MGMT	O6-methylguanine-DNA-methyltransferase
MMP	Matrix metalloproteinase
MRP1	Multi-drug resistance-associated protein-1
Msi	Mushashi
MW	Molecular weight
NADPH	Nicotinamide adenine dinucleotide phosphate
NAIP	Neuronal Apoptosis Inhibitory Protein
NAMPT	Nicotinamide phosphoribosyltransferase precursor
NANOG	homeobox protein NANOG
Nes	Nestin
NHA	Normal human astrocytes
NOXA	Pro-apoptotic member of Bcl-2 protein family
NSCs	Normal Stem Cells
Oct4	Octamer-binding transcription factor 4
p53	Protein 53
PBS	Phosphatase buffer saline
PDGFRA	Alpha platelet-derived growth factor receptor
PDK1	Pyruvate Dehydrogenase kinase 1
PE	Phyco Erythrin
PGK1	Phosphoglycerate kinase 1
PGM1	Phosphoglycerate mutase 1
P-gp	Permeability glycoprotein
PI	Propidium Iodide
pI	Isoelectric points
PTEN	Phosphatase and tensin homolog

rCSCs	Recurrence cancer stem cells
REDD1	Regulated in development and DNA damage responses 1
RHB-A	Serum free media
RNA	Ribonucleic acid
siRNA	Small interfering RNAs
SOX2	Sex-determining region Y-box-2
SOX9	Sex determining region Y box 9
SPRP3	Small proline-rich protein 3
SPTLC2	Serine palmitoyltransferase, long chain base subunit 2
STAT	Signal Transducers and Activators of Transcription
Taxol	Paclitaxel
TCR	Transcription-coupled repair
TIMP-1	Tissue Inhibitor of Metalloproteinases-1
TMZ	Temozolomide
TNF	Tumour necrosis factor
TNFSF8	Tumour Necrosis Factor (ligand) Super Family, member 8
TR	Texas Red
TRP1	Tyrosinase-related protein 1
TRPC1	Transient receptor potential cation channel 1
UDG	Uracil DNA glycosylase
UNG	Uracil DNA glycosylase gene
UTF1	Undifferentiated embryonic cell transcription factor
VEGF	Vascular endothelial growth factor
VEGF-R1	Vascular endothelial growth factor receptor
Vim	Vimentin
VIP	Vasoactive intestinal peptide
XIAP	X-linked Inhibitor of Apoptosis Protein
α	Alpha
β	Beta

Chapter 1

Introduction

1.1 Glioma

Gliomas or brain tumours originate from glial cells of the brain. Glial cells unlike neurones have a property of cell division, a loss of controlled cell proliferation is found to result in a brain tumour. The abnormality of cells combined with the efficiency of their growth rate categorizes brain tumours into grades 1 to 4. Grades 1 and 2 indicate a low grade of glioma and grades 3 and 4 represent a higher stage of brain tumour (Shinohara *et al.*, 2008). Glioma can be both benign and malignant, where approximately more than 50 % of them show highly malignant and aggressive behaviour (Weil *et al.*, 2006). A low grade glioma is less aggressive and grows slowly, whereas, high grade brain tumours are highly vascular with a tendency to infiltrate in the surrounding tissues. Most of the high grade tumours are found to reoccur even after surgical resection (Nobuyoshi *et al.*, 2006). Brain tumours are reported to be highly heterogeneous expressing phenotypes of cells belonging to more than one neuronal lineage which could be either differentiated or undifferentiated (Pomeroy *et al.*, 2002). There are several types of brain tumours such as astrocytomas that grow throughout the brain, ependymomas develops in the lining of the ventricles and oligodendrogliomas develop in the cerebrum (Kondziolka and Bilbao 1988). The progression from low to high grade glioma involves a series of accumulated genetic mutations inactivating specific tumour suppressor genes namely *TP53*, *p16*, *RB* or *PTEN* or are found to activate oncogenes *MDM2*, *CDK4* and *CDK6* (Kleiheus and Cavenee, 2000; Maher *et al.*, 2001). The most common treatment employed to treat glioma includes surgical resection of the tumour, stereotactic radio surgery, radiation and chemotherapy with the application of approved drugs (Weil *et al.*, 2006). However,

chemotherapeutic drug strategies together with surgery and radiation therapies have till now been unable to completely cure cancer, tumour metastasis and relapse.

1.2 Cancer Stem Cells (CSCs)

The human brain accommodates a group of self-renewing stem cells throughout their life (Gage *et al.*, 2000). This small population of stem cells are predominantly maintained in an undifferentiated state, accompanied by a potential of self-renewal and multi-lineage differentiation. Normal stem cells (NSCs) assist in the repair and regeneration of damaged areas of the CNS. However, mutations (Fig. 1.1) and epigenetic alterations can coerce them to be transformed into cancer stem cells (CSCs) giving them the indefinite potential to differentiate into a tumorigenic lineage (Reya *et al.*, 2001).

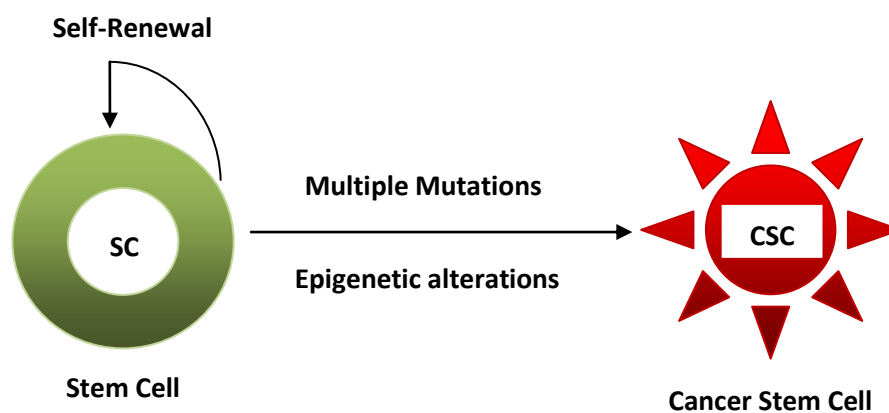


Figure 1.1: Cancer stem cell hypotheses. Transformation of a stem cell (SC) into a CSC on account of multiple mutations. (Adapted from http://www.allthingsstemcell.com/wp-content/uploads/2009/09/p53_cancer_cell_formation-copy2.png)

It has been observed that most of the tumours arise from the zone where stem cells reside, specifically the sub-ventricular zone in proximity to the walls of the ventricular system (Globus *et al.*, 1944). The majority of the therapies focus on eliminating the tumour mass, while ignoring the chemo- and radio-resistance capability of CSCs, providing them the opportunity to repopulate (Fig 1.2).

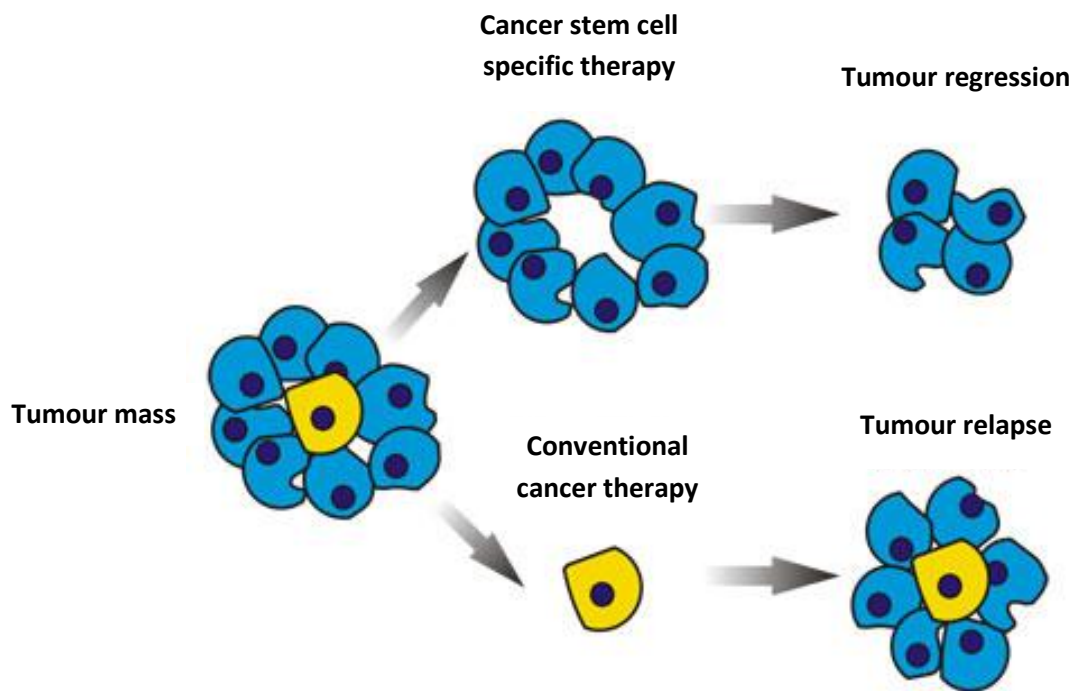


Figure 1.2: Cancer therapies. Illustration of efficiency cancer therapies when targeting at tumour mass and cancer stem cells respectively. (Modified from http://drugdiscoveryopinion.com/images/cancer_stem_cells.jpg)

CSCs are known to elicit a genetically defective response towards the epigenetic stimuli leading to cancer progression by compromising tumour suppressor genes (Rajaraman *et al.*, 2006). A genetic alteration in the pathway resulting in the loss of the tumour suppressor gene *Ink4a-Arf* can transform the astrocytes to a tumour progenitor cell (Bachoo *et al.*, 2002). The signalling pathways such as *Bmi 1* and *Wnt* have been proven to have similar effects on NSCs and CSCs self-renewal. This indicates that there exists a common molecular pathway regulating both populations. The deregulation of signalling pathways culminate in the actual loss of stemness control in NSCs and this needs to be further explored (Fargeas *et al.*, 2003).

Stem cells at present have therefore become one of the crucial targets to study the diverse aspects of cancer intensification and maintenance. This small group of cells have been identified by means of a marker expression showing an extensive proliferation to form tumours (Singh *et al.*, 2003). Common markers for NSCs and CSCs include prominin-1 (CD133; CSC marker), nestin (Nes; NSC marker), mushashi (Msi; NSC marker, cell fate determinant), octamer-binding transcription factor 4 (Oct4; undifferentiated stem cell marker) and bone morphogenetic proteins (BMPs; stem cell fate determinant, differentiation) (Bao *et al.*, 2006). Elevated levels of nestin have been considered as a prognostic marker for glioma malignancy, whereas, a relatively weak mushashi expression with loss of its regulatory function has reduced its clinical significance in treating glioma (Strojnik *et al.*, 2007). The existence of stem cells in both normal and malignant brain tissue has been successfully identified by the presence of CD133, a designated stem cell surface marker (Singh *et al.*, 2003).

1.3 Stem cell markers

1.3.1 CD133

Various human tissue samples express CD133; however, the glycosylated epitope AC133 of the CD133 antigen is found only on stem cells and is down regulated after the onset of differentiation (Kemper *et al.*, 2010). CD133 is a 20kDa, 5-transmembrane domain surface glycoprotein (Fig 1.3) with an unknown function. Prominin-1/CD133 has been reported to be localised in the protrusions of the apical membrane in the neuroepithelial cells where it plays an important role in the maintenance of apical-basal polarity (Kosodo *et al.*, 2004).

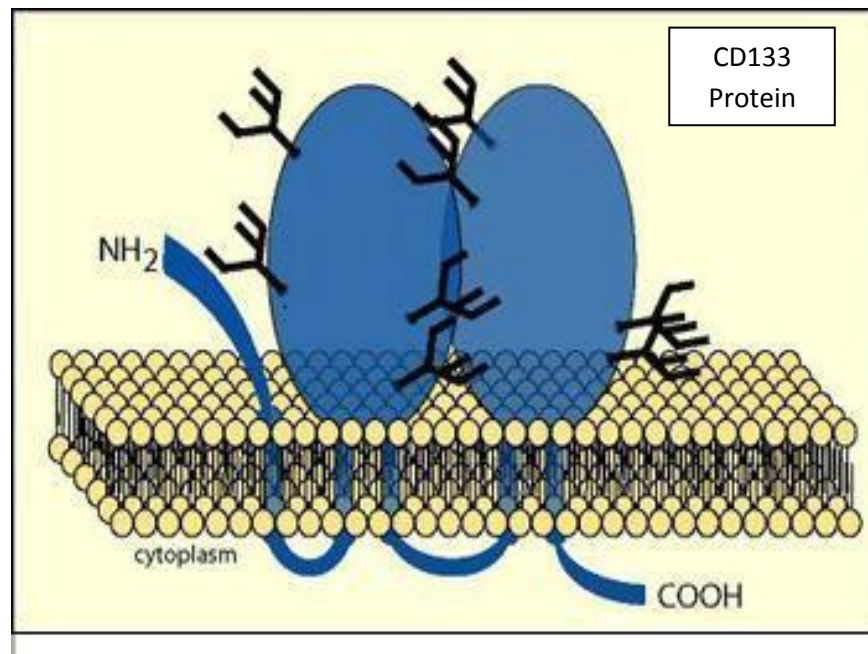


Figure 1.3: CD133, transmembrane glycoprotein. Localisation of CD133 on the cell surface. (Modified from <http://www.biotec.tu-dresden.de/research/corbeil/>)

The initial identification and characterisation of CSCs from glioma tissue was based on the sorting of CD133⁺ cells within a dissociated tumour cell mass (Singh *et al.*, 2003). In glioblastoma, CD133⁺ cells maintained a dormant state, however, when required they could enter the proliferative cell cycle phase to produce a highly progressive progeny (Lui and Zhang, 2009). As a requisite for a stem cell, CD133⁺ cells express a sex-determining region called the Y-box-2 (SOX2; regulates self-renewal and undifferentiated state of stem cells) and extracellular matrix receptor III genes (CD44; stem adhesion and invasion), required for self-renewal and could differentiate into CD133⁻ cell progeny, representing a major portion of the glioblastoma (Liu *et al.*, 2009). The percentage of CD133⁺ cells were found to increase following radiation therapy, further contributing to radio-resistance by activation of deoxyribonucleic acid (DNA) damage checkpoints (Bao *et al.*, 2006). These cancer causing cells in comparison to NSCs were found to be resistant to the tumour necrosis factor (TNF) related apoptosis ligand (TRAIL/Apo2L) (Capper *et al.*, 2009). The expression of the CD133 protein and the drug resistant genes such as the multi-drug resistant gene product 1 (MDR1; neurospheres formation, stem cell self-renewal and drug resistance) and B-cell lymphoma 2 (Bcl-2; anti-apoptotic protein, drug resistance) were evaluated in glioblastoma and normal human cell lines (Shervington and Lu, 2008). The expression profile of CD133⁺ cells was higher in glioma cells compared to the normal astrocytes, however, both normal and glioma CD133⁺ cells showed an increased drug resistance capability as compared to CD133⁻ cells (Shervington and Lu, 2008). These data further advocates a link between chemotherapy and multi-drug resistance in brain tumours. In addition, histological analysis and the quantitative expression of CD133 antigen within various glioma cell populations draw a correlation, where a high expression of CD133

protein was associated with a reduced probability of patient survival (Zeppernick *et al.*, 2008). An elevated CD133 protein level was considered to be a risk factor for tumour proliferation and progression of malignancy. These results provide sufficient evidence proving that CD133⁺ cells are CSCs, and thus increase the feasibility to utilize it as a potential therapeutic target in the treatment of glioma (Shervington and Lu, 2008).

The concept of CD133⁺ as CSCs, however, does not address tumour relapse even after the administration of potent therapies (Bao *et al.*, 2006). The methods used for the purification and sorting of CD133⁺ cells from CD133⁻ cells have been re-examined in fresh human gliomas and gliomasphere cultures. The data showed that there are no significant differences found in the expression of stemness genes or the long-term self-renewal capacities of CD133⁺ and CD133⁻ cells (Clement *et al.*, 2009). *In vivo* experiments showed that CD133⁻ cells obtained from glioma patients when implanted in nude rats, yielded tumours and only a few of the resultant tumours were found to comprise of CD133⁺ cells (Wang *et al.*, 2008). CD133 protein was also detected on the neural progenitor cells isolated from the post-mortem human cortex and its expression was noticeably reduced in high-passage lineage-restricted cultures (Schwartz *et al.*, 2003). Such variation in the expression of CD133 protein poses a question mark on its stemness status and raises a doubt as to whether CD133⁺ cells are tumour-initiating stem cells or progenitors that have acquired stem cell functions.

A stem cell is required to self-renew and differentiate into various progenitors, and simultaneously maintain itself in an undifferentiated state. CD133⁺ cells maintain only a subset of primary glioblastoma, whereas the origination of other tumours is inherited from the CD133⁻ cells. The differential growth characteristic of CD133⁺ and

CD133⁻ cells reflects two dissimilar subtypes of glioblastoma; however, they specify an equal potency to develop into brain tumours (Beier *et al.*, 2007). In addition, the cell cycle profile of CD133 cells shows that CD133⁻ cells reside in the G1/G0 phase while the CD133⁺ cells are mainly inhabited in the S/G2 or S/M phase (Sun *et al.*, 2009). This increases the likelihood of CD133⁻ cells to generate tumours even while residing in a quiescent state. The detection and isolation of substantial quantities of CD133⁺ cells still remains uncertain due to the non-specific binding of glioma cells to micro-beads (Clement *et al.*, 2009).

1.3.2 Oct4-A

Oct4 (Pou5f1), a POU-homeodomain transcription factor, plays a crucial role in self-renewal, pluripotency (Fig. 1.4), and lineage commitment of the stem cells. Being an essential factor for differentiation during the early embryonic stages, Oct4 gene is silenced in somatic tissues (Lengner *et al.*, 2007).

An abnormal Oct4 expression in an adult tissue may consequently indicate a discrepancy in the process of cell differentiation. In addition, the expression of Oct4 gene has been reported to enhance tumorigenicity in a dose-dependent manner (Gidekel *et al.*, 2003). The Oct4 gene on chromosome 6, encodes for two different alternatively spliced variants Oct4-A and Oct4-B, respectively. Oct4-A is composed of 360 amino acids and is sited within the nucleus, whereas, Oct4-B comprises of 265 amino acids and is predominant in the cytoplasm (Wang and Dai, 2010). Although both isoforms have a similar 225 C-terminal amino acid sequence, they differ with respect to the N-terminal (Lee *et al.*, 2006). This structural disparity endows them with different functional properties. Comparative studies have shown that Oct4-A is responsible for pluripotency and transcription of various genes, whereas, Oct4-B does

not sustain stem cell properties. The expression of Oct4 gene has been linked to several aspects of self-renewal in the embryonic and adult stem cells (Nichols *et al.*, 1998; Boyer *et al.*, 2005). However, its occurrence in the somatic tissue is questionable due to the presence of Oct4 pseudo genes. The resemblance of the pseudo genes was found to be higher towards the Oct4-A compared to Oct4-B, resulting in multiple probabilities depicting false positive results. Adult stem cells expressing Oct4 gene can be used to define the initiation point of cancer (Atlasi *et al.*, 2008).

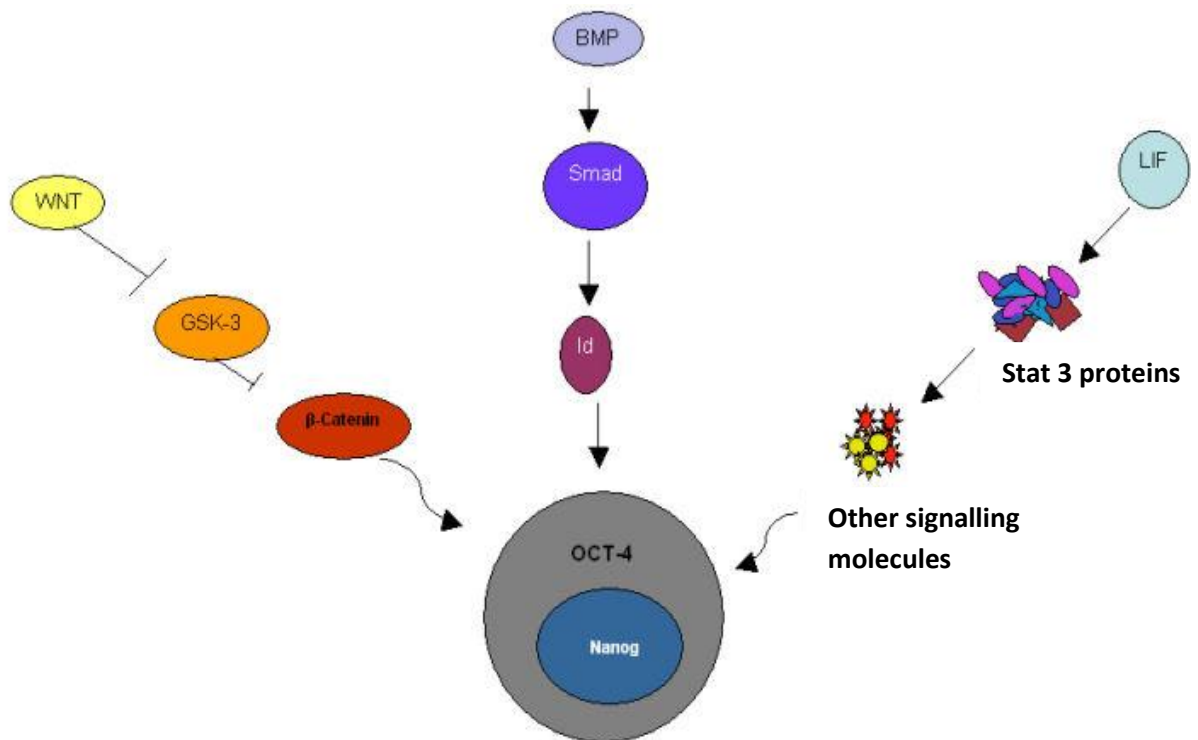


Figure 1.4: Pluripotency pathways. Pathways contributing to stem cell pluripotency via Oct4. (Adapted from <http://njms.umdnj.edu/gsbs/stemcell/scofthemoth/esc/2.jpg>)

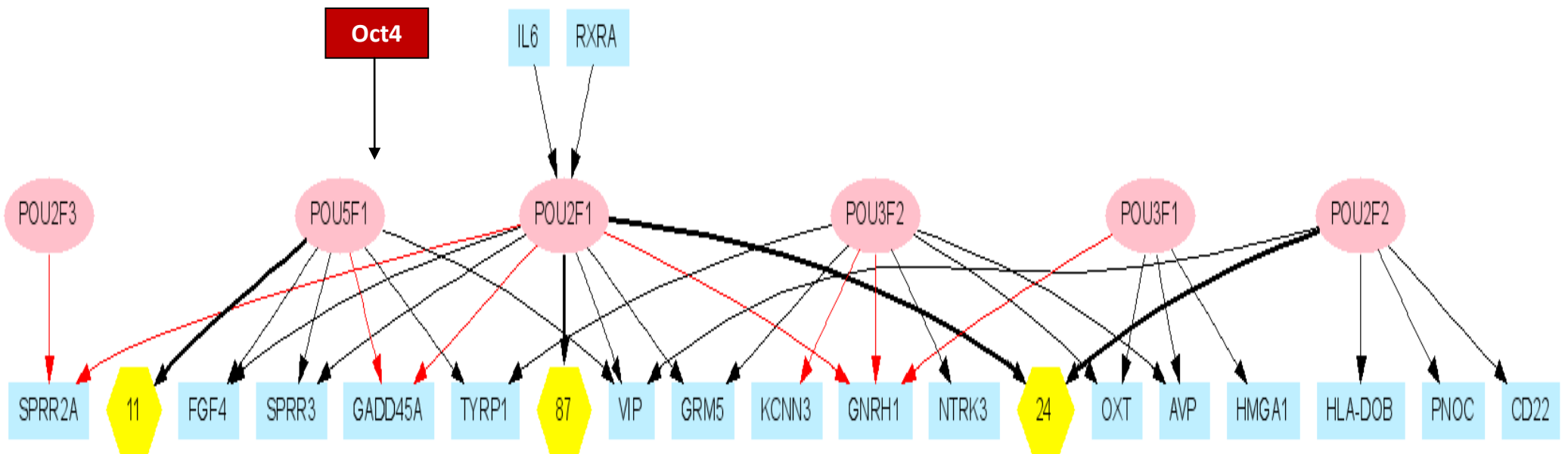


Figure 1.5: Gene Regulatory Network of Transcription Factor family Oct4 in human. **Ellipses** represent the transcription factors belonging to the POU family. **Boxes** symbolize the genes. In case of Oct4 /POU5F1 genes regulated include fibroblast growth factor-4 (FGF4), Small proline-rich protein 3 (SPRP3), Growth arrest and DNA-damage-inducible protein GADD45 alpha (GADD45A), Tyrosinase-related protein 1 (TRP1) and Vasoactive intestinal peptide (VIP). **Hexagons** correspond to the number of clustered genes. **Red lines** indicate that the protein-DNA binding is known. The 11 regulated clustered genes are: Friend leukaemia virus integration 1 (FLI1), Sex determining region Y { SRY } - box 9 (SOX9), Chorionic gonadotropin beta (CGB), Collagen type II alpha 1 (COL2A1), Dopamine Decarboxylase (DDC), Forkhead box D3 (FOXD3), High-mobility group protein B1 (HMGB1), High-mobility group protein B2 (HMGB2), Interferon epsilon 1 (IFNE1), Alpha platelet-derived growth factor receptor (PDGFRA) and Undifferentiated embryonic cell transcription factor 1 (UTF1). (Adapted from <http://rulai.cshl.edu/TRED/GRN/Oct.htm>).

1.3.3 BMP-2

While Oct4-A is associated with stem cell pluripotency, the bone morphogenetic proteins (BMPs) produce a promotion or inhibition of the astrocytic lineage (Nakano *et al.*, 2008). The gene expressions of the two BMP isoforms, BMP2 and BMP4 have been observed extensively in glioma, performing diverse functions. BMP4 protein has been found to promote astro-gial differentiation by reducing symmetric divisions, thereby depleting the CSCs population (Piccirillo and Vescovi, 2006). This inhibition is achieved by the FRAP-STAT pathway involving FKBP12/rapamycin associated protein (FRAP), the Signal Transducers and Activators of Transcription (STAT) proteins (Rajan *et al.*, 2003). *In vivo* data illustrated that the delivery of BMP4 down regulated CD133 expression by 50 % and BMP4 pre-treated CD133⁺ cells formed defined, non-invasive tumours in immune-deficient mice compared to untreated cells which developed large tumours (Piccirillo *et al.*, 2006).

On the other hand, BMP2 regulates cell differentiation and proliferation (Rios *et al.*, 2004). BMP2 is down regulated in differentiated somatic cells, and contributes to stem cell survival and self-renewal. Astrocytic tumours express a high level of BMP2 protein in comparison to the normal human astrocytes (NHA). Inhibition of this protein using small interfering ribonucleic acids (RNAs) {siRNA} reduced glioma cell proliferation and migration (Lu *et al.*, 2006). Furthermore, a high expression of BMP2 in different grades of glioma has been shown to increase its clinical relevance and makes it a selective marker for the prognosis of glioma (Liu *et al.*, 2009). The level BMP2 protein within the glioma cell population would help predict the extent of undifferentiated state of brain tumour cells attained on induction of micro-environmental changes.

1.4 Undifferentiation

Undifferentiation is one of the key features of stem cells. Changes in the properties of the undifferentiated brain tumour cells were studied by induction of micro-environmental changes in order to obtain an insight into the deregulated pathways in glioma. A differentiated U87-MG cell line was subjected to serum deprivation and hypoxia in order to promote their undifferentiation and to focus on the stem cell-like properties. The expression of CD133, Oct4-A was thus evaluated to confirm the presence of stem-like cells or its progenitors.

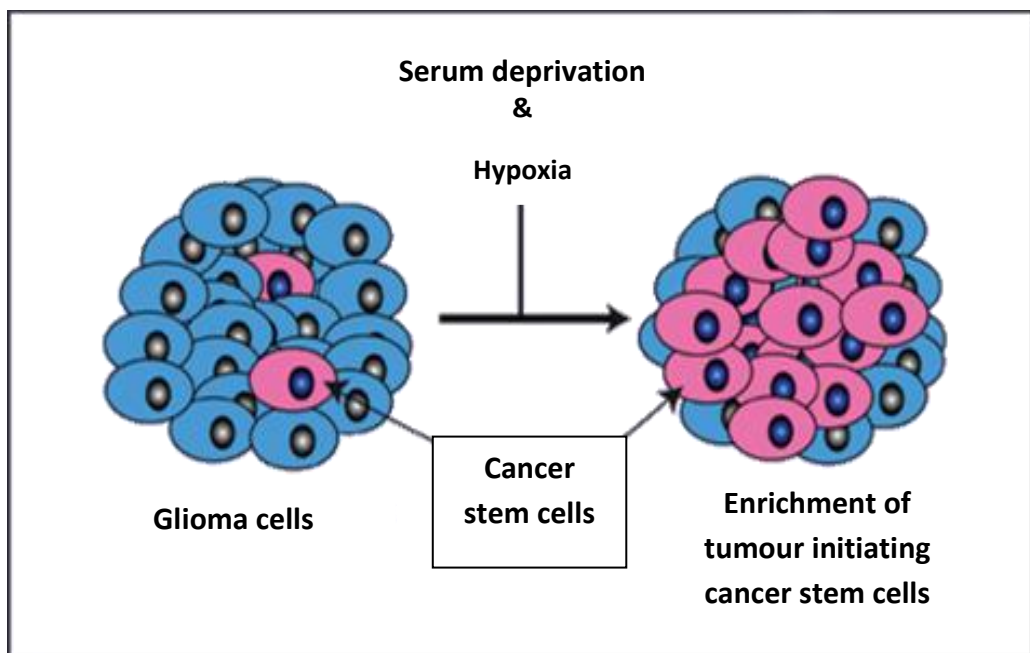


Figure 1.6: Glioma cell undifferentiation. Enrichment of CSCs on induction of serum deprivation and hypoxia. (Modified from <http://www.mmf.umn.edu/initiatives/wh/2009/Spring/funding.cfm>)

1.4.1 i) Serum deprivation

Cancer cells attain immortality by ignoring growth inhibitory signals and proliferating in the absence of stimulatory growth signals. They propagate in lack of serum as their cell cycle phase is independent of the interactions between growth factors and surface located receptors (Karp, 2009). Breast cancer cells when exposed to serum deprivation indicated an increased tumour cell invasion mediated by Phosphoinositide 3-kinase (Reshkin *et al.*, 2000). Evaluation of cells under serum-deprived conditions was undertaken in order to study the response of human glioblastoma. A gradual increase in the concentration of serum-free neural stem cell culture medium with and without vincristine has been reported to be a simple and effective method of isolating CSCs from U87-MG cells (Yu *et al.*, 2008). In addition, an up-regulation of CD133 was observed as a result of decreasing serum supplement levels in GOS-3 cells (Shervington and Lu, 2008). As proposed by stem cell sciences (UK), cancer cells when subjected to serum free media (RHB-A) undergo differentiation, whereas the addition of supplements such as human epidermal growth factor (hEGF) and basic fibroblast growth factor (bFGF) drives the cells towards undifferentiation. The growth factor EGF induces motility owing to chemotaxis and chemokinesis stimulation and also contributes to drug resistance (Garcia *et al.*, 2006). In addition, the fast acting FGF mediates mitosis supporting the EGF action of cancer cell proliferation (Fischer *et al.*, 2008). The combination of growth factors and serum starvation could provide an insight of the mechanism of glioma cell adaptation to the new tumour micro-environment and indicate an increase in the expression of stem cell-related genes.

ii) Hypoxia

Hypoxia is an important feature of solid tumours characterised by decreased oxygen availability and promoting tumour progression (Brahimi-Horn *et al.*, 2007). The cells inhabited in the hypoxic environment show chemoresistance due to the limited supply of therapeutic drugs delivered via circulation (Cardone *et al.*, 2005). Hypoxia activates hypoxia-induced alpha/beta (α/β) heterodimeric transcription factors (HIFs) leading to induction or repression of various genes related to angiogenesis, cell death/survival, pH regulation, metabolism, matrix remodelling and metastasis (Brahimi-Horn *et al.*, 2007 and Pouyssegur *et al.*, 2006).

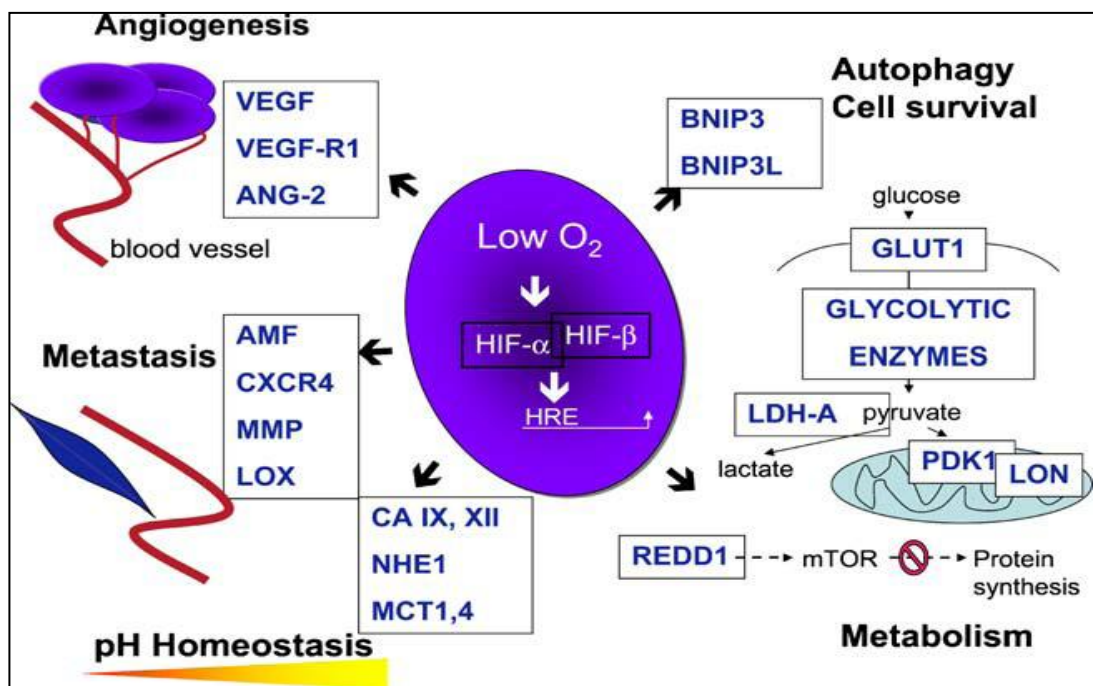


Figure 1.7: Functions of HIF induced gene products. HIF α/β bound to the hypoxia-response elements mediates functions such as angiogenesis, metastasis, pH homeostasis, autophagy and metabolism via expression of various proteins. Regulated proteins include AMF autocrine motility factor; ANG-2 angiopoietin-2; BNIP3 Bcl-2/adenovirus E1B 19 kDa-interacting protein 3; BNIP3L Bcl-2/adenovirus E1B 19 kDa-interacting protein 3 like; CA IX, XII carbonic anhydrase; CXCR4 cytokine (C-X-C motif) receptor 4; GLUT1 glucose transporter 1; LDH-A lactate dehydrogenase-A; LON, a mitochondrial protease; LOX lysyl oxidase; MCT1, 4, monocarboxylate transporter; MMP matrix metalloproteinase; NOXA pro-apoptotic member of Bcl-2 protein family; PDK1 pyruvate dehydrogenase kinase 1; REDD1/RTP801; VEGF vascular endothelial growth factor; VEGF-R1, vascular endothelial growth factor receptor (Adapted from Brahimi-Horn *et al.*, 2007).

The behaviour of CSCs is affected by external signals that originate from the niche disrupting their regime of receptor mediated pathways (Li *et al.*, 2009). HIFs are known to directly alter cellular differentiation and stem cell function (Keith and Simon, 2007). Cells under hypoxic conditions stabilise HIFs and trigger the activity of gene products such as Notch, Oct4, avian myelocytomatosis virus oncogene cellular homologue (c-myc; proto-oncogene), ABC transporters (ABC-T), and telomerase to promote a stem cell-like state (Fig 1.8). Furthermore, dedifferentiation and stem cell-like characteristic of self-renewal is promoted by factors such as KLF4 and Sox2 (Keith and Simon, 2007).

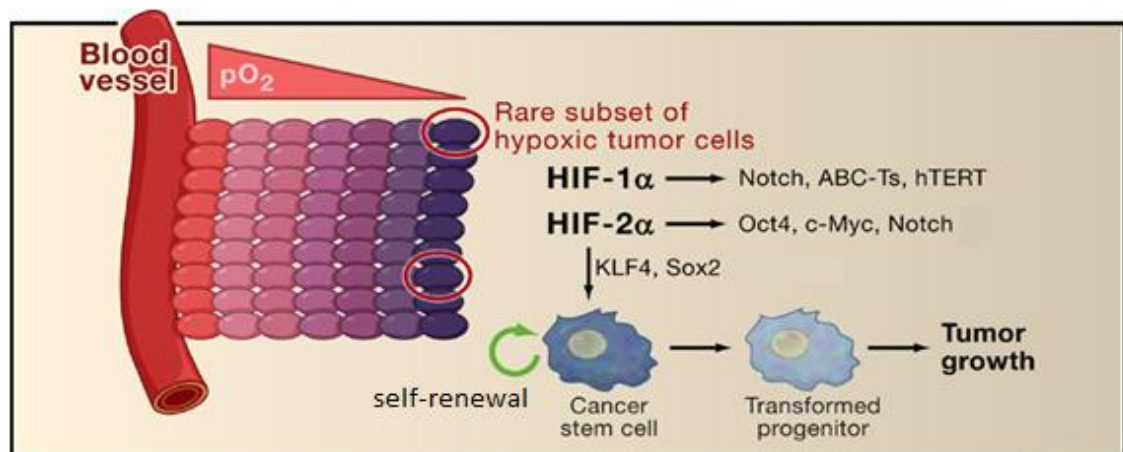


Figure 1.8: Generation of stem cell induced by HIFs under hypoxic conditions (Adapted from Keith and Simon, 2007).

Hypoxia-induced factor 2 α (HIF2 α ; promotes tumorigenesis) has been reported to stimulate the expression stem cell marker protein CD133 in non-stem cells together with an up regulation of stemness related genes such as OCT4, homeobox protein NANOG (NANOG; self-renewal of undifferentiated stem cells) and c-Myc (Heddleston *et al.*, 2009). The stem cell-like properties of CD133⁺ cells derived from glioblastoma were enhanced by reducing the optimum oxygen levels from 20 to 7 %, resulting in the simultaneous increase in the expression of other stem cell markers (nestin, Oct4 and SOX2) (McCord *et al.*, 2009). The induction of hypoxia in glioma cells may provide an insight of the stem cell function of undifferentiation and self-renewal, respectively.

1.5 Focus of current research

The main aim of the investigation entails an evaluation of stem cell-like features in the differentiated and undifferentiated cohort of brain tumour cells in order to define a suitable stem cell marker(s). U87-MG cells grown under normal cell culture conditions and those subjected to serum deprivation and hypoxia (undifferentiation) were initially checked for the expression of CD133, Oct4-A and BMP2 proteins. Flow cytometry provided detailed measurements of the quantitative expression, whereas immunofluorescence facilitated qualitative analysis of the candidate proteins. The cells were subsequently subjected to a chemosensitivity assay, cell cycle analysis and proteomic studies in order to achieve an in-depth understanding of the altered protein level within the undifferentiated glioma cells.

1.5.1 Chemosensitivity

Drug resistance remains one of the crucial attributes enabling stem cells to proliferate and repopulate even after the administration of effective chemotherapeutic drugs. In glioma, a high expression of multi-drug resistance genes such as *MDR1* and multi-drug resistance-associated protein-1 (*MRP1*) together with anti-apoptotic proteins such as permeability glycoprotein (*P-gp*), B-cell lymphoma 2 (*B-cl2*), Bcl-x_L, FLICE-inhibitory protein (FLIP), cellular inhibitor of apoptosis-1 (c-IAP2), X-linked inhibitor of apoptosis protein (XIAP), neuronal apoptosis inhibitory protein (NAIP), and survivin in CD133⁺ cells has been associated with the chemoresistance mechanism (Bi *et al.*, 2007; Shervington and Lu, 2008; Liu *et al.*, 2006). Most of the chemotherapeutic drugs target the DNA affecting cell division to induce cell death. However, the DNA repair mechanism of CSCs helps to restore the integrity of the alkylated DNA bases following drug therapy failure (Johannesen *et al.*, 2008). The

present study included exposure to chemotherapeutic drugs such as Temozolomide (TMZ) and Paclitaxel (Taxol) to test the drug resistant ability of the undifferentiated cells with respect to the control (differentiated) U87-MG cells. The effectiveness of the specified drugs was assessed by performing cell viability assay.

- **Temozolomide (TMZ)**

The drug, TMZ is a widely used anti-cancer agent in the treatment of various tumours due to its predictable bioavailability and minimal toxicity (Friedman *et al.*, 2000). TMZ leads to cell death by inducing O6-guanine methylation creating cytotoxic lesions recognized by DNA mismatch repair (Gupta *et al.*, 2006; Fig 1.9).

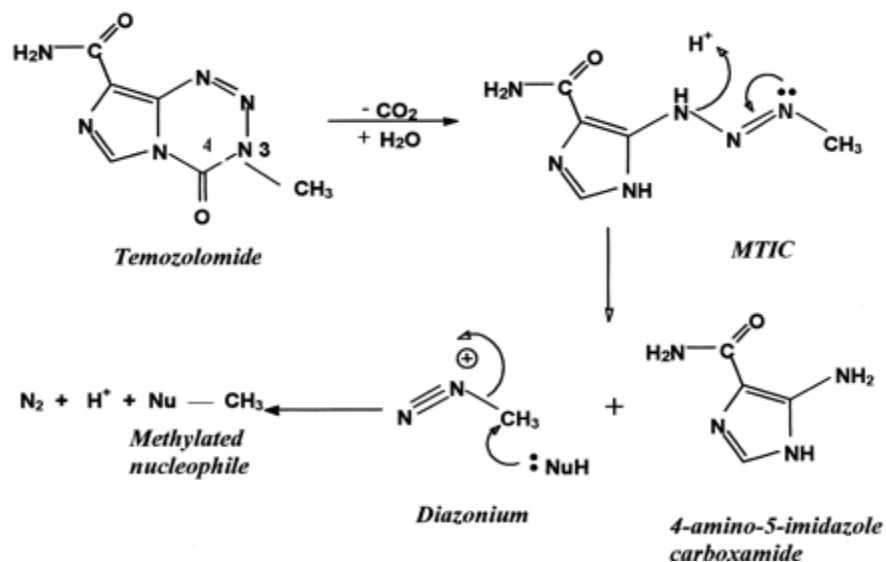


Figure 1.9: Mechanism of action of TMZ. TMZ alkylates DNA at N-7/O-6 position of guanine residues to cause DNA damage (Adapted from <http://cureglioma.info/>).

It is known that glioma cells demonstrate G2/M arrest in response to TMZ, whereas stem cells resist the effect with a down-regulation of autophagy-related proteins such as Beclin-1, autophagy protein 5 (Atg5) and light chain 3 (LC3) (Kanzawa *et al.*, 2004 and Fu *et al.*, 2009). Therefore, if the cell is driven to an undifferentiated state populates a cohort of stem-like cells then they should exhibit resistance towards TMZ as compared to the control U87-MG cells.

- **Paclitaxel (Taxol)**

Taxol is cytotoxic group of taxane that disrupts microtubule integrity (Tseng *et al.*, 1999). It affects the function of mitosis; cellular morphology and secretion by causing an arrest of the cell cycle in the G2/M phase (Fruehauf *et al.*, 2006). Cancer cells resist the cytotoxic effect of Taxol by taking advantage of the drug efflux mechanism with the help of P-gp (Gottesman *et al.*, 1993). Furthermore, Taxol alters the tubulin structure, deregulates the cell cycle, and also changes the drug binding affinity of the microtubules (Zhou *et al.*, 2010).

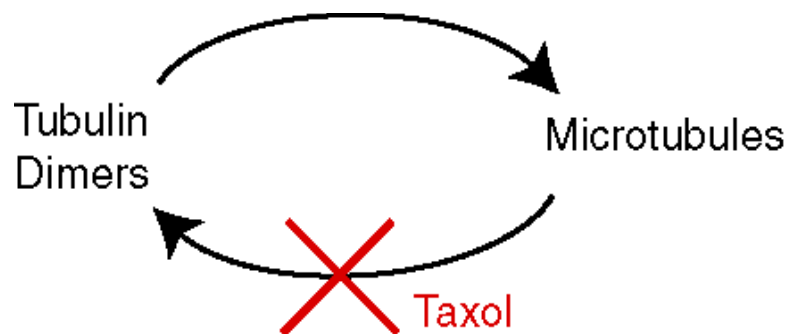


Figure 1.10: Stabilization of microtubules by Taxol in order to bring about mitotic arrest. (Adapted from <http://course1.winona.edu/sberg/308s10/Lec-note/CytoskeletonA.htm>).

Since, CD133⁺ cells show a high expression of P-gp (Shervington and Lu, 2008); the existing group of undifferentiated stem cells inhabited within U87-MG cells may possibly indicate a resistance towards Taxol.

1.5.2 Cell cycle analysis

A normal eukaryotic cell cycle comprises of four consecutive phases, i.e. G1, S, G2 and M phase. Chromosomal replication and separation occur in the S and M phase, whereas G1 and G2 phases represent the gap phase which favours cell growth. Stem cells have a unique cell cycle structure and control mechanisms that help to maintain the stem cell state (White and Dalton, 2006). Glioma stem cells display minimal DNA repair mechanism with an elongated cell cycle and enhanced basal activation of checkpoint proteins that may contribute to their radio resistance (Ropolo *et al.*, 2009). Monitoring the cell cycle changes induced in the U87-MG cell line would explain the altered mechanism in their state of differentiation, under the influence of micro-environmental changes and administration of chemotherapeutic agents (TMZ and Taxol).

1.5.3 Proteomics

Proteomics primarily involves the study and comprehensive analysis of proteins. In a population of stem cells, it helps to unravel the molecular mechanism of self-renewal and multi-lineage differentiation (Whetton *et al.*, 2008). A complete developmental change in stem cells and its protein interactions cannot be examined by means of transcriptome analysis (Heck *et al.*, 2007). Proteomics characterises and quantifies a range of proteins involved in drug resistance, signalling cascade, cell-to-cell interactions and membrane proteins that function as surface markers for cell identification (Zhang *et al.*, 2010).

Malignant gliomas show an increased concentration of soluble growth factors and cytokines which function to attract NSCs towards tumours (Heese *et al.*, 2005).

Furthermore, a combined study using proteomics and microarray showed seven specific proteins namely Annexin A2 (ANXA2; receptor expressed on tumour cells), Tissue Inhibitor of Metalloproteinases-1 (TIMP-1), Collagen alpha-1(XI) (COL11A; malignancy), bax (Bax; anti- and pro-apoptotic regulator), Cluster of Differentiation 74 (CD74; cancer metastasis), Tumour Necrosis Factor (ligand) Super Family, member 8 (TNFSF8; Hodgkin lymphoma marker, cell proliferation/inhibition) and Serine palmitoyltransferase, long chain base subunit 2 (SPTLC2; associated with hereditary neuropathy type 1) to participate in the migration of stem cells towards malignant tumours (An *et al.*, 2009). Analysis and quantification of post-translational modifications and investigation of pathways involved in embryonic stem cell (ESC) differentiation have been readily achieved through the proteomic approach (Whetton *et al.*, 2008). In addition, it helps in the identification of novel protein/peptide markers on the cell surface which could be distinguished between two different cell lines with an equal potential.

The current research aims to investigate changes in protein expression of the differentiated (grown under normal cell culture conditions) and undifferentiated (serum-deprived and hypoxia) U87-MG cells using a proteomic approach. Proteins from the control and the treated samples were extracted and quantified in our laboratory and the rest of experimental protocol was carried out by Applied Biomics (U.S.A). The techniques used included Two-Dimensional Polyacrylamide Gel Electrophoresis (2D-PAGE), 2D Fluorescence Difference gel electrophoresis (2D-DIGE), DeCyder analysis, Mass spectrometry analysis and Mascot (Database search). The experiment resulted in differential, elevated and decreased dataset for the protein expression profile.

The protein dataset provided by the Applied Biomics (U.S.A) was then subjected to IPA (Ingenuity® Systems), Data mining and knowledge-based software to identify molecular functions and pathways which correlate with the protein datasets. Each protein was studied in detail in relation to the aspect of cell differentiation status and features of stemness.

1.6 Previous studies from our laboratory

Previous studies focused on the characterisation of CD133⁺ stem-like cells in glioma with respect to the expression of multi-drug resistance (MDR)-related molecules (i.e. *mdr1* and *bcl-2*). High levels of nestin, P-gp, Bcl-2, and telomerase in CD133⁺ astrocytoma/oligodendroglioma cells (GOS-3) and a significantly high expression of Bcl-2 at both the genotypic and phenotypic levels in CD133⁺ normal astrocytes compared to the autologous CD133⁻ cells were observed (Shervington and Lu, 2008). The results indicated a possible contribution of MDR molecules to chemoresistance in CD133⁺ stem-like cells. It was concluded that Bcl-2 may play a crucial role in supporting the significant chemoresistance of CD133⁺ glioma and normal cells as compared to the corresponding CD133⁻ cells. In addition, CD133⁺ glioma cells and CD133⁺ normal astrocytes share similar regulatory mechanisms with respect to the drug efflux protein P-gp, the anti-apoptotic protein Bcl-2 and the immortalisation protein telomerase (Shervington and Lu, 2008).

The use of serum deprivation (without supplements) enriched the CD133⁺ cells in astrocytoma/oligodendroglioma (GOS-3) cells with *nestin*, *mdr1* and *bcl-2* proteins and down-regulated *hTERT*, *bmi1*, *c-myc* and telomerase activity. Thus, a first direct link between *CD133* and other molecules e.g. *mdr1*, *bcl-2*, *hTERT*, *bmi1*, and *c-myc* was

provided. Serum deprivation also highlighted that CD133⁺ originated from secondary glioblastomas, putting forward a query on its derivation from a NSC, progenitor or a differentiated glioma cell (Lu, 2008).

Based on the above data, the current study focused on evaluating the differentiated and undifferentiated state of glioma cells for stem cell-like traits. Glioma cells grown under normal cell culture conditions were considered as differentiated cells since they arise from a process of differentiation from stem cell progeny (Sell, 2006). On the other hand, the undifferentiated state of the differentiated glioma cells was achieved by induction of two independent micro-environmental changes (hypoxia and serum deprivation) (Fig. 1.11). The present study mainly focused on the regulation of the proteins CD133, Oct-A and BMP2 and the cell cycle phase when the brain tumour cells were driven from a differentiated to an undifferentiated state. In addition, the chemosensitivity assay performed may provide an insight into the drug resistance potential of the undifferentiated glioma cells.

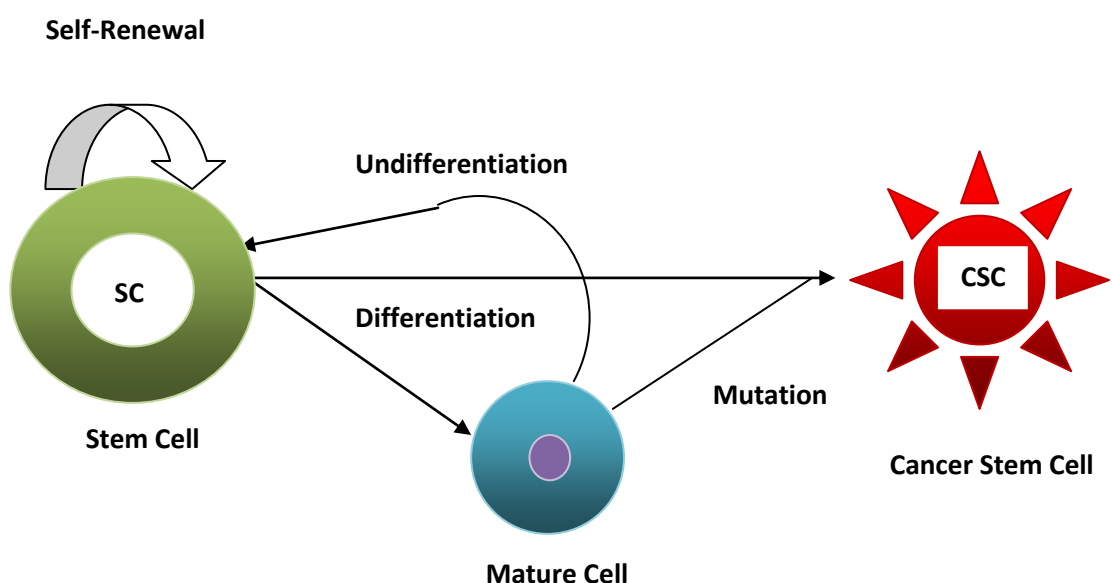


Figure 1.11: Differentiation and undifferentiation of cells. (Adapted from http://www.allthingsstemcell.com/wp-content/uploads/2009/09/p53_cancer_cell_formation-copy2.png)

1.7 U87-MG cell line to evaluate stemness status

Previous data from our laboratory have demonstrated the isolation of CD133 from astrocytoma/oligodendroglioma cells (GOS-3) (Lu 2008, PhD thesis). In the present study, U87-MG (grade IV) being the highest form astrocytic brain tumour cell line was used for all the experiments. These cells have been widely used as an *in-vitro* model of human glioblastoma cells to study the cytotoxic effect of chemotherapeutic drugs towards cancer cells. In 2008, Yu *et.al* demonstrated that U87-MG cells inhabited a fraction of neurosphere forming cells with a capability of self-renewal and multipotency. Similar to CSCs, these cells showed histological features identical to glioblastoma together with cellular pleomorphism, hyperchromatic nuclei, pseudopalisades surrounding necrosis, high density of micro vessels and invasion to the brain parenchyma (Yu *et. al.*, 2008). In addition, U87-MG cells elicit receptors for CD133 and epidermal growth factor receptor VIII (EGFRVIII). A biphasic antibody directed against CD133⁺ and EGFRVIII⁺ has been successful as a therapeutic agent for specifically targeting CD133⁺/EGFRVIII⁺ cancer stem cells (Wong *et. al.*, 2009). Vascular endothelial growth factor (VEGF) has been a vital factor in promoting angiogenesis in glioma. U87-MG cells when subjected to hypoxia, displayed an aggressive growth with an up-regulation of VEGF by means of transient receptor potential cation channel 1 (TRPC1) (Wang *et. al.*, 2009). Some of the characteristics of U87-MG cells resemble to CSCs, and thus, it was decided to use it as a suitable target under differentiated and undifferentiated conditions in order to study the stem cell-like properties.

1.8 Questions to be addressed concerning the investigation (Working Hypothesis)

1. Is CD133 a reliable glioma stem cell marker?
2. Should the research focus on the differentiated and undifferentiated aspects of glioma cells in order to trace stemness properties?
3. What would be the requirements of desired glioma stem cell marker/s?

1.8.1 Main Aim

1. To address the complexity of identifying glioma stem cell biomarker.

1.8.2 Specific Aims

The specific aims of this study were:

1. To evaluate the expression of CD133, Oct4-A and BMP2 in differentiated and undifferentiated glioma cells.
2. To study the proteomic change influenced by hypoxia and serum deprivation.

1.8.3 Novelty of the current research project

1. The current research focuses on exploring the undifferentiated and differentiated aspects of brain tumour cells in order to define CSCs.
2. Introduction of pluripotency factor of Oct4-A in glioma and checking its expression as a potent CSC marker with respect to CD133.
3. Studying the proteomic changes on account of hypoxia and serum deprivation (undifferentiation) in order to obtain an insight into the deregulated pathways in glioma.
4. Propose selective marker/s for the detection of glioma stem cells.

Chapter 2

Materials and Methods

2.1 Cell Culture

2.1.1 Cell lines

The experiments were carried out using different grades of human glioma cell lines (Table 2.1) with Grade I astrocytoma expressing a mutant p53 (1321N1), a grade II/III astrocytoma/ oligodendroglioma (GOS-3) and a grade IV glioblastoma (U87-MG). The human cell lines were purchased from the European Collection of Cell Cultures (ECACC) and the American Type Culture Collection (ATCC) with no evidence of the presence of infectious viruses or toxic products. The handling instructions were followed as recommended by the Advisory Committee on Dangerous Pathogens (ACDP) for Category 2 containment. The cells were received as frozen ampoules in 1 ml plastic cryotubes in an appropriate freezing medium. The freezing medium was supplemented with 10 % foetal bovine serum (FBS), 2 mM L-glutamine and 10 % (v/v) dimethyl sulphoxide (DMSO). Cells were grown by incubating at 37 °C in a humidified 5 % CO₂ atmosphere and maintained in 75 cm² or 25 cm² tissue culture-treated polystyrene flasks (Sigma, UK) as monolayer cultures. All cells were harvested when they reached 70-80 % confluence.

Table 2.1: Cell lines used and their media formulation.

Cell lines	Description	WHO grade	Culture Media	Suppliers
1321-N1	Astrocytoma	II	DMEM, 10 % (v/v) FBS, 2 mM L-glutamine	ECACC, UK
GOS-3	Astrocytoma/Oligodendro- glioma	II/III	DMEM, 10 % (v/v) FBS, 4 mM L-glutamine	DSMZ, Germany
U87-MG	Glioblastoma	IV	EMEM, 10 % (v/v) FBS, 2 mM L-glutamine, 1 % (v/v) non-essential amino acid RHB-A [®] , 20 ng/ml EGF, 20 ng/ml FGF	ECACC, UK

2.1.2 Media and reagents

Media preparations were carried out under aseptic conditions by the addition of required supplements as recommended by the suppliers (Table 2.2). The prepared medium was labelled with the date of preparation and stored at 4 °C. Serum-free basal medium (RHB-A) was foil-wrapped to protect from light as it contained light-labile components. The reconstituted medium was stable for 4 weeks.

The volume of the supplement that was to be added was calculated using the formula:

$$V_1 C_1 = V_2 C_2$$

$$V_1 = \frac{V_2 C_2}{C_1}$$

Where: V_1 = Initial volume

C_1 = initial stock concentration

V_2 = final volume

C_2 = final concentration

This formula was adopted to determine volume and concentrations in appropriate calculations throughout this study.

Table 2.2: Media, reagents, supplements and storage conditions

Reagents	Abbreviation & storage temp	Formulations	Suppliers
Dulbecco's modified eagle's medium	DMEM, 2-8 °C	25 mM hepes, 1.0 g/l glucose 1.0 mM sodium bicarbonate, 0.011 g/l phenol red	Sigma, UK
Eagle's minimum essential medium	EMEM, 2-8 °C	2.0 g/l sodium bicarbonate 4.5 g/l glucose, 10 mM hepes 1.0 mM sodium pyruvate, 0.0053 g/l phenol red	Sigma, UK
Serum free basal medium	RHB-A®, 2-8 °C	Company patency	Stem cell sciences, UK
Foetal bovine serum	FBS, -20 °C	Heat inactivated FBS	GIBCO, UK
L-glutamine	-20 °C	200 mM L-glutamine	Sigma, UK
Non essential amino acid	2-8 °C	100 x non essential amino acid	Sigma, UK
Phosphatase buffer saline (PBS, 1x)	2-8 °C	8 g/l NaCl, 0.2 g/l KCl, 1.44 g/l Na ₂ HPO ₄ 0.24 g/l KH ₂ PO ₄ , pH 7.4	BDH, UK
Trypan blue (0.4 %)	Room temperature	0.81 % sodium chloride 0.06 % potassium phosphate, dibasic	Sigma, UK
Dimethyl sulfoxide	DMSO, Room temperature	99.5 % dimethyl sulfoxide, 0.81 % sodium chloride	Sigma, UK
Recombinant Human Epidermal growth factor	hEGF, -20 °C	Recombinant (<u>E.coli</u>)	BD Biosciences, UK
Basic Fibroblast growth factor	bFGF, -20 °C	Recombinant (<u>E.coli</u>)	BD Biosciences, UK

2.1.3 Resuscitation of frozen cells

The cell lines supplied were stored in cryotubes in liquid nitrogen. The protocol was carried forward as recommended by ECCAC. The medium was pre-warmed at 37 °C in a water bath for approximately 30 min. The external surfaces of the media bottle were decontaminated with 70 % ethanol and then transferred to a sterile field. Frozen cell cryotubes were completely thawed by placing them in a water bath at 37 °C for 1-2 min. The contents of the cryotube were then resuspended in 4 ml of appropriate media in a 15 ml centrifuge tube. The resuspended cells were then centrifuged at 150 x g for 5 min at room temperature. The supernatant was discarded and the cell pellets were aliquoted into 25 cm² tissue culture-treated polystyrene flasks with 5 ml of medium in each flask. The flasks were gently shaken back and forth manually to enhance equal distribution of the cells within the medium and were labelled with the name of the cell line, passage number and date. The cells were then incubated at 37 °C in 5 % CO₂ and 95 % oxygen and the medium was changed every alternate day. For slow growing cells the medium was changed after every 48 hours of incubation to maintain sufficient nutrient levels for the cells. Cells were observed under the microscope after overnight incubation.

2.1.4 Subculture and cell treatment

i) Subculture

When the monolayer of the cells reached 70-80 % confluence, they were scraped to enable sub-culture. The cells were washed 3 times with PBS (0.5 ml, pH 7.4, 37°C) to remove excess culture media and then were scraped using a sterile disposable scraper. To ensure approximately 95 % cell detachment, the cells were observed under the microscope. The cells were re-suspended in 8 ml of media and transferred into a 15 ml centrifuge tube. A 20 µl suspension was taken for a cell count and the remaining cells were centrifuged at 1000 rpm (112 g) for 5 min. The cell pellets were re-suspended in growth media in a new flask seeding at $2-4 \times 10,000$ cells/cm² for cancer cells (1321N1, GOS-3, U87-MG). The flasks were suitably labelled with the name of the cell line, passage number and date and then incubated under ordinary culture conditions.

ii) Cell treatment (hypoxia and serum deprivation)

Hypoxia and serum deprivation were implemented to study the cell differentiation status.

a. Hypoxia

U87-MG cells (70-80 % confluence) were subjected to 100 % nitrogen for 30 min (previously optimised technique in our laboratory) under sterile conditions to enhance undifferentiation (Lu, 2008, PhD thesis). The cells were incubated for 24 hours under cell culture incubation conditions and later scraped and used for further experiments.

b. Serum deprivation

U87-MG cells (70-80 % confluence) were replaced with serum free RHB-A[®] media supplemented with 20 ng/ml of hEGF and bFGF, respectively. The cells were observed for morphological changes within 3-5 days after which the cells

transformed completely into neurospheres, indicating their undifferentiation state. The media was replaced with supplements every alternate day. The hypoxia-treated and the serum-deprived cells were then subjected to multiple experimental procedures which included flow cytometry, cell viability and cell cycle analysis.

2.1.5 Cryopreservation

The cell pellets after scraping were alternatively cryopreserved for future use. 1×10^6 cells were re-suspended in a cell freezing medium (complete culture medium with 10 % DMSO) in 1 ml cryoprotective ampoules, labelled with the cell line name, passage number and date. The ampoules were then placed in a 'Mr. Frosty' freezing container (Nalgene, UK) filled with isopropanol, stored at -80°C overnight and then transferred into -195°C liquid nitrogen container. For mRNA isolation 2×10^6 cells were frozen and stored as pellets at -80°C without the freezing medium. Cells required for immunofluorescence were cultured in chamber slides and fixed with paraformaldehyde. In order to carry out cell cycle analysis a pellet containing 1×10^6 cells was washed once with PBS and then fixed by re-suspending them in 70 % ice cold ethanol. These fixed cells were stored for a minimum of 24 hours at -20°C before following the cell cycle analysis protocol. For the waste disposal as recommended by ECCAC, the culture medium, pipette and tips were placed in 1 % Virkon solution (Anachem Ltd, UK) overnight before being autoclaved and incinerated.

2.1.6 Cell library maintenance

Cell library was maintained to manage cell stocks of different cell lines. A data entry log book was maintained having a record of the position of storage of cryotubes in the liquid nitrogen. This allowed easy traceability of specific cells for future reference. The level of liquid nitrogen was monitored regularly to ensure an appropriate cryopreservation.

2.1.7 Quantification of cells and cell viability using a haemocytometer

Cell aliquot (20 μ l) was diluted 1:1 with trypan blue (Freshney, 1987) to identify the number of viable cells. A cover slip was attached to the haemocytometer to create Newton's refraction rings. Both sides of the chamber were filled with the stained cell suspension and the cells were counted under a light microscope using x 20 magnification. Cell viability was calculated as a percentage using the following equation:

$$\text{Total number of cells counted/ml} = \text{total viable cells} + \text{total dead cells} \times 10^4$$

$$\text{Percentage of viable cells} = \frac{\text{viable cells}}{\text{Total cell number}} \times 100$$

2.2 Messenger RNA (mRNA) isolation and quantification

mRNA from cell lines was extracted using an mRNA Isolation Kit (Roche, UK) according to the Manufacturer's instructions provided. The isolation kit worked on the basis that the poly (A)⁺ tail of mRNA hybridised to a biotin-labelled oligo (dT)₂₀ probe. A Streptavidin-coated magnetic particle captured the biotinylated hybrids and by means of a magnetic separator, the magnetic particles were captured. The fluid was then removed by washing the particles with the washing buffer and finally the mRNA was eluted from the particles by incubation using redistilled water. This method enabled to achieve a highly purified form of mRNA without the preparation of total RNA. Table 2.3 shows the reagents used in the process of mRNA isolation and figure 2.1 illustrates the principle of mRNA isolation.

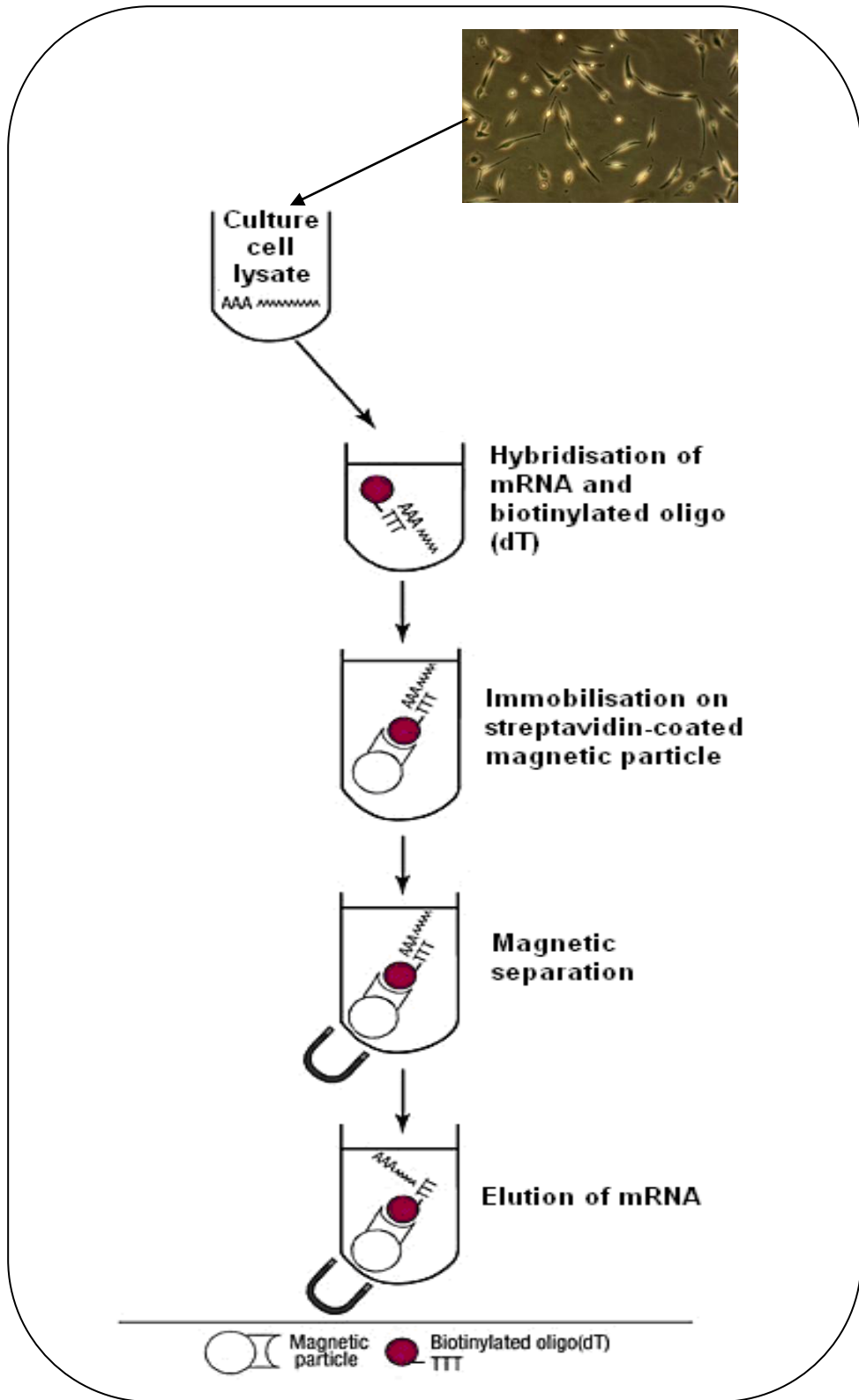


Figure 2.1: Schematic representation of the principle of mRNA isolation (Roche diagnostic, UK). (Modified from http://www.roche-applied-science.com/US/ProdInfo/images/mrna_isolation_kit_flow01n.jpg)

2.2.1 mRNA isolation

The sample and reagents employed in this study were kept on ice throughout the isolation protocol. A total of 2×10^6 cells was washed three times using ice cold 1 x PBS and was resuspended with 500 μ l lysis buffer. Cells were then sheared mechanically by passing six times through a 21 gauge needle to prepare a cell lysate. 0.5 μ l of biotin-labelled oligo (dT)₂₀ probe was added to the lysate and allowed to hybridise with mRNA at 37 °C for 5 min. Simultaneously, streptavidin magnetic particles were prepared as follows: they were resuspended thoroughly before appropriate amount of magnetic particle (Table 2.3) was transferred to a fresh microcentrifuge tube. Using a magnetic separator the Streptavidin magnetic particles were separated from its storage buffer. Storage buffer was discarded and the particles were then washed once in 75 μ l of lysing buffer to remove any excess storage buffer. The supernatant was again discarded and the particles were resuspended in the dT-mRNA hybrid mixture and incubated at 37 °C for 5 min to attain immobilisation. The hybrid-linked particles were magnetically separated from the fluid and the supernatant was discarded. Magnetic particles were then resuspended thrice in washing buffer (3 \times 200 μ l) in order to remove all contaminants quantitatively. Subsequent to the final wash, the supernatant was discarded and the mRNA was eluted from the magnetic particles by the addition of 10 μ l redistilled water. This was followed by an incubation at 65 °C for 2 min. mRNA was separated from the magnetic beads using a magnetic separator. The supernatant containing the mRNA was analysed quantitatively stored at -20 °C in an RNase free eppendorf tube. The mRNA isolated was further transcribed into single-stranded cDNA to perform PCR.

Table 2.3: reagents used in this study for mRNA isolation

Reagents	Preparation	Contents	2 x 10⁵ cells	2 x 10⁶ cells
PBS	Autoclaved	1x, pH 7.4, ice cold	3 x 500 µl	3 x 500 µl
Lysis buffer	Used from the kit (Roche , UK) Stored at 2-8 °C	0.1 M Tris buffer 0.3 M LiCl 10 mM EDTA 1 % lithium dodecylsulfate 5 mM DTT (dithiothreitol) pH 7.5	0.1 ml	0.5 ml
Streptavidin magnetic particles		10 mg/ml in 50 mM hepes 0.1 % bovine serum albumin 0.1 % chloracetamide 0.01 % methylisothiazolone, pH 7.4	50 µl	50 µl
Oligo(dT)₂₀ probe, biotin labelled		100 pmol biotin-labelled oligo(dT) ₂₀ per µl of redistilled water	0.5 µl (50 pmol)	0.5 µl (50 pmol)
Washing buffer		10 mM Tris buffer 0.2 M LiCl 1 mM EDTA pH 7.5	3 x 200 µl	3 x 200 µl
Redistilled water		RNase-free	5 µl	10 µl

2.2.2 mRNA quantification

The mRNA was quantified spectrophotometrically using a Helios gamma spectrophotometer (Thermo spectronic, UK) by measuring the absorbance at 260 nm (A_{260}) and 280 nm (A_{280}).

The Isolated mRNA was diluted 1: 250 1 x Tris-Acetate-EDTA (TAE) buffer. The optical density (OD) of the diluted mRNA sample was measured using the absorbance reading taken at 260 nm. A blank containing 2 μ l of dH₂O and 498 μ l 1x TAE buffer was used as reference for each sample.

Concentration of extracted mRNA was calculated using the formula:

An emission of one OD (One A_{260} unit) = 40 μ g/ml for single-stranded (ss) mRNA.

Dilution factor = 250

\therefore Concentration of mRNA (μ g/ml) = $A_{260} \times 250 \times 40$

A ratio of A_{260}/A_{280} represents the level of contamination (e.g. protein) in a RNA sample. $A_{260}/A_{280} > 1.8 - 2.0$ suggested a pure preparation of (ss) mRNA.

2.3 Introduction to bioinformatics

Application of computer science and statistics to molecular biology is termed as bioinformatics. Bioinformatics by means of multiple disciplines such as mathematics, artificial intelligence, computer science, chemistry, biochemistry, and statistics helps to facilitate data analysis. The ease of data analysis not only provides an insight of the various biological processes but also addresses many unanswered biological questions (Kim, 2000).

The subject areas covered under this field range from structural biology, genomics to gene expression studies and assists in storing and organizing data. It provides specialized tools to view and analyze the explosive data generated by biological scientists throughout the world (Kim, 2000). The World Wide Web has become an essential feature to the world of bioinformatics as it makes DNA, RNA and protein data available to users throughout the world through databases such as National Centre for Biotechnology Information (NCBI), GenBank (USA), European molecular biology laboratory (EMBL) (Europe) (Fenstermacher, 2005). The present achievements of bioinformatics hold substantial promise to transform the medical world.

2.3.1 Gene sequence and location

In the present study, bioinformatics was used to locate the genes of interest among the human DNA sequences. Location of the target genes with its diagrammatic representation was obtained online with the help of GeneCards[®] (Weizmann Institute of Science, <http://www.genecards.org/>). GeneCards[®] is an integrated database of human genes providing a concise integrated summary on various genes, extracted from major public and proprietary database. A gene annotation from over 40 mined

resources can be managed using GeneCards[®] (Shmueli *et al.*, 2003). The whole template DNA sequence of target genes was found online at National Center for Biotechnology Information (NCBI, <http://www.ncbi.nlm.nih.gov/>) which provides the GenBank DNA sequence database.

For this study genes without any identified mutation were chosen for the design of sequence-specific primers (required for qRT-PCR) using Primer3 software. Primer3 software helps to choose oligonucleotide primers for the template DNA sequence as also displays information about the sequences and average length of the primer, amplicon size, melting temperature (T_m) and GC content (GC%).

2.3.2 Primer design

The primer used for a PCR commercially synthesised single-stranded oligonucleotide having a short length of 18 to 22 bp. Primers used in the technique of PCR amplified the gene of interest. The following parameters were generally taken care of while designing primers for a PCR to give yields of the specific amplicon:

- a. A primer should be between 18 to 22 bp. Long primers having longer annealing temperatures are more specific, but their efficiency is low because thermodynamically the annealing takes longer.
- b. G/C and A/T content of the primer should be similar to or higher than that of the sequence to be amplified. For example, a primer, which is 20 nucleotides long, normally corresponds to 45-55 % GC content. Therefore its melting temperature should be between 55 and 65°C (Dieffenbach *et al.*, 1993).

Primers with melting temperatures above 65°C have a tendency for secondary annealing. Within a primer pair, the GC content and T_m should be well matched. Poorly matched primer pairs could prove to be less efficient and non-specific because loss of specificity arises with a lower melting temperature (T_m). Thus, PCR primers should maintain a reasonable GC content. Oligonucleotides 20 bases long with a 50 % G + C content generally have a melting T_m values in the range of 52-58 °C offering a sufficient thermal window for efficient annealing (Dieffenbach *et al.*, 1993). Figures 2.2, 2.3, 2.4 and 2.5 represents the output from gene locations and primer designs for *CD133*, *Oct4-A*, *BMP-2* and *GAPDH*, respectively. Primer 3 was accessed from: http://frodo.wi.mit.edu/cgi-bin/primer3/primer3_www.cgi.

2.4 Complementary DNA (cDNA) synthesis

An amount of 100 ng of isolated mRNA was reverse transcribed to cDNA using a 1st Strand cDNA Synthesis Kit (Roche, UK). Figure 2.6 showed the principle of converting mRNA to cDNA while table 2.4 enlisted the reagents with its formulations provided in the 1st Strand cDNA Synthesis kit.

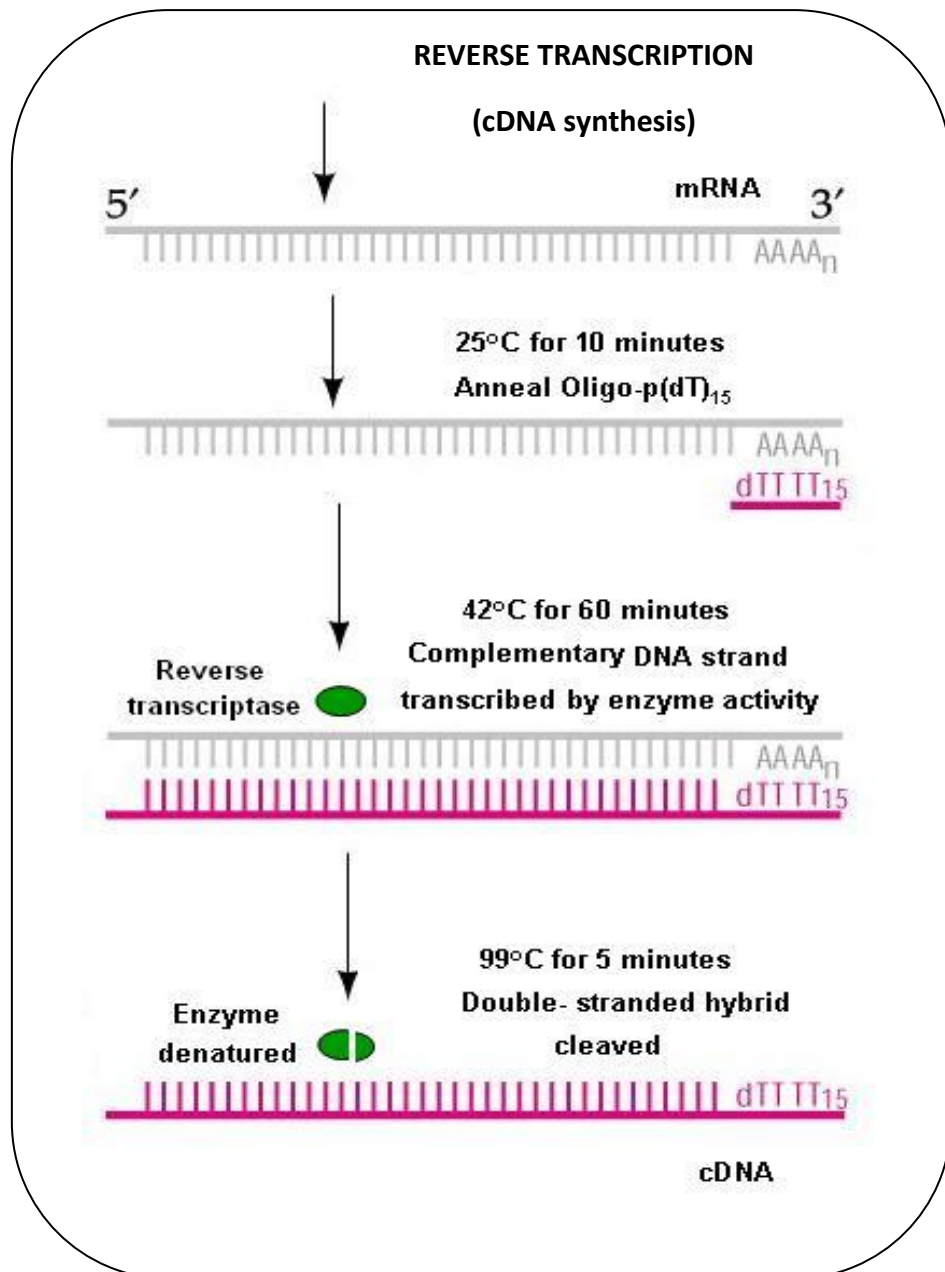


Figure 2.6: Principle of Reverse transcription of mRNA to cDNA. (Modified from <http://8e.devbio.com/images/ch04/0405fig2.jpg>)

Table 2.4: Reagents used for cDNA synthesis

Reagents	Formulation & concentrations	Volume of reagents (Final volume: 20 μl)	Final concentrations
10x Reaction buffer	100 mM Tris, 500 mM KCl, pH 8.3	2 μ l	1 x
MgCl₂	25 mM	4 μ l	5 mM
Deoxynucleotide mix	dATP, dCTP, dTTP, dGTP, 10 mM	2 μ l	1 mM
Oligo-p(dT)₁₅ primer	0.02 A ₂₆₀ units/ μ l (0.8 μ g/ μ l)	2 μ l	0.04 A ₂₆₀ units (1.6 μ g)
RNase inhibitor	50 units/ μ l	1 μ l	50 units
AMV reverse transcriptase	-----	0.8 μ l	\geq 20 units
Sterile water	-----	20 μ l – 11.8 μ l – mRNA sample volume	-----

2.4.1 cDNA synthesis protocol

An amount of 50 - 100 ng of mRNA was required for successful cDNA synthesis. Therefore, 100 ng of isolated mRNA was used to obtain cDNA in this study. Samples and reagents were kept on ice throughout the cDNA preparation. All reagents were thawed on room temperature except for RNase inhibitor and AMV reverse transcriptase which were thawed on ice. A mixture containing all the reagents was prepared to sum up to a total volume of 11.8 µl (volume as mentioned in table 2.4). An appropriate volume of mRNA sample was added to the mixture based on its quantification value to achieve a final concentration of 100 ng. Sterile water was added to obtain a final volume of 20 µl in each sample and the mixture was briefly vortexed and centrifuged. The mixture was incubated at 25 °C for 10 min to allow mRNA and primer annealing. The mRNA template was reverse transcribed into single-stranded cDNA by further incubating the mixture at 42 °C for 60 min. AMV reverse transcriptase was denatured by incubating the reaction at 99 °C for 5 min and then further cooled at 4 °C for 5 min. The synthesised cDNA was stored at at -20 °C until required.

2.5 Quantitative Real Time Polymerase Chain Reaction (qRT-PCR)

qRT-PCR was a technique used detect the genetic expression of the targeted mRNA. This was a sensitive and simple technique that logarithmically amplified a short sequence of DNA (100-600 bases) within a longer double stranded DNA/cDNA molecule. The level of *CD133*, *OCT4A*, *BMP2* and *GAPDH* expressions was calculated by qRT-PCR using the Light Cycler 2.0 system. (Roche Diagnostics, UK) and Light Cycler® Fast Start DNA Master^{PLUS} SYBR Green I kit according to the manufacturer's

instructions. Prior to the study the PCR of each targeted gene was optimised. Figure 2.7 illustrated the basic steps of denaturation , annealing and extension in a PCR.

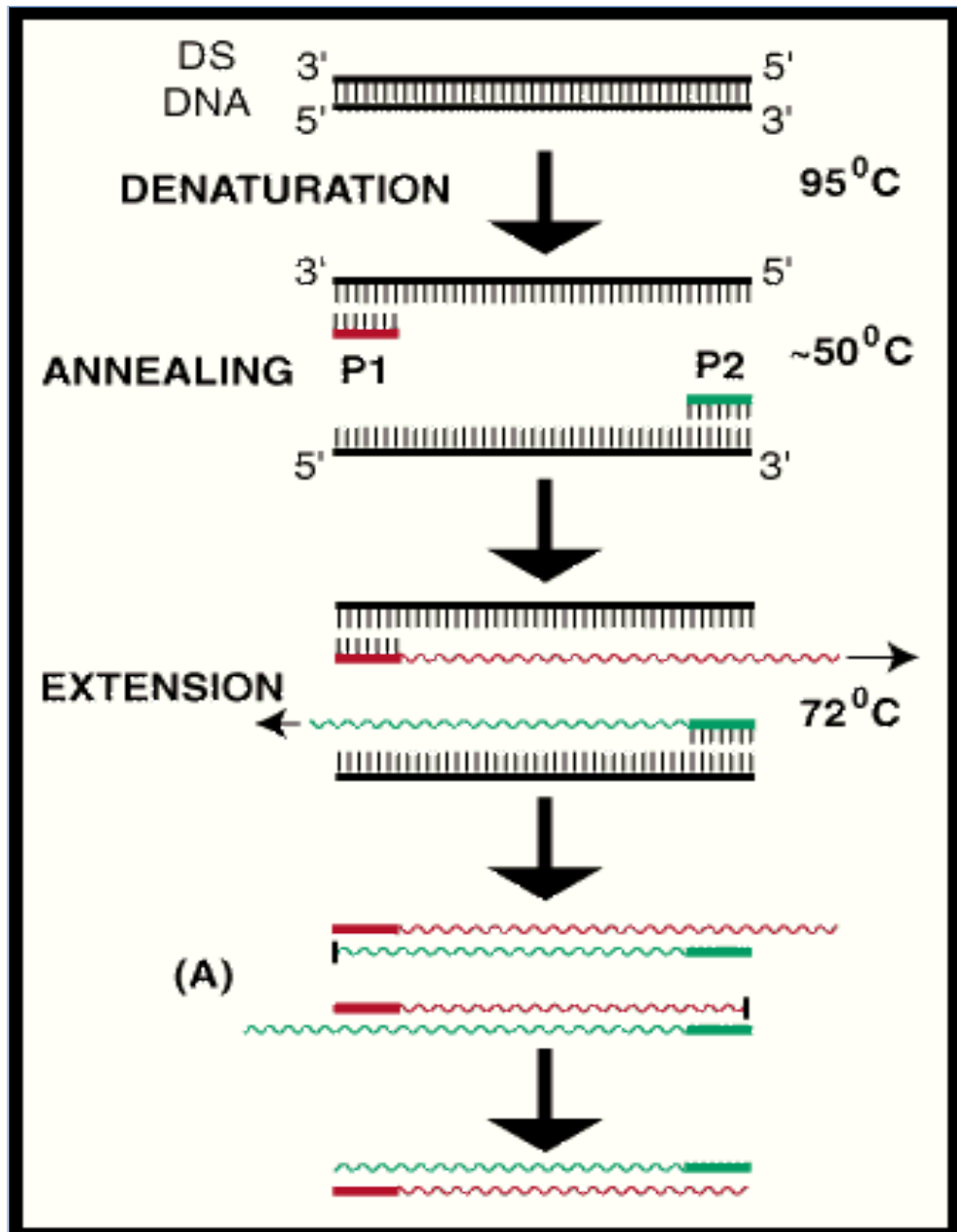


Figure 2.7: Steps involved in a PCR. Denaturation of double-stranded DNA into two complementary single strands at 95°C, annealing of the primers P1 and P2 to the target region of DNA at about 56°C (temperature varies according to the primers used) and extension of the primers from 3 prime to the 5 prime direction at 72 °C by DNA polymerases. (Modified from <http://www.flmnh.ufl.edu/cowries/PCR.gif>).

Table 2.5: Reagents provided in the PCR kit (Roche, UK) and volume of reagents required to make PCR master mix.

Kit reagents		
Reagents	Compositions	Quantity
Light Cycler® Fast Start Enzyme (1a)	Fast Start Taq DNA Polymerase	1 vial
Light Cycler® Fast Start Reaction Mix SYBR Green (1b)	Reaction buffer, dNTP mix (with dUTP instead of dTTP), SYBR Green I dye and 10 mM MgCl ₂	3 vials
H₂O, PCR-grade	RNase-free H ₂ O	2 ml
PCR master mix (total =20µl)		
PCR primer mix	Left + right primer (1:1)	2 µl
Enzyme Master Mix	14µl of Light Cycler® Fast Start Enzyme (1a) added to Light Cycler® Fast Start Reaction Mix SYBR Green (1b)	4 µl
Single-stranded cDNA template	-----	2 µl
H₂O, PCR-grade	-----	12 µl

2.5.1 Primer Preparation

Each primer (right/sense and left/antisense) was dissolved in 250 µl of molecular biology grade water to obtain 20 µM stock solutions and stored at -20°C as recommended by the manufacturer. Table 2.6 represented the specific primer sequence of the targeted genes and their specific annealing temperature.

Table 2.6: Primer sequence and the annealing temperature of the targeted genes

Gene	Primer Sequences	Product size (bp)	Annealing Temperature (°C)			
			Primer3	TIB MOLBIOL	Wallace rule*	Experimental Temperature after optimisation
<i>CD133</i>	Sense: 5' -TTGTGGCAAATCACCAGGTA-3' Antisense: 5' -TCAGATCTGTGAACGCCTTG-3'	248	59.96 59.98	55.80 55.50	58.00 60.00	64.00 64.00
<i>Oct4-A</i>	Sense: 5' -GACACCTGGCTTCGGATTT-3' Antisense: 5' -GAATCCCCCACACCTCAGA-3'	174	Self designed	56.5 56.3	58.00 60.00	56.00 56.00
<i>BMP-2</i>	Sense: 5' -CCCAGCGTGAAAAGAGAGAC-3' Antisense: 5' -GAGACCGCAGTCCGTCTAAG-3'	168	59.99 60.01	56.5 56.3	62.00 64.00	56.00 56.00
<i>GAPDH</i>	Sense: 5' -GAGTCAACGGATTTGGTCGT-3' Antisense: 5' -TTGATTTTGGAGGGATCTCG-3'	194	59.83 59.99	56.20 54.80	60.00 58.00	56.00 56.00

Wallace rule(GC/AT rule): calculates the primer annealing temperature for short DNA oligo consisting of 14-20 base pairs: $T = 2^{\circ}\text{C}(A + T) + 4^{\circ}\text{C}(G + C)$, where A, C, G and T represent the number of adenine, cytosine, guanine and thymine bases in each primer sequence, respectively (Wallace *et al.*, 1979).

2.5.2 PCR protocol

All reagents and samples were kept on ice throughout the experiment. The PCR enzyme reaction mix was prepared by adding 14 μl of Light Cycler[®] Fast Start Enzyme (1a) to Light Cycler[®] Fast Start Reaction Mix SYBR Green vial (1b). The prepared enzyme was then labelled and stored at 2-8 °C and it was also protected from light. PCR master mix was prepared by adding 12 μl molecular biology-grade H₂O, 2 μl of 10 μM PCR primer mix, 4 μl of Master Mix and 2 μl single-stranded cDNA template to give a total volume of 20 μl . PCR grade H₂O was substituted for cDNA to serve as a negative control for the experiment. The protocol involved hot-start induction, with the Fast Start *Taq* DNA polymerase enzyme activated by pre-incubating the reaction mixture at 95 °C for 10 min. Hot start induction was crucial in this method to prevent non specific elongations and thus increased PCR specificity, sensitivity and yield (Dang and Jayasena, 1996). The single-stranded cDNA template was then subjected to 35 amplification cycles. Amplification cycles included the following parameters:

- Denaturation at 95 °C for 15 seconds.
- Annealing at the primer-dependent temperature for 15 seconds.
- Amplicon dependent extension at 72 °C for 25 bp/second.

The cycle ended by producing a data for quantification analysis which was obtained by a single step emitted fluorescence (in channel F1, gain value 3). After the 35th cycle, the produced amplicon was prepared for melting curve analysis, thus heated to 95°C (denaturation). This was then rapidly cooled to the previous annealing temperature (+10°C) for 40 seconds. Up to this stage all heating and cooling steps were performed with a slope of 20 °C/s.

Further, to obtain data for the melting curve analysis, the temperature was then raised to 95°C (melting) with a slope of 0.1 °C/s and the emitted fluorescence was measured continuously. The specificity of the amplified PCR product could be assessed via the melting curve which differentiates between primer-dimers and the specific product. The PCR product was cooled to 40 °C for 30 sec and stored at -20 °C until required.

Table 2.7: Default conditions for all amplifications for a qRT-PCR

Analysis Mode	Cycles	Segment	Specific Temperature (°C)	Holding Time (min)
-	Pre-Incubation	-	-	-
None	1	-	95	10
-	Amplification	-	-	-
Quantification	35	Denaturation	95	1
-	-	Annealing	variable	2
-	-	Extension	72	1
-	-	-	72	7
-	Cooling	-	-	-
None	1	-	4	∞

2.5.3 Analysis of qRT-PCR product.

Agarose gel electrophoresis helped to assess the length and purity of the qRT-PCR product. Reagents used in the process as mentioned in table 2.8.

2.5.4 Agarose gel electrophoresis.

The 1 x TBE buffer (working solution) was prepared from 10 x TBE (stock solution). Agarose gel 2 % (w/v) was prepared in dH₂O and heated in a domestic microwave at maximum power for 3-4 min until all the crystals dissolved. The solution was cooled to 70 °C and poured into a gel tray set with a comb. The gel was allowed to set for 30-45 min. The 1 x TBE buffer (Running buffer), was poured into the gel tank with solidified gel in place. Thereafter, the comb was removed carefully. A 10 µl of PCR product was mixed with 2 µl of tracking dye and loaded in the wells. A molecular marker of 100bp was also loaded with the sample as a reference. The gel was electrophoresed for 3-4 hours at 70 volts and then stained with 0.5 µg/ml ethidium bromide (EtBr) for 20-30 min followed by destaining with water for 15-20 min. The banding patterns were visualised using a GENE GENIUS Bioimaging system and Genesnap software (Syngene, UK).

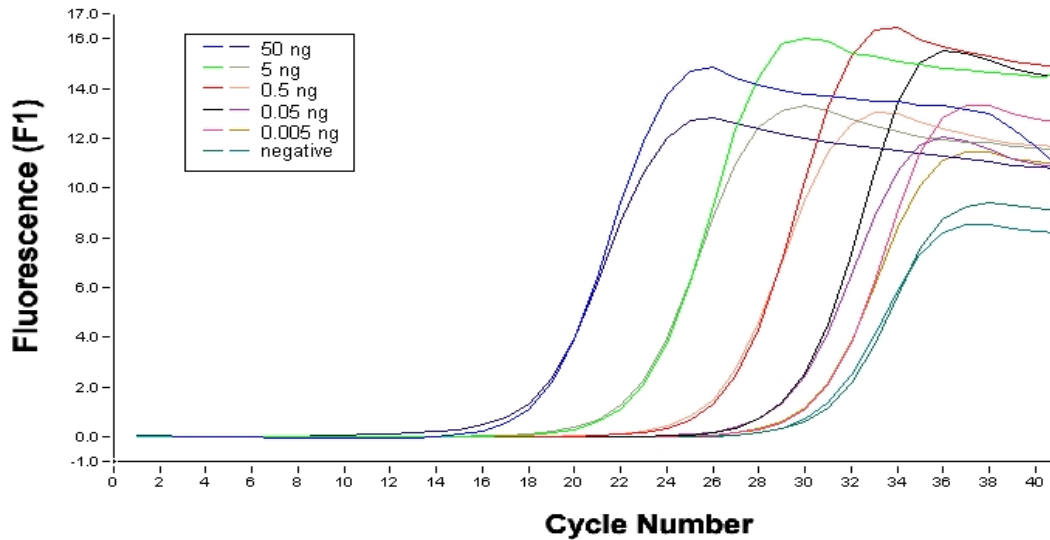
Table 2.8: Reagents used for agarose gel electrophoresis.

Reagents	Working concentrations	Suppliers
TBE (10x Ultrapure 10x Tris borate EDTA electrophoresis buffer)	1 x = 150 ml of 10x TBE in 1350 ml of dH ₂ O	Sigma, UK
Agarose	2 % (w/v) = 3 g Agarose in 150 ml 1xTBE	GIBCO, UK
Tracking dye	40 % (w/v) Sucrose , 0.25 % (w/v) Bromophenol blue and 0.25 % (w/v) Xylene Gyanole	Sigma, UK
Molecular marker (100 bp DNA ladder)	0.5 µg/sample = 1 µl of 500 µg/ml ladder in 6 µl of tracking dye	New England BioLabs, UK
Ethidium bromide (10 mg/ml)	0.5 µg/ml = 25 µl EtBr in 500 ml dH ₂ O	Amresco, USA

2.5.5 Quantification analysis of qRT-PCR

The absolute amount of target amplicon was determined by an external standard of known concentration or copy number. The quantification of copy numbers from crossing point was previously established in our lab using genomic DNA as a template (Mohammed, PhD thesis, 2007). A standard curve was plotted from the quantitative method established on the Light Cycler® 2.0 Real-Time PCR (Mohammed, PhD thesis, 2007). A standard genomic DNA (QIAGEN, UK) with known concentration of 1 µg equal to 3.4×10^5 copies of a single gene, was prepared in five different concentrations (0.005, 0.05, 0.5, 5 and 50 ng, refer table 2.9). This was then amplified by the LightCycler® using *GAPDH* reference gene with its threshold cycle (Ct) numbers to obtain a standard curve. A standard curve generated was plotted with the crossing point or Ct value against copy numbers in order to calculate the copy numbers of the unknown samples (*CD133*, *Oct4-A*, *BMP-2* and *GAPDH*).

A.



B.

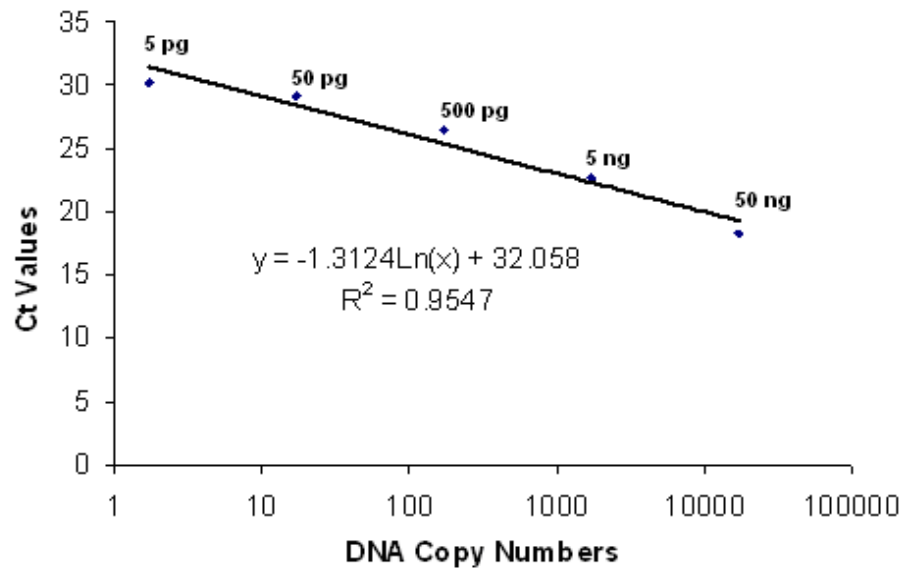


Figure 2.8: Standards to calculate the copy number of the targeted gene. A. Light Cycler quantification curve generated with known concentration of genomic DNA amplified, showing that the higher the concentration of DNA the lower the Ct values i.e. earlier the acquisition of fluorescence. The negative control (Primer alone, NTC) shows no fluorescence acquisition until after 30 Ct (straight line). **B.** The standard generated from the crossing points showing the relationship between Ct values and the copy numbers of the amplified genomic DNA using *GAPDH* as a reference gene (Mohammed, PhD thesis, 2007).

The equation generated ($y = -1.3124\ln(x) + 32.058$) from this standard graph was rearranged to $(=EXP \{Ct \text{ value} - 32.058\} / -1.3124)$ to determine the copy numbers of the mRNA expression of all the genes used throughout the study.

Table 2.9: Genomic DNA correspondence to its average Ct values and equivalent copy number.

Concentration of Genomic DNA (ng)	Average Ct	Copy number
0.005	30.15	1.7
0.05	29.10	17
0.5	26.42	170
5	22.60	1700
50	18.30	17000

2.6 Chemosensitivity Assay

2.6.1 Chemosensitivity

Glioma cell line U87-MG was subjected to a chemosensitivity assay and was evaluated for cell viability. The undifferentiated U87-MG cells (hypoxic and serum-deprived) together with the control cells were treated with two drugs Taxol and TMZ for a period of 48 hours. An untreated cohort of U87-MG cells served as a negative control without the addition of the drugs. The drugs were prepared based on their IC₅₀ values (Table 2.10) (Lu, 2008). After 48 hours the cells were scraped and their viability was measured by means of propidium iodide (PI) staining.

Table 2.10: Drug preparation

Drugs	Molecular weights	Solvents	Stock Concentrations (mM)	Suppliers	Cat #
Taxol (Paclitaxel)	853.91	Dissolved in methanol, subsequently in culture medium	0.3903	Sigma, UK	T7402
Temozolomide (TMZ)	194.15	Culture medium	2.5753	Schering Plough, UK	25774612

2.6.2 Cell Viability

Previous studies showed cell viability as a quantitative parameter to assess the cytotoxicity of drugs in this study (Lu, 2008, PhD Thesis). For this experimental process, a non-permeant dye propidium iodide (PI) was used which intercalated into the major groove of the DNA of the dead cells. The binding of the dye produced a high fluorescent adduct indicating the presence of non-viable cells.

Cells were scraped and their culture medium was discarded. The cells were then washed 3 x with PBS (0.5 ml, 0.1 M) and centrifuged at 1000 rpm for 5 min. An amount of 500 μ g of PI solution (concentration 10 mg/ml) was added to the cells and incubated in the dark for 5 min. The cells were subjected to the viability analysis using the flow cytometer. The excitation wavelength for PI is 488 nm whereas its fluorescence is detected from 550 nm to 670 nm. An untreated cell line (no staining) served a negative control. For every sample a minimum of 10,000 events/sample was considered. All the reagents and samples were kept on ice throughout the experimental process. Figure 2.9 demonstrated a typical example of a histogram illustrating a cell viability assay performed on the flow cytometer.

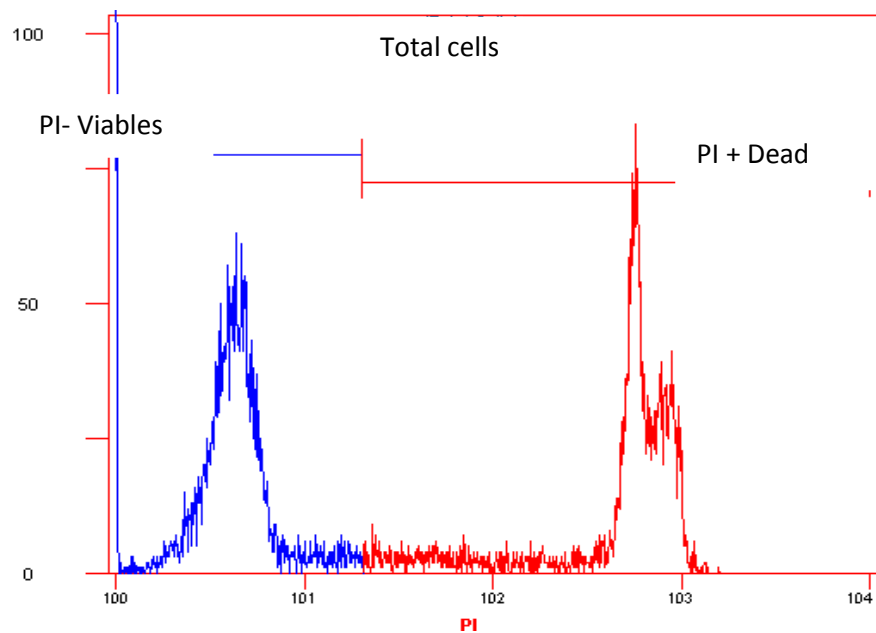


Figure 2.9: A typical example of a histogram plot of cell viability assay using the flow cytometer. Blue histogram represented the population of viable cells and the red histogram denoted the population of dead cells stained with PI (Adapted from <http://www.cdbss.com.cn/?p=2&a=view&r=12>).

2.7 Cell cycle analysis

The cells subjected to undifferentiation and chemotherapeutic drugs were evaluated for altered cell cycle phases. Table 2.11 listed the reagents and their formulation/concentrations used for cell cycle analysis. The cells (1×10^6 cells) were scraped and washed with 1 x PBS (0.5 ml, 0.1M) and then centrifuged at 112 g for 5 min. The supernatant was discarded and the cells were fixed by resuspending it in 2 ml of 70 % ice cold ethanol. Ethanol was added drop wise to the cell pellet to avoid clumping of the cells. The cell sample was then stored at -20°C for a minimum of 24 hours. The fixed samples were centrifuged at 112 g for 5 min and the supernatant consisting mainly of ethanol was discarded and the cells were washed with 1 x PBS (0.5 ml, 0.1 M). The cells were resuspended in PBS containing PI (50 $\mu\text{g}/\text{ml}$) and RNase (100 $\mu\text{g}/\text{ml}$) and incubated at 37°C for 30 min. Stained samples were kept at 4°C in the dark until subjected to flow cytometric analysis.

Table 2.11: Reagents used for cell cycle analysis

Reagents	Concentrations	Suppliers
PBS	0.1 M	Sigma, UK
Ethanol	70 %	Fisher Scientific, UK
PI	50 µg/ml	Sigma, UK
RNAse	100 µg/ml	Sigma, UK

2.8 Flow cytometry

Flow cytometry was a previously described technique that helped to measure the properties of an individual cell. The cells were labelled with a specific antibody conjugated to a fluorochrome and by means of hydrodynamic focusing. Each cell was passed through a single or multiple beam of light. The emitted fluorescence (light scattering) provided knowledge about the cellular properties. Fluorescence measurements taken at different wavelengths provided quantitative and qualitative data about fluorochrome-labelled cell surface receptors and/or intracellular molecules within a cell (e.g. DNA and cytokines) {Fig. 2.10}

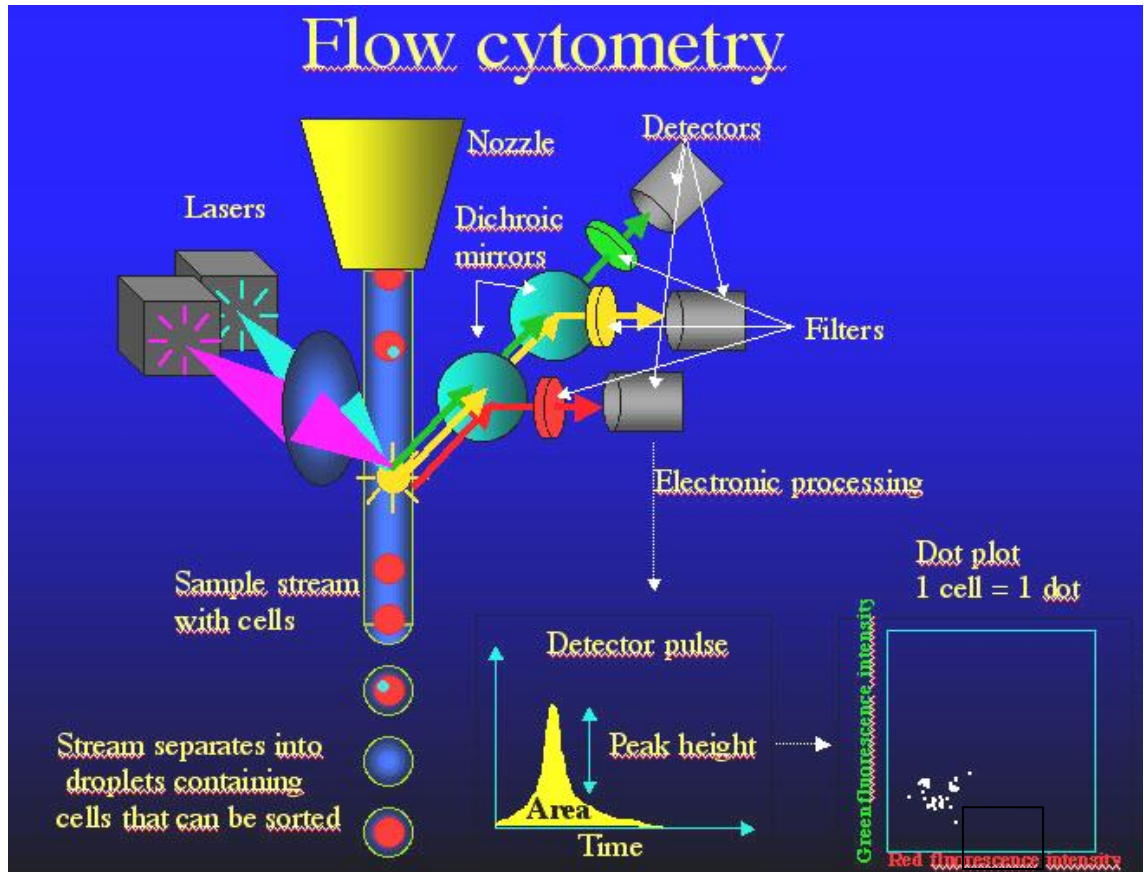


Figure 2.10: An illustration of flow cytometry. (Modified from <http://www.rudbeck.uu.se/showpic.php?id=54>).

2.8.1 Sample preparation (adapted from Abcam, UK; modified according to the experimental requirement)

Control and treated cells ($>1 \times 10^6$ cells) were collected by scraping. The cells were washed 3 x with bovine serum albumin (BSA) (0.5 ml and 0.1 %) made in PBS (0.5 ml and 0.1 M). After each wash the cells were centrifuged at 112 g for 5 min at 4 °C. The supernatant was carefully discarded in order to achieve maximum number of cells for the analysis. The cells were permeabilised by incubating with 0.1 % of triton-X in (100 μ l, 0.1 M) PBS for 15 min in the dark, followed by 3 washes with BSA (0.5 ml, 0.1 %). Blocking solution (made up in 5 % serum in (0.1M) PBS based on the animal in which the antibody was raised) was added to the cells and incubated for 30 min at

4 °C. After 30 min the cells were centrifuged and the blocking solution was discarded. This was followed by the addition of a specific primary antibody (made up in 5 % serum with PBS {0.5 ml, 0.1 M}) for 30 min. The primary antibody was removed by 3 x washes with BSA (0.5 ml, 0.1 %). Secondary antibody prepared similar the primary antibody preparation was added to cell sample and incubated in dark for 30 min. A number of 3 x washes with BSA (0.5 ml, 0.1 %) was carried out in order to remove any traces of secondary antibody. The cells were finally resuspended in BSA (250 µl, 0.1 %) and then filtered to remove clumps using a sterile filter for flow cytometric sample preparation. The samples were stored at 4 °C in the dark until analysed on the flow cytometer. The negative control was prepared by replacing the labelling with the primary antibody. Throughout the experimental process the cell samples and the reagents were kept on ice to minimize cell death. The samples during each wash were gently pipetted to achieve single cell suspension.

2.8.2 Data analysis

The cells were gated selectively by eliminating cell debris or dead cells. For each sample, a maximum of 10,000 events/samples were taken into consideration. It was possible to demonstrate the flow cytometric data by means of a density plot, contour diagrams and histograms (Le *et al.*, 2007). Throughout this study histogram graphs were used to display relative fluorescence (single parameter) on the x-axis and the number of events on the y-axis. Fig. 2.11 represented a histogram plot for flow cytometric analysis. A statistical view of the data could be achieved after acquiring 10,000 events/ sample to identify the exact number of positive cells in a given sample.

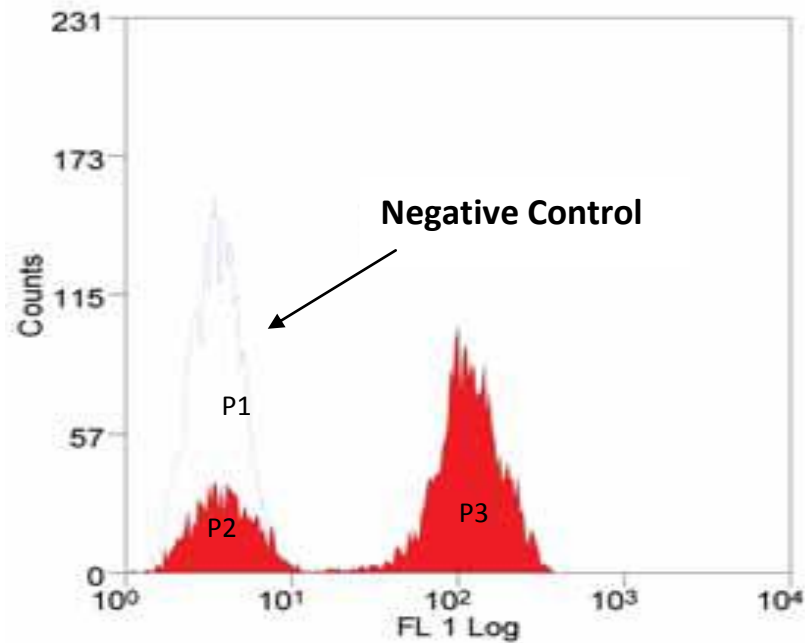


Figure 2.11: A histogram graph demonstrating flow cytometric data. P1-negative control, P2- negative population of cells from sample and P3-positive population of the stained cells. (Modified from <http://keck.bioimaging.wisc.edu/Neuro670/Introduction%20to%20Flow%20Cytometry.pdf>).

Table 2.12: Antibodies used in this study with the dilution factor as recommended by the supplier.

Proteins	Antibodies	Types	Dilution Factor	Suppliers
CD133	Primary	Rabbit polyclonal IgG	1:100	Abcam, UK
	Secondary	Goat polyclonal to Rabbit IgG (Cyanine 5-Cy 5)	1:200	
OCT4-A	Primary	Mouse monoclonal IgG2B	1:50	Santacruz biotechnology, UK
	Secondary	Goat anti-mouse IgG2B (Phyco erythrin-PE)	1:400	
BMP2	Primary	Mouse monoclonal IgG	1:100	Abcam, UK
	Secondary	Rabbit polyclonal to Mouse IgG (Texas Red-TR)	1:200	

2.9 Immunofluorescence (IF)

The technique of Immunofluorescence helped to determine the presence and localisation of the target protein or antigen in fixed cells or tissue samples. Immunofluorescence was carried out by two methods of staining i) Direct staining - where the primary antibody was itself conjugated with fluorescent dye and ii) Indirect staining - where the primary antibody was detected with the help of a secondary antibody conjugated to the fluorescent dye. For this study, the antigen was detected using an indirect staining method to localise the proteins of interest with the aid of a LSM510 Confocal microscope (fig 2.12).

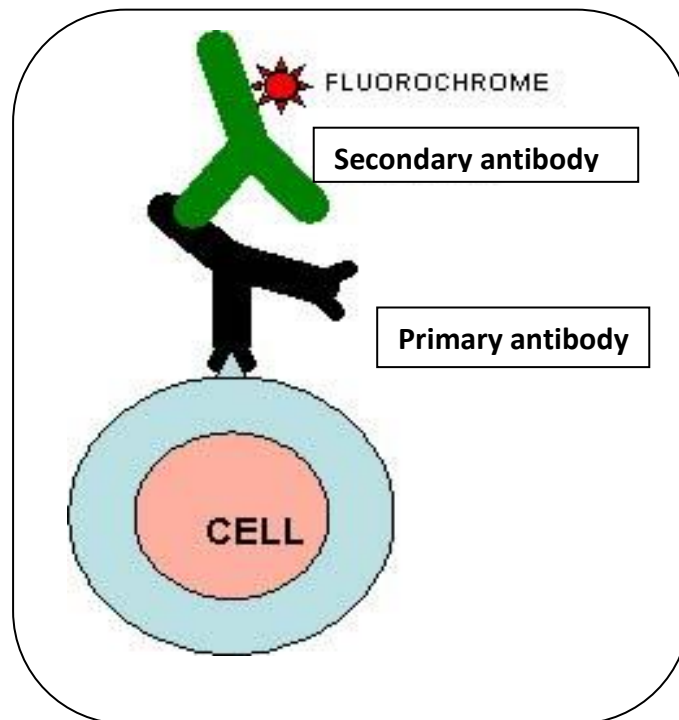


Figure 2.12: Indirect immunofluorescent staining. Primary antibody binds to the antigen on the cell and the secondary antibody conjugated to the fluorochrome recognises the primary antibody and binds to it. The cells are then visualised under a confocal microscope. (Adapted from http://www.biotech.uiuc.edu/images/Indirect_stain_second_image.jpg)

2.9.1 Cell culture IF

The culture medium was removed from the chamber slides and the cells were washed 3 x with warm PBS (0.5 ml, 0.1 M) {all the washing steps were carried out for 5 min on a shaker}. The cells were then fixed at room temperature with freshly prepared 4 % paraformaldehyde (w/v) in PBS (0.5 ml, 0.1 M). The cells were washed 3 x with warm PBS (0.5 ml, 0.1 M). After this step, the cells could be stored for a period of 6 months at -20 °C for immunofluorescent staining. Permeabilisation was carried out by incubating the fixed cell with 0.3 % (v/v) Triton X-100 in PBS (100 µl) at room temperature for 7 min. The cells were incubated with a blocking solution with serum (based on the species in which the secondary antibody was raised) for 30 min at room temperature. The blocking solution minimizes the probabilities of non-specific binding within the sample. After the removal of the blocking reagent, the cells were incubated with their corresponding primary antibodies (Table 2.12) for 1 hour at room temperature. The primary antibody was then removed by washing the cells 3 x with warm PBS (0.5 ml, 0.1 M). The cells were then incubated with light sensitive fluorochrome (Table 2.12) conjugated secondary antibody (Abcam, UK) diluted in blocking solution for further 60 min in a dark room. The secondary antibody was removed with three consecutive PBS (0.5 ml, 0.1 M) washes and the cover slips were placed on the slides by addition of 1.5 µg/ml VECTASHIELD mounting medium (Sigma, UK) and allowed to dry for 10 min. The negative control cells from each sample received identical preparations for immunofluorescent staining with no addition of primary antibodies. The cells were then visualised and scanned using an Axiovert 200 LSM 510 laser scanning confocal microscope (Carl Zeiss, UK) (Long *et al.*, 2005)

2.10 Proteomics

Proteomics refers to a large scale study of the characterisation and functions of various types of proteins present within a cell, organ, or organism (Adams 2008). Although the human genome harbours 26000-31000 protein encoding genes (Baltimore *et al.*, 2001) one million proteins have been identified as human protein products, including splice variants and proteins essential for post-translational modifications (Godovac-Zimmermann and Brown, 2001). Proteomics displayed patterns of hundreds of thousands of proteins that were differentially regulated at any time point being dynamically modified by different treatments (Whiteley, 2006). Proteomic analysis included a combination of complex and sophisticated analytical techniques such as 2D Gel electrophoresis for protein separation, image analysis, mass spectrophotometry and bioinformatics tools for quantification and characterization of the complex proteins (Bensmail and Haoudi, 2003).

For the present study, proteins were extracted from the U87-MG control and treated cells (hypoxia and serum deprivation) and were subsequently quantified. Proteomic analysis was performed by Applied Biomics (Hayward, CA). Fig 2.13 illustrated an overview of different proteomic strategies and summarised the workflow of 2D-DIGE via DeCyder analysis. Highlighted in yellow was the proteomic methodologies used in this study.

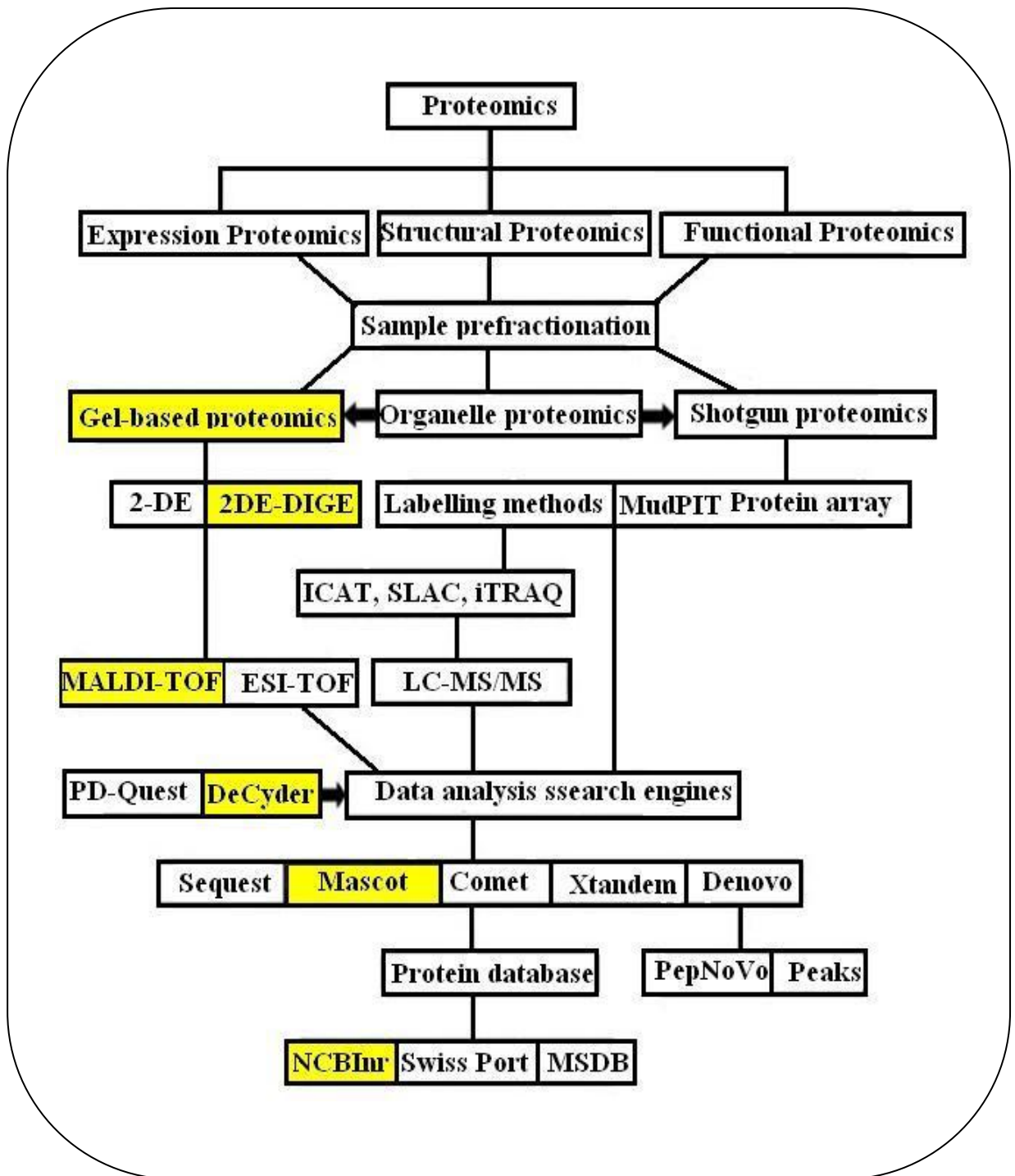


Figure 2.13: An overview of proteomic strategies. Methods used in this project are highlighted. (Adapted from Chandramouli and Quian, 2009).

2.10.1 Protein extraction

The freshly collected cell pellets were washed 3 x with washing Buffer (10 mM Tris-HCl, 5 mM magnesium acetate, pH 8.0) to remove any excess culture medium. For 10 mg of cultured cell pellet, a volume of 200 µl of 2-D cell lysis buffer (400 mM Tris, 0.01 M EDTA; pH 8.3) was added. The mixture was sonicated at 4 °C followed by shaking for 30 min at room temperature. The samples were then centrifuged at 14,000 rpm for 30 min. The supernatant was collected. Protein concentration was measured using Bio-Rad protein assay method.

2.10.2 Protein quantification

The Bio-Rad Protein Assay is based on the Bradford method previously designed for protein quantification. This dye-binding assay produced a differential colour change in response to various concentrations of protein (Bradford, 1976). The dye reagent concentrate was purchased in a kit with BSA (Biorad, UK) which was used as a standard.

Lyophilized BSA standards were reconstituted by adding 20 ml of deionised water and were mixed thoroughly until dissolved. The standard was aliquoted and stored at -20 °C for future use. The dye reagent was prepared by diluting 1 part Dye Reagent Concentrate with 4 parts of distilled deionized water and this was then filtered through Whatman #1 filter. The protein solution was prepared by pipetting 100 µl of each standard and sample solution into a clean and dry test tube. Diluted dye reagent (5 ml) was added to each tube. The mixtures were vortexed and incubated at room temperature for 5 min. The absorbance was measured at 595 nm using gamma thermo

Helios spectrophotometer (Thermospectronics, UK). A standard curve was plotted and the value of the unknown protein was extrapolated. Each protein assay was repeated in triplicate. The protein with additional cell line samples were shipped to the U.S.A on dry ice supplemented with ice bags following the instructions recommended by Applied Biomics.

2.10.3 Over view of work carried out by Applied Biomics (U.S.A) (Fig. 2.14)

- a. **Two-Dimensional Polyacrylamide Gel Electrophoresis (2D-PAGE)** - This technique was used for protein separation under denaturing conditions. The principle of separation being that a combination of two orthogonal electrophoretic processes {molecular size and isoelectric focusing (IEF)} on a gel yields a greater degree of resolution than obtained by a single process (Issaq *et al.*, 2002).
- b. Following separation, the gels were stained to visualize separated protein spots using various dyes such as colloidal Coomassie brilliant blue G, silver stain and fluorescent stain SYPRO Ruby (Gygi *et al.*, 2000).
- c. **2D Fluorescence Difference gel electrophoresis (2D-DIGE)** - Samples were labelled with one of three spectrally different succinimidyl esters of the fluorescent cyanide (Cy) dyes: Cy2, Cy 3 or Cy 5 before the first dimension IEF separation. These fluorophores were similar in charge and molecular weight, however, they had distinct fluorescent properties which aided their discrimination when scanned using appropriate optical filters (Marouga *et al.*, 2005; Timms and Cramer, 2008; Minden, 2007). In a 2D-DIGE experiment, three different samples were covalently labelled, with a different Cy dye. One of the sample was a control which could either be an untreated sample or a mixture of all samples pooled together, thus, forming a control. The gel was then

scanned using a fluorescence imager at specific wavelengths for Cy2 (488 nm - control), Cy3 (532 nm – hypoxic) and Cy5 (633 nm – serum-deprived), and a gel image for each of the different samples was obtained. The images were then merged and analyzed using imaging software to check the differential regulation amongst the proteins (Minden, 2007).

- d. **DeCyder analysis** - this software that contained proprietary algorithms to perform co-detection of differently labelled samples within the same gel. DeCyder permitted automated detection, background subtraction, quantitation, normalization and inter-gel matching and spot picking. This resulted in high throughput, minimum introduction of human error and greatly increased the reproducibility. Figure 2.14 showed a typical workflow of 2D-DIGE using DeCyder software.
- e. **Mass spectrometry analysis** - A mass spectrometer such as Matrix-assisted laser desorption/ionization-time of flight (MALDI-TOF) is used primarily for protein identification. MALDI measured the mass of peptides derived from a trypsinized parent protein and generated a list of experimental peptide masses, often referred to as “mass fingerprints” (Vestling and Fenselau, 1994; Medzihradszky *et al.*, 2000). The TOF measurement was used as a procedure where instead of operating continuously, the pulsed laser took individual shots (Duncan and Hunsucker, 2008).
- f. **Database search** - The peptide masses derived from the mass spectrometer analysis correlated with peptide fingerprints of known proteins in a protein sequence database using search engines like Sequest, MASCOT, Comet, X!tandem, MOWSE , PeptIdent-2 and Profound (Pappin, 1993; Mann, 1993;

Yates, 1993; Colinge, 2003; Geer, 2004). These search engines provided a list of the best matching peptide sequences for an individual tandem mass spectrum. In addition, they provided scores that were related to the confidence level in the match. In this project MASCOT search engine developed by Matric science was used.

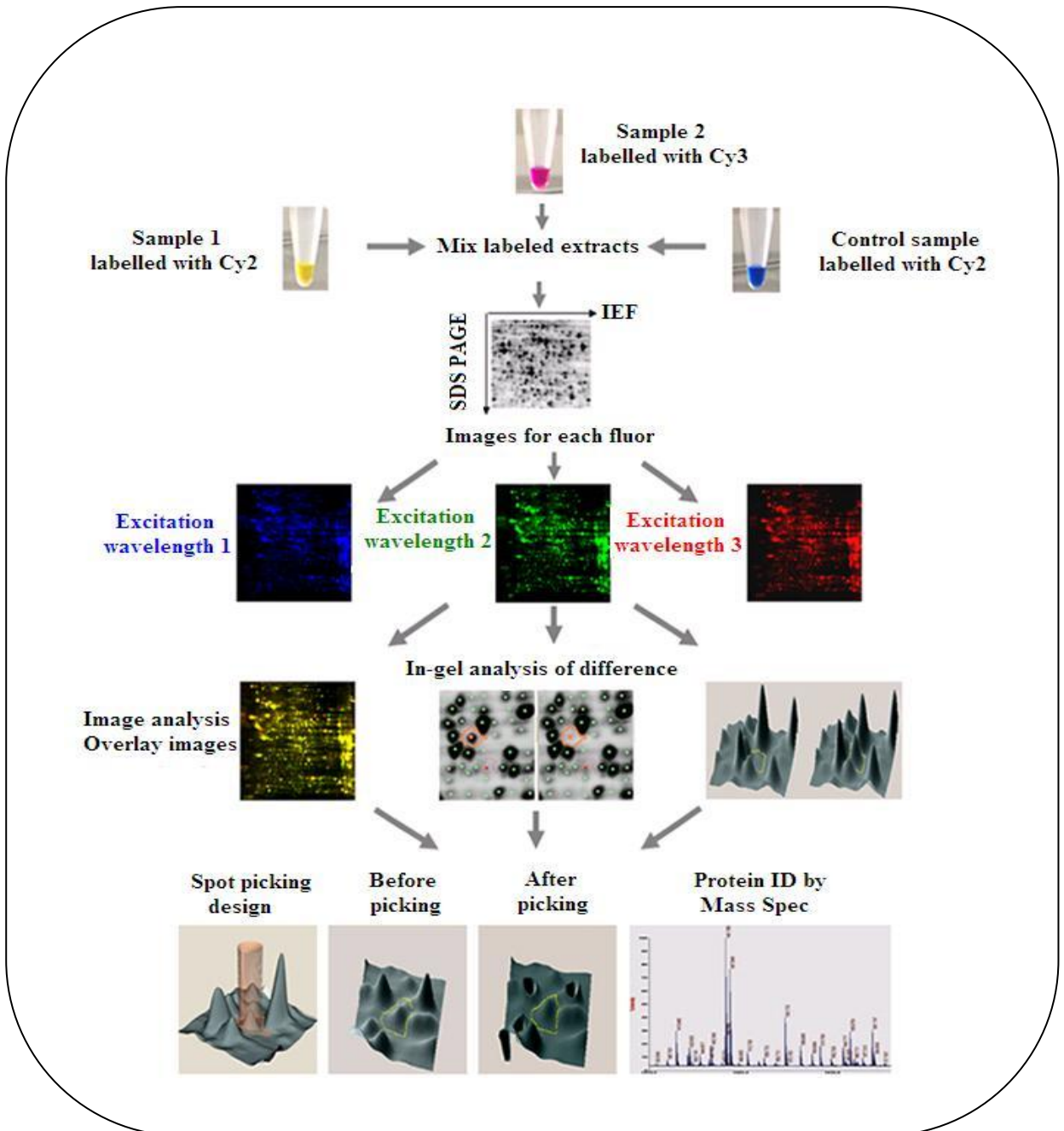


Figure 2.14: Workflow of 2D-DIGE via DeCyder (Adapted from Ettan DIGE User Manual, 2002)

2.11 Statistical Analysis

The experimental data such as PCR, Flowcytometry data, chemosensitivity and cell cycle analysis were analyzed by PASW package using One-Sample Student's T-test and paired T-test. A value of * $p < 0.05$ and ** $p < 0.001$ was considered as significant.

Chapter 3

Results

The current investigation primarily deals with changes in the protein expressions of the differentiated and undifferentiated brain tumour cells. The three proteins measured in this study included CD133, Oct4-A and BMP2. The initial experiments included gene expression analysis of the three candidate proteins by means of qRT-PCR. Flow cytometry has been extensively used to evaluate the expression of the candidate proteins. For analysis, the cells were labelled with the appropriate primary antibodies and detected using fluorochrome conjugated secondary antibodies. CD133 protein has been detected by an antibody conjugated to Cyanine 5 (Cy-5), Phyco erythrin (PE) used to detect Oct-A protein and Phyco erythrin Texas Red (PE-Texas Red) to detect the BMP2 protein in the glioma cell lines (Chapter 2; Table 2.4). For the cell viability assay and cell cycle analysis, the cells were labelled with PI followed by analysis using a flow cytometer.

The results of the present study are presented as follows:

- 3.1 Gene expressions of candidate proteins in the control glioma cell lines.
- 3.2 Protein expression profiles in the undifferentiated U87-MG cell line.
- 3.3 Chemosensitivity assay.
- 3.4 Cell cycle analysis.
- 3.5 Proteomics.

3.1 mRNA, cDNA and qRT-PCR

mRNA was extracted from the three glioma cell lines namely 1321-N1, Gos-3 and U87-MG. Spectrophotometry was carried out to evaluate the purity and quantification of the isolated mRNA. The mRNA absorbance was measured at wavelengths 260 nm and 280 nm respectively. Based on the spectrophotometric readings the quantity of mRNA required for cDNA conversion was calculated.

A total of 100 ng of mRNA was reverse-transcribed into c DNA followed by real time PCR which helped to measure the expression of the candidate proteins *CD133*, *Oct4-A*, *BMP2* and housekeeping gene *GAPDH*. Note that there was no significant difference observed in the expression of the candidate genes *GAPDH*, *CD133*, *Oct4-A* and *BMP2* in all the three glioma cell lines

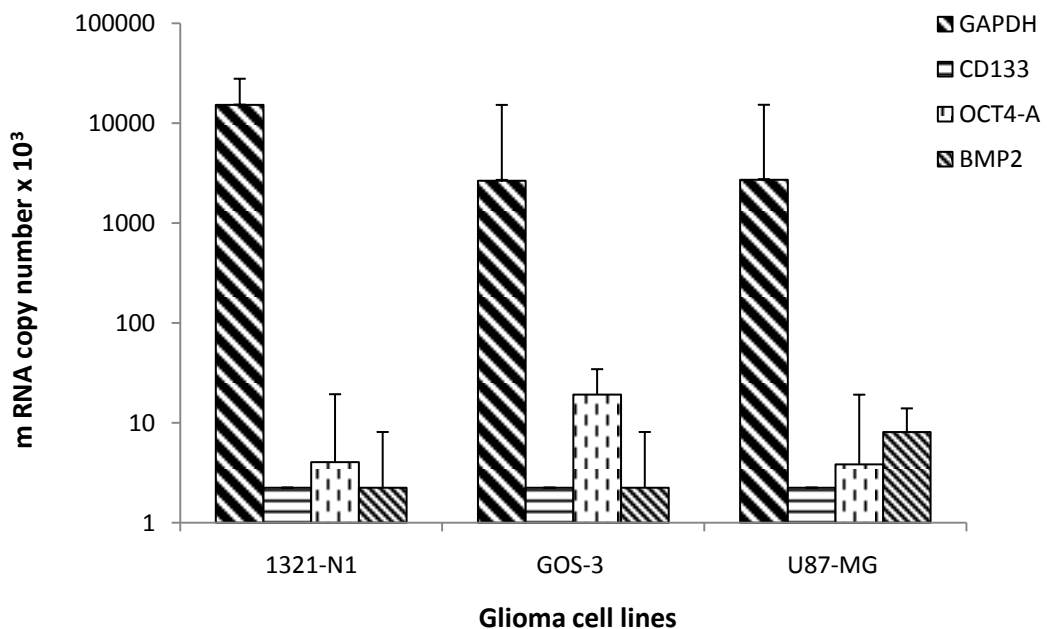


Figure 3.1: Gene expressions of *GAPDH*, *CD133*, *OCT4-A* and *BMP2* in all the three glioma cell lines. The respective mean values \pm standard error of the copy number of *GAPDH*, *CD133*, *OCT4-A* and *BMP2* genes expressed in each cell line were included (Data obtained from 3 independent experiments, $n = 3$). No statistically significant difference was observed in the expressions of the candidate genes when compared between the three different glioma cell lines.

Figure 3.1 showed the expression of the target candidate genes with respect to the expression of housekeeping gene *GAPDH* which was consistently expressed in all the three glioma cell lines compared to the other genes. The qRT-PCR results demonstrated that expression of *CD133* gene was not noticed whereas, *BMP2* expression was only observed more prominently in the U87-MG cells. The expression of the pluripotency gene *OCT4-A* was observed to be marginally elevated in the GOS-3 cell line as compared to 1321-N1 and U87-MG cells. Statistical analysis using Student's one sample T-test did not show any significance difference in the expression of the gene *CD133*, *OCT4-A* and *BMP2* in the glioma cell lines.

3.2 Expressions of candidate protein levels in the control glioma cell lines

Figure 3.2 displays the nuclear restricted Oct4-A protein in different grades of glioma cell lines. The results show that immunofluorescent staining was negative in the glioma cell lines stained with *CD133* and *BMP2* antibodies. Oct4-A protein was detected within the nucleus of all three glioma cell lines 1321-N1, GOS-3 and U87-MG.

3.2.1 Oct4-A protein levels in the control glioma cells using IF.

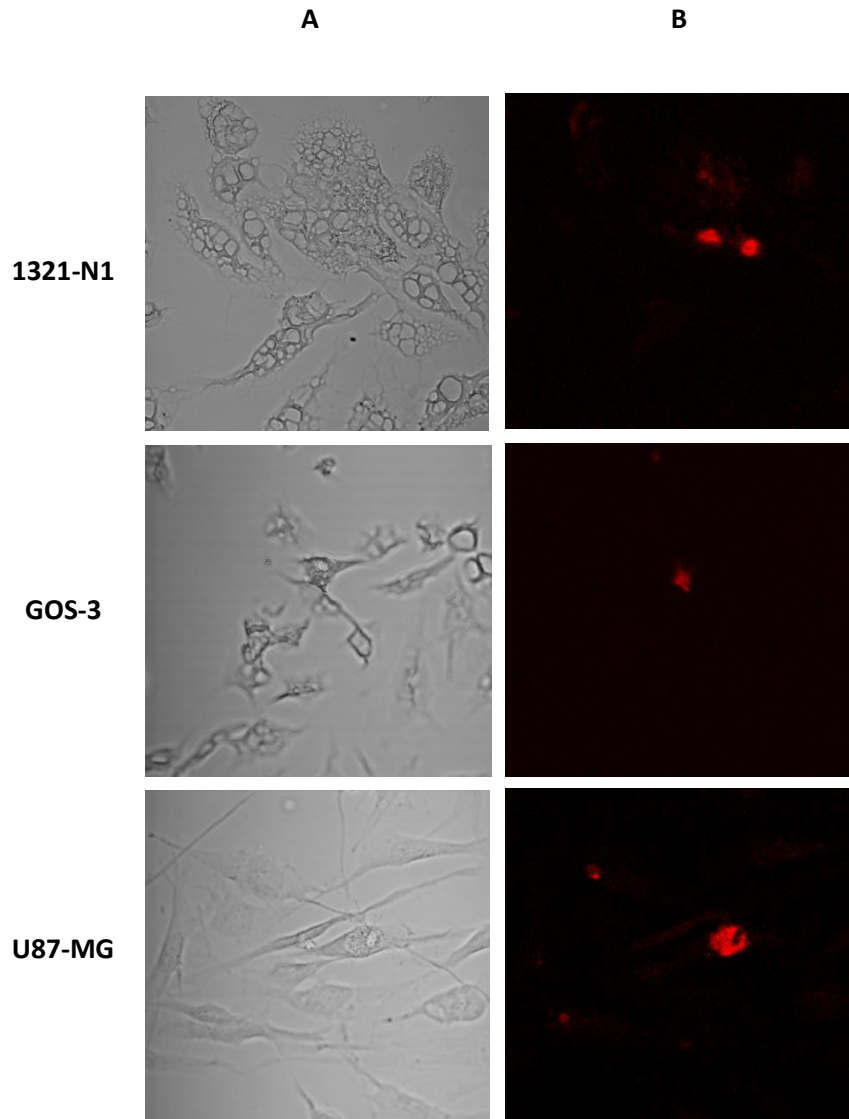


Figure 3.2: A typical example of nuclear located Oct4-A protein in different grades of glioma cell lines. A. phase contrast images of 1321-N1, GOS-3 and U87-MG cell lines. B. Oct4-A protein visualised in the nucleus 1321-N1, GOS-3 and U87-MG cell lines. Protein was identified using antibodies conjugated to PE. Images were observed using a confocal microscope (X 40 magnification, n=3).

3.2.2 Candidate protein expressions in the control cells (1321-N1, GOS-3 and U87-MG) using flow cytometry.

i) Expression profile of CD133, Oct4-A and BMP2 protein in glioma cell line 1321-N1.

Figure 3.3 illustrates the percentage of positive cells for the candidate proteins. The results show that no CD133 and BMP2 proteins were detected in the 1321-N1 cell line using flow cytometric analysis. However, a large number of cells were found to be positive for Oct4-A. Histograms A denotes the absence of CD133 protein in the 1321-N1 cell line, B indicates 75 % of the 1321-N1 cell positive with Oct4-A protein whereas, histogram C shows the absence of BMP2 protein in the glioma cell line 1321-N1.

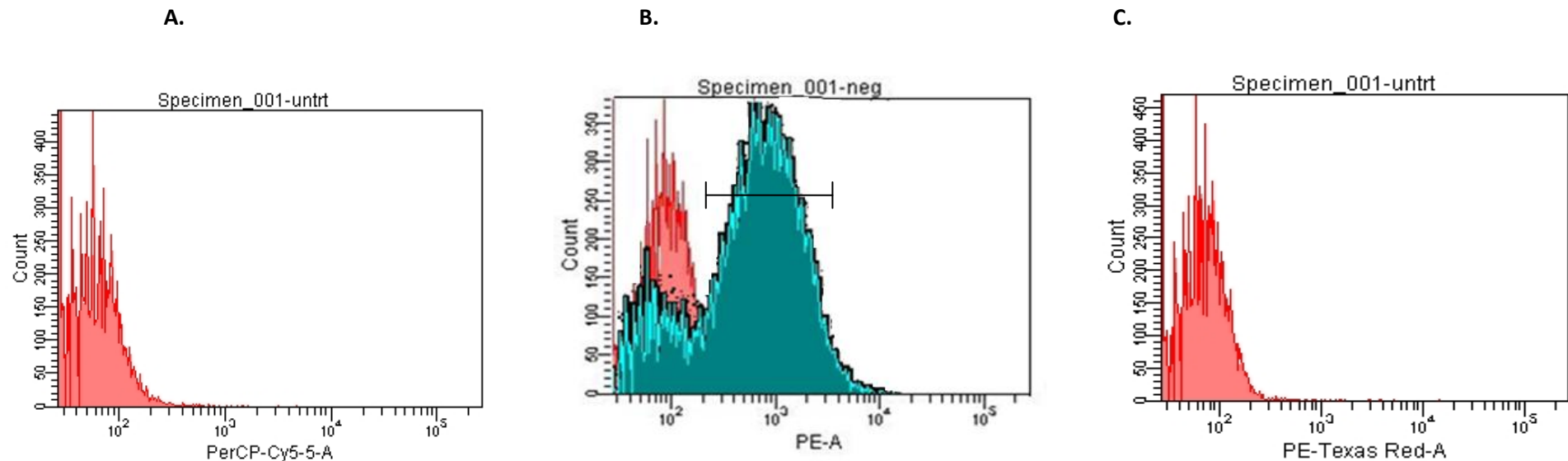


Figure 3.3: A typical example of expression profiles of CD133, Oct4-A and BMP2 protein in glioma cell line 1321-N1. A. Cells stained with Cy-5 shows no cells positive for CD133. B. Gated cell population (blue) represents the cells positive with the Oct4-A protein labelled with PE. C. Cells stained with PE-Texas Red display an absence of BMP2 protein. (Data obtained from three independent experiments, n = 3).

ii) Expression profile of CD133, Oct4-A and BMP2 protein in glioma cell line GOS-3.

Figure 3.4 shows the quantitative protein expression profile of CD133, Oct4-A and BMP2 in the GOS-3 cell line. The results indicated that no CD133 and BMP2 proteins were detected in the GOS-3 cells using flow cytometric analysis. The cell line was found to be positive for a substantial quantity of the Oct4-A protein. Absence of CD133 protein has been demonstrated by histogram A, histogram B represents approximately 84 % of the GOS-3 cells positive with Oct4-A protein and histogram C indicates an absence of the BMP2 protein within the GOS-3 cell line.

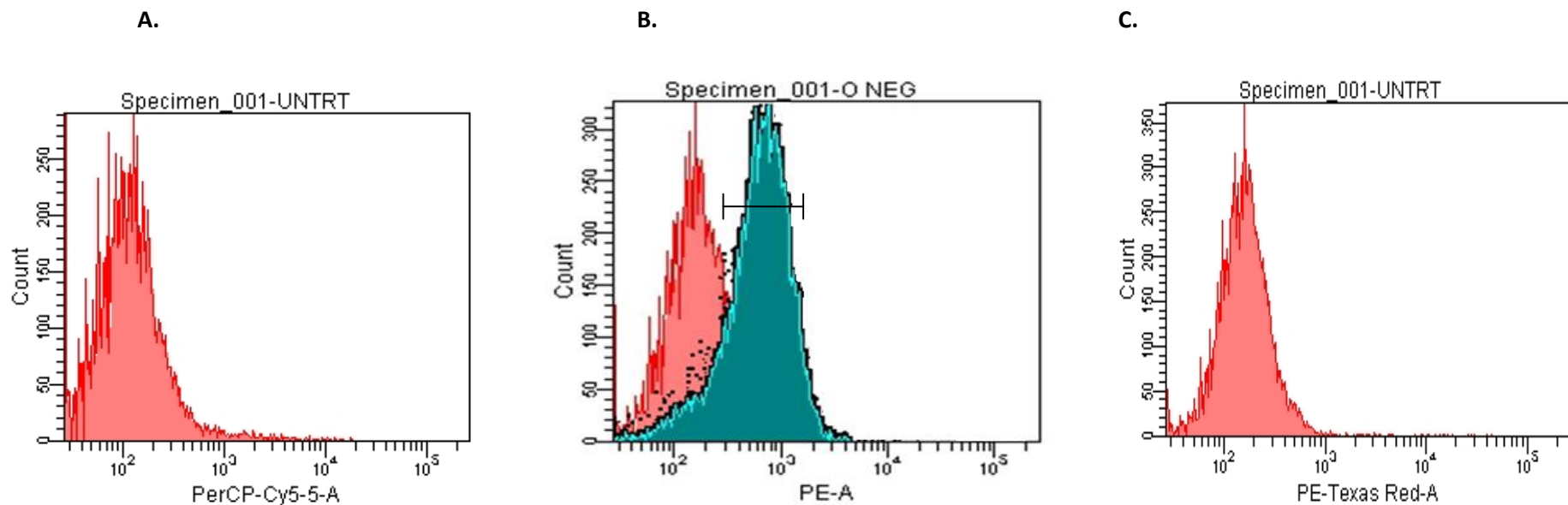


Figure 3.4: A typical quantitative protein expression profiles of CD133, Oct4-A and BMP2 proteins in the GOS-3 cell line. A. Cells stained with Cy-5 shows no cells positive for CD133. **B.** Gated cell population (blue) stained with PE, represents a positive percentage for Oct4-A protein compared with the negative. **C.** Cells stained with PE-Texas Red show an absence of BMP2 protein. (Data obtained from three independent experiments, n = 3)

iii) Expression profile of CD133, Oct4-A and BMP2 proteins in glioma cell line U87-MG.

Figure 3.5 presents the data indicating the percentage of cells positive for CD133, Oct4-A and BMP2 proteins. The results showed that the control U87-MG cell line when evaluated for the candidate protein expression showed the presence of only the Oct4-A protein. The expression of CD133 and BMP2 proteins were not observed. U87-MG cells did not indicate a presence of CD133 protein represented by histogram A, 72 % of the cells were positive for Oct4-A protein and no cells were detected positive for BMP2 protein demonstrated by histogram C.

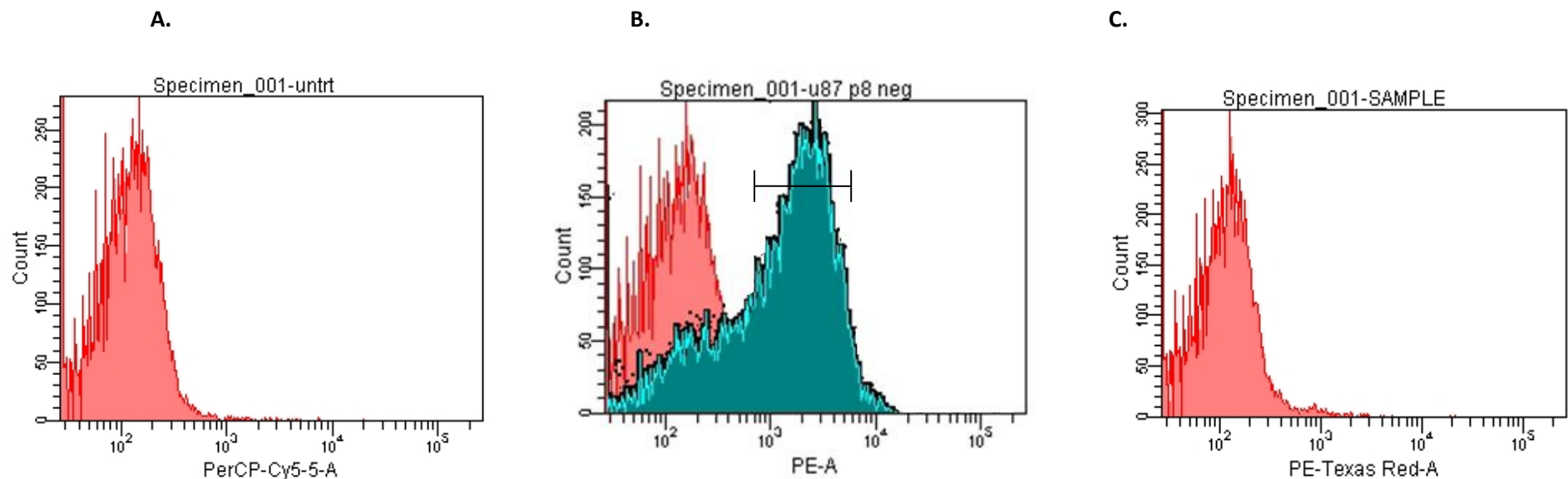


Figure 3.5: Percentage of cells positive for CD133, Oct4-A and BMP2 proteins in the U87-MG cells. A. No cells were detected positive for the CD133 protein analysed by staining with Cy-5. B. Approximately 73 % of the cells indicated a presence of Oct4-A protein detected by the PE stain. C. U87-MG cells displayed an absence of the BMP2 protein. (Data obtained from three independent experiments, n = 3).

Table 3.1 shows the quantitative expression of the candidate proteins in different grades of glioma cell lines. The control glioma cells were analysed using flow cytometry for the presence of proteins CD133, Oct4-A and BMP2. A total event of 10,000 cells was considered for each sample. All three cell lines showed a positive expression of Oct4-A protein and an absence of CD133 and BMP2 proteins. The highest expression of the Oct4-A protein was observed in the GOS-3 cells followed by a similar expression in the 1321-N1 and U87-MG cells. However, on carrying out Student's one sample T-test it was found that the number of GOS-3 and U87-MG cells expressing Oct4-A protein was statistically significant (*p < 0.05) as compared to the 1321-N1 cell lines.

Table 3.1: Quantitative expression of CD133, Oct4-A and BMP2 proteins in the control glioma cell lines 1321-N1, GOS-3 and U87-MG. Data values are mean \pm standard deviation (SD), n = 3. *p < 0.05 was considered statistically significant.

Note that the expression of the candidate proteins was compared between different grades of glioma cell lines. There was observed to be a significant increase ($p < 0.05$) in the expression of Oct4-A protein in the GOS-3 and U87-MG cell line compared to 1321-N1 cells. Expression of CD133 and BMP2 protein was not detected in all the three cell lines.

Cell lines	Proteins (Positive percentage {%))		
	CD133	OCT4-A	BMP2
1321-N1	0	75.6 \pm 11.8	0
GOS-3	0	84.3 \pm 6.2*	0
U87-MG	0	72.7 \pm 5*	0

3.3 Protein expression profiles in the undifferentiated U87-MG cell line.

Based on the literature search (chapter 1, section 1.7), the U87-MG cell line was found to display characteristics similar to CD133, a designated glioma stem cell marker. The following results are based on the protein profile evaluated in the U87-MG cells by shifting them from a differentiated state to an undifferentiated state. The conditions used for the experimental procedure involve two types of micro-environmental changes namely Hypoxia and Serum deprivation. The U87-MG cells grown under normal cell culture conditions and those subjected to micro-environmental changes were observed for morphological changes under the light microscope, followed by a qualitative study of the candidate protein expression using immunofluorescence.

3.3.1 i) Morphological changes observed in U87-MG cell line subjected to micro-environmental changes.

Figure 3.6 displays the morphological differences between the differentiated and undifferentiated U87-MG cells. The differentiated state was considered to be the normal cell culture conditions required for the growth of U87-MG cells. The results show that treatment with either hypoxia (100 % nitrogen) for 30 min or serum deprivation for a period of 3-7 days induced a state similar to undifferentiation within the cells.

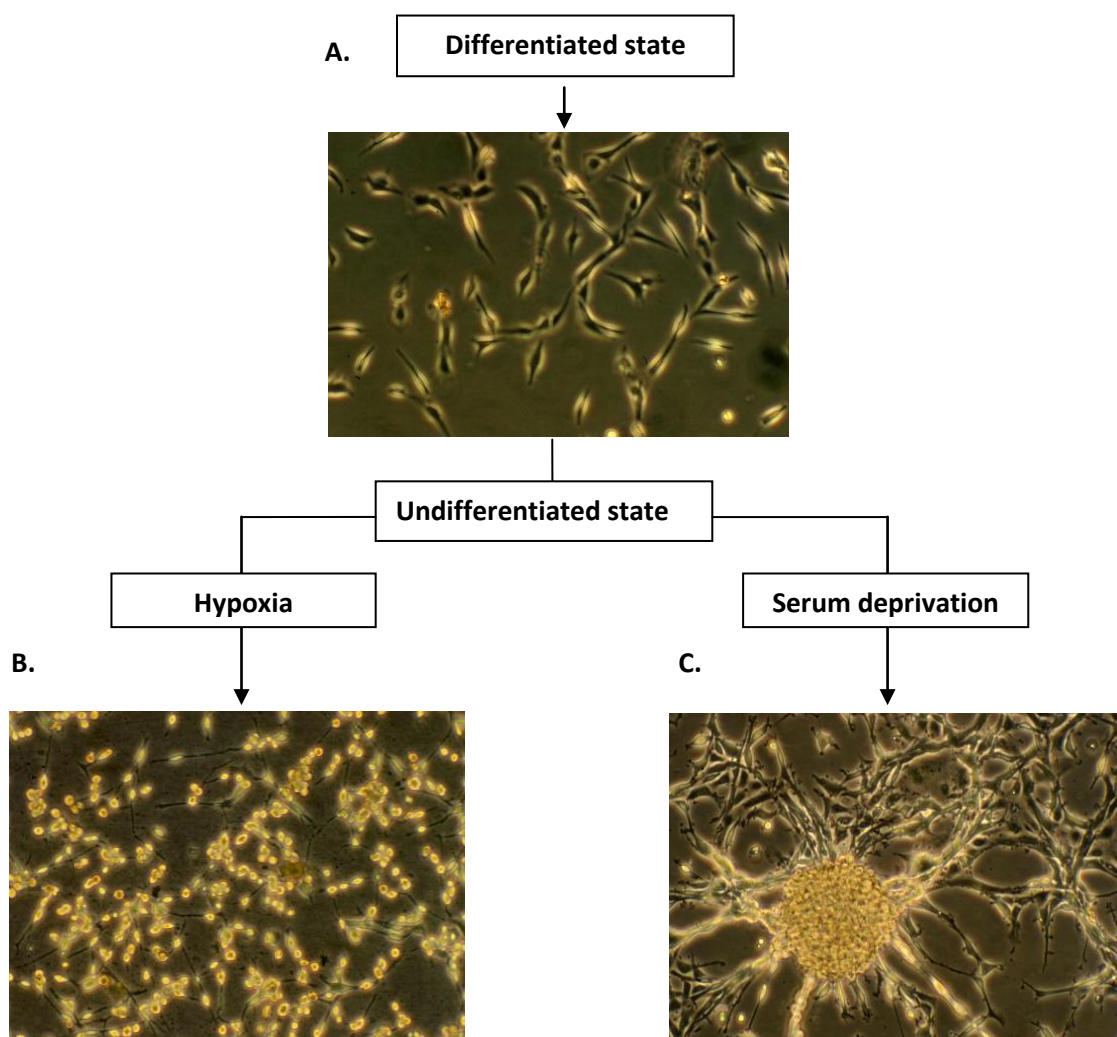


Figure 3.6: A typical example of morphological changes induced in U87-MG cells due to micro-environmental changes. A. Control U87-MG cell line grown in EMEM media. B. U87-MG cells observed after 24 hrs of treatment with hypoxia for 30 min. C. Serum-deprived U87-MG cell transformed into neurospheres when grown in RHB-A media supplemented with hEGF and bFGF to enhance their undifferentiation. Cells were observed under a light microscope (magnification x 20, n=3).

ii) Qualitative protein expressions by immunofluorescent staining.

Cells were studied for the presence of candidate proteins using immunofluorescence.

The results demonstrated in figure 3.7 display the peripheral localisation of the CD133 protein in the hypoxia-treated U87-MG cells. The presence of Oct4-A was visualised in the nucleus of the U87-MG cells in a state of differentiation and undifferentiation. The

BMP2 protein was not detected in the U87-MG cells.

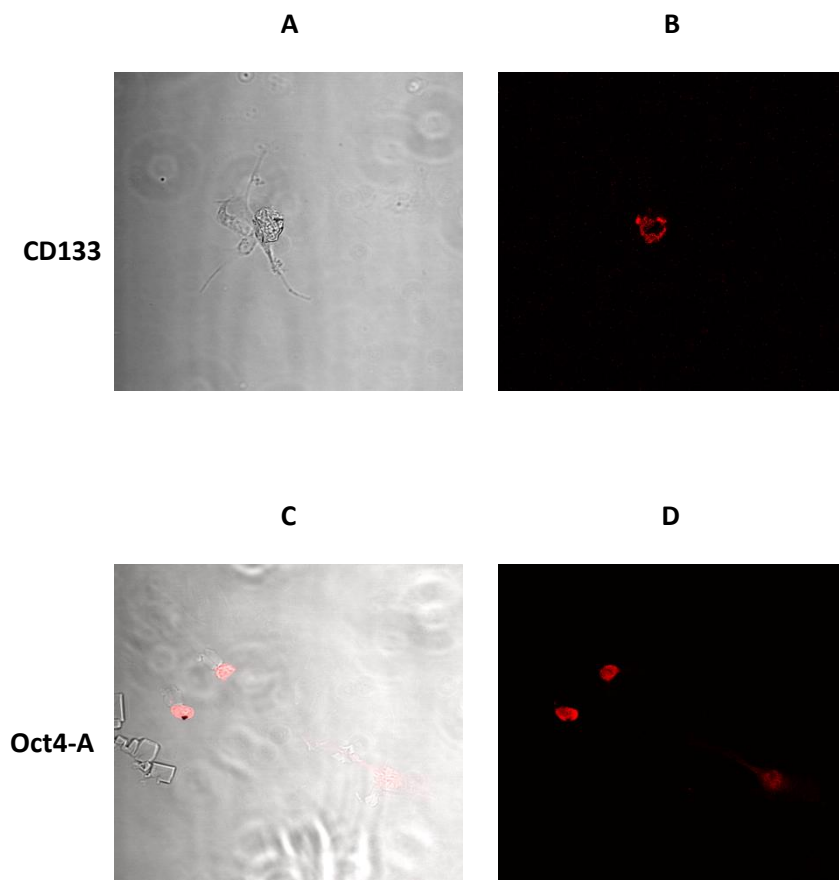


Figure 3.7: A typical example displaying CD133 and Oct4-A proteins in the hypoxic U87-MG cells. A, C. phase contrast images of hypoxia-treated U87-MG cell line. B. Cell surface localisation of CD133 on the hypoxic U87-MG cells detected by Cy-5 staining. D. Nuclear location of Oct4-A protein in the U87-MG cell line identified using antibody conjugated to PE. Image observed confocal microscope (X 40 magnification, n=3).

3.3.2 Analysis of CD133, Oct4-A and BMP2 protein expressions in the U87-MG control cells.

Figure 3.8 displays the measurement of the protein expression profiles in the control U87-MG cells. Under normal cell culture conditions (differentiated state) the U87-MG cells did not display presence of CD133 and BMP2 protein as demonstrated in histograms A and C, respectively. Approximately 65 % of U87-MG cells were noticed to be positive for Oct4-A protein as represented by histogram B.

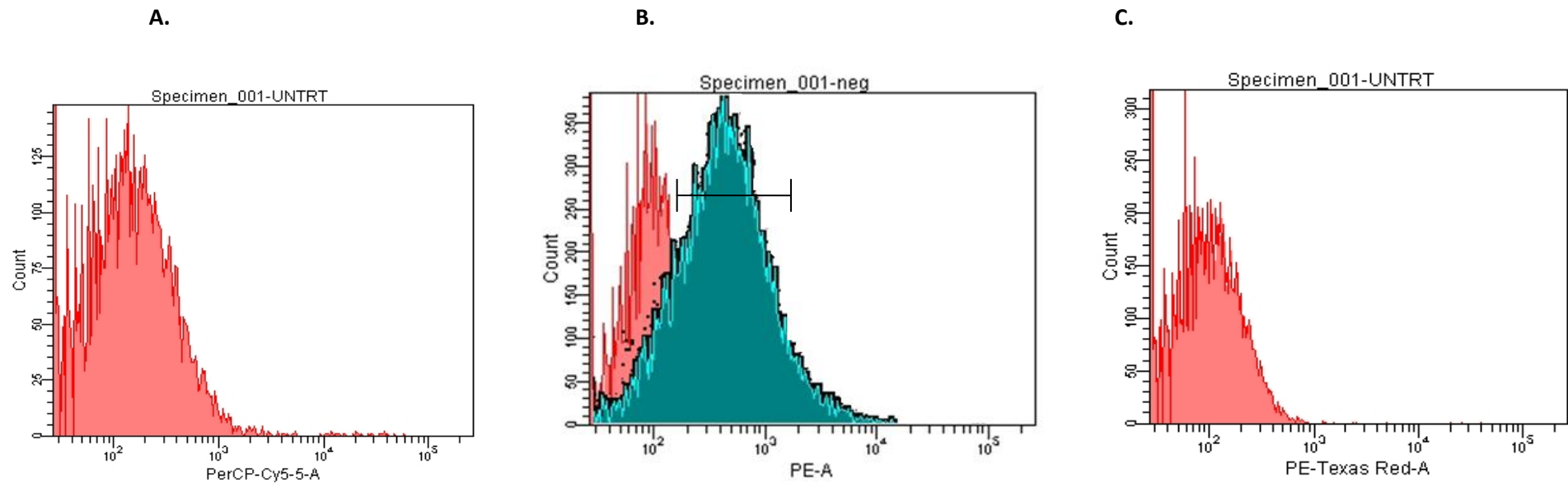


Figure 3.8: Percentage of cells positive for CD133, Oct4-A and BMP2 proteins in the U87-MG control cells. A. No cells were detected positive for CD133 protein, stained using Cy-5. B. Blue histogram indicate cells positive for the Oct4-A protein detected by staining the cells with PE. C. U87-MG cells display an absence of the BMP2 protein. (Data obtained from three independent experiments, n = 3).

3.3.3 Analysis of CD133, Oct4-A and BMP2 protein expressions in U87-MG cells treated 30 min with hypoxia (followed by 24 hr incubation).

Figure 3.9 displays the protein expression profiles in the hypoxia-treated U87-MG cells. Flow cytometric analysis of hypoxia-treated cells showed a basal expression (2 %) of CD133 protein in U87-MG cells as observed in histogram A. The expression of the Oct4-A protein was found to be significantly increased ($p < 0.05$, 84 %) as compared to the control U87-MG cells demonstrated in histogram B. Histogram C indicates that the presence of the BMP2 protein was not observed in the hypoxic U87-MG cell line.

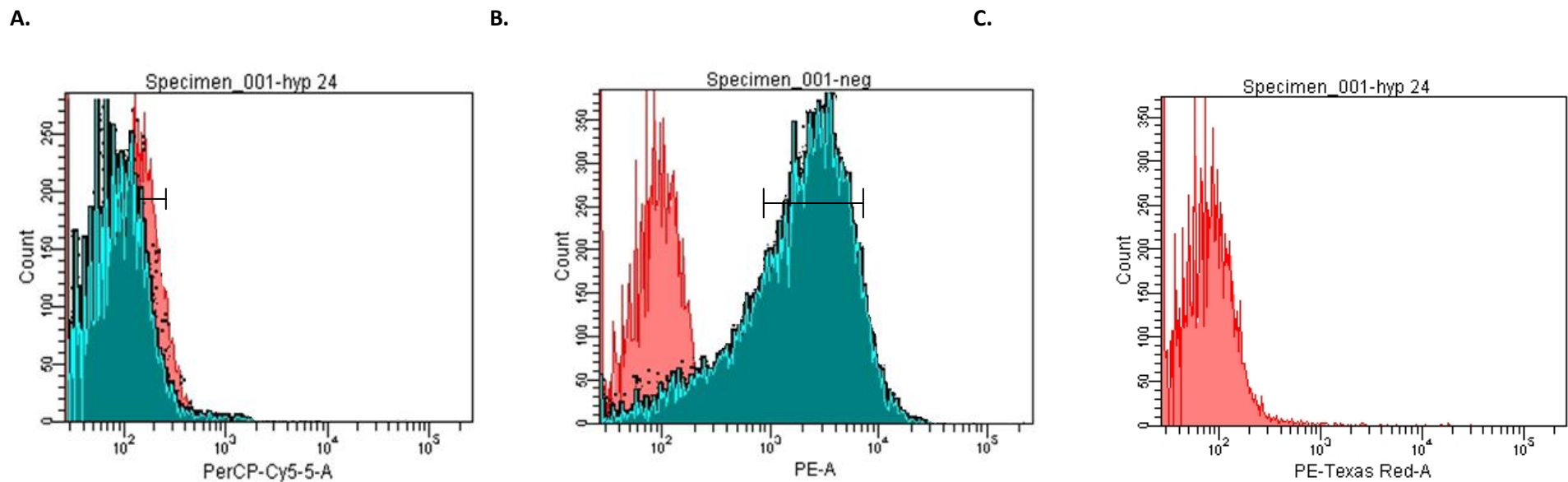


Figure 3.9: Analysis of the protein expression profile followed by hypoxia treatment. A. Red coloured histogram displays a minimal expression of the CD133 protein expression observed on account of hypoxia. Cells detected through fluorophore Cy-5. B. Cells positive for Oct4-A, stained with PE represented by the blue colour gated histogram. C. No cells observed to be positive for the presence of the BMP2 protein, perceived using PE-Texas Red. (Data obtained from three independent experiments, $n = 3$).

3.3.4 Analysis of CD133, Oct4-A and BMP2 protein expressions in U87-MG cells after serum deprivation (5 days).

Figure 3.10 displays the protein expression profiles in the serum-deprived U87-MG cells. Histogram A indicates that the serum-deprived U87-MG cells did not display presence of CD133 protein. Similarly, an absence of BMP2 was observed in the U87-MG cells under serum-deprived conditions, displayed in histogram C. Histogram B shows that serum deprivation for a period of 5 days led to a decrease in the expression of Oct4-A protein (43 %) as compared to the control U87-MG cell.

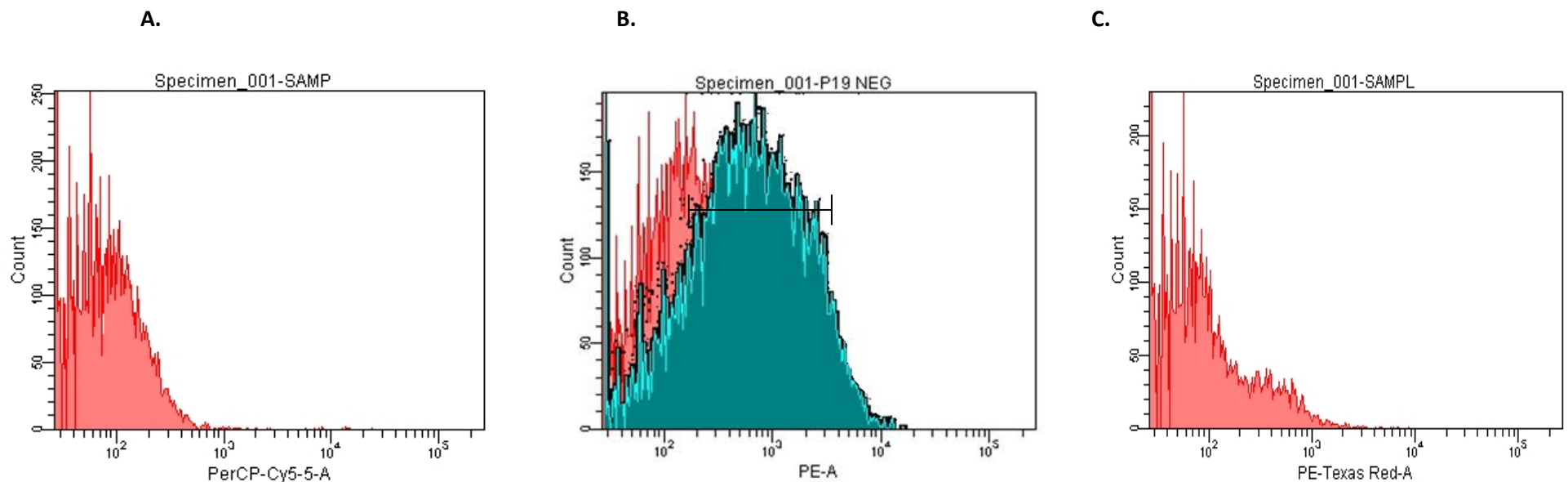


Figure 3.10: Proteins detected in serum-deprived U87-MG cells. A. Histogram indicates the absence of CD133 protein following serum deprivation. B. A marginal expression of the Oct4-A protein in the U87-MG cells detected using PE fluorochrome. C. No cells display positive for protein BMP2 stained with PE-Texas Red. (Data obtained from three independent experiments, n = 3).

U87-MG cells were studied for changes in the candidate protein expression when shifted from the differentiated state to an undifferentiated state. An attempt to shift the cells towards the undifferentiated state was carried out by induction of micro-environmental changes such as hypoxia and serum deprivation. Table 3.2 enlists the number of cells positive for the expression of candidate proteins as a result of micro-environmental changes.

Table 3.2: Quantitative expression of proteins CD133, Oct4-A and BMP2 in the U87-MG glioma cell line when subjected to treatment of hypoxia and serum deprivation compared to the untreated cells. Data values are mean \pm standard deviation (SD), n = 3. *p < 0.05 was considered statistically significant.

Note that there was no significant difference observed in the expression of CD133 and BMP2 proteins in the treated U87-MG cells. the expression was Oct4-A protein changed significantly in the hypoxic and serum-deprived cells as compared to the control U87-MG cells.

U87-MG	Proteins (Positive %)		
	CD133	OCT4-A	BMP2
Control	0	69.9 \pm 11.4	0
Hypoxia	2.3 \pm 2	84 \pm 7.7*	0
Serum deprivation	0	43.2 \pm 4.9*	0

While no expression of BMP2 was observed in the U87-MG cells, the percentage of Oct4-A protein expression increased by 14.1 % in the hypoxia-treated cells and decreased by 26.7 % in serum-deprived cells compared to the control. A basal expression of the CD133 protein (2.3 %) was observed only in the cells treated with hypoxia. Statistical analysis proved a significance difference in the expression of Oct4 protein (*p < 0.05) when the cells were subjected to hypoxia and serum deprivation as compared to the control U87-MG cells.

3.4 Chemosensitivity and Cell viability using Taxol and TMZ

Differentiated and undifferentiated U87-MG cells were tested for the toxicity of chemotherapeutic drugs Taxol and TMZ. The experiments were performed by treating the control, hypoxic and serum-deprived cells with the drugs and then subjected to the cell viability assay. The analysis was carried out by staining the cells with PI which displayed the number of dead cells using the flow cytometer. U87-MG cells grown under normal cell culture conditions served as a reference for the cell viability assay (PI staining) and U87-MG cells grown under normal cell culture conditions with the respective drug treatment served as a control for the chemosensitivity assay.

3.4.1 Cell viability assay for the U87-MG cells treated with Taxol.

Figure 3.11 demonstrates the cytotoxic effect of Taxol on the control, hypoxic and serum-deprived U87-MG cells. The flow cytometric histograms display the percentage of dead cells indicating the toxicity of Taxol on the U87-MG cells. Histogram A represents the untreated cells displaying maximum number of live cells when stained with PI. Control and hypoxic cells displayed an identical number of dead cells (9 %) when treated with taxol are demonstrated in histogram B and C, respectively. Histogram D displayed 36 % of dead cells when treated with taxol under serum-deprived conditions.

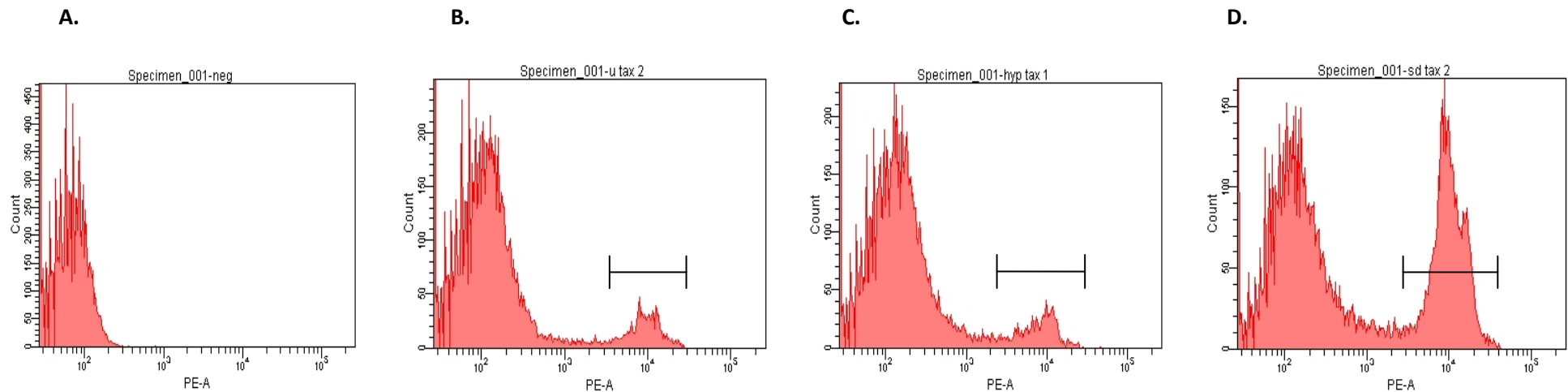


Figure 3.11: Cell viability assay results of U87-MG cells treated with Taxol. A. Control U87-MG cells without drug treatment. B. Control U87-MG cells treated with Taxol. C. Hypoxic U87-MG cells treated with Taxol. D. Serum starved U87-MG cells when treated with Taxol. Cells stained with PI indicate the percentage of dead cells (gated population) on treatment with Taxol. (Data obtained from three independent experiments, n = 3).

3.4.2 Cell viability assay for the U87-MG cells treated with TMZ.

Figure 3.12 displays the cytotoxic effect of the drug TMZ on the control, hypoxic and serum starved U87-MG cells. The results show the percentage of dead U87-MG cells when treated with TMZ. Histogram A represents maximum number of live U87-MG cells when treated with TMZ. Histogram B shows approximately 6 % of control dead U87-MG cells on TMZ treatment. Histogram C shows a minimum of 3 % cell dead percentage in the hypoxic U87-MG cells when treated with TMZ. Serum-deprived U87-MG cells displayed 26 % of dead cell when subjected to TMZ as displayed in histogram D.

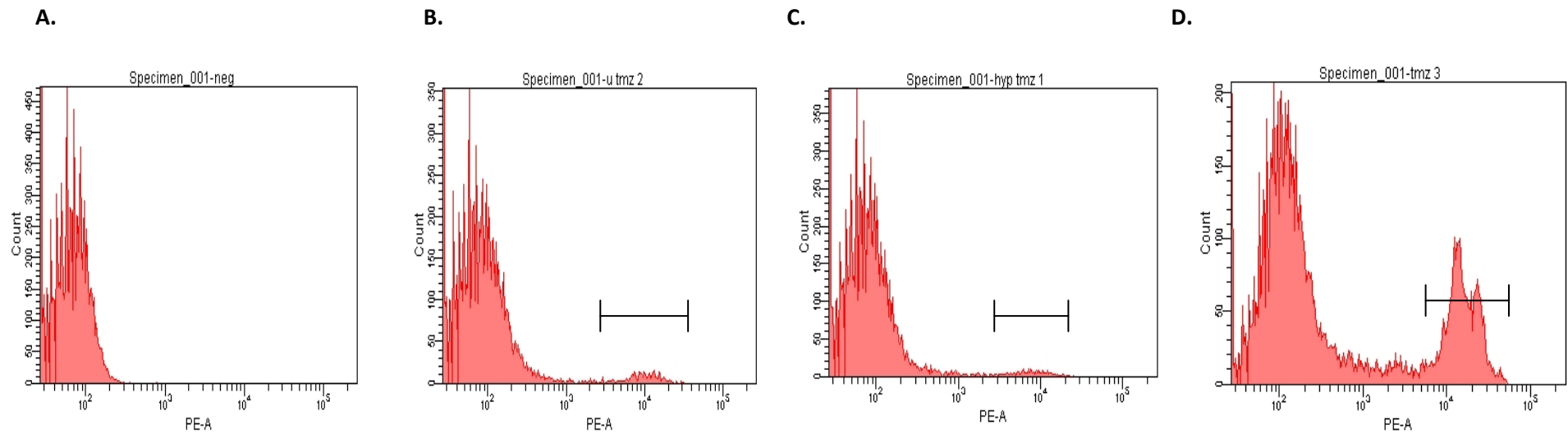


Figure 3.12: Percentage of dead U87-MG cells on treatment with TMZ following cell viability count. A. Control U87-MG cells without drug treatment. B. Control U87-MG cells treated with TMZ. C. Hypoxic U87-MG cells treated with TMZ. D. Serum starved U87-MG cells when treated with TMZ. Cells stained with PI indicate the percentage of dead cells (gated population) on treatment with TMZ. (Data obtained from three independent experiments, $n = 3$).

The results show that the percentage of dead cells with Taxol remained identical for both the control and hypoxic U87-MG cells. Serum-deprived cells responded to Taxol treatment with a 36.5 % cell death. Similar effects were observed when the cells were treated with TMZ; however, serum-deprived cells indicated a 26 % cell death. The cytotoxic effect of Taxol was found to be enhanced by 3 % in the control and hypoxic U87-MG cells, whereas the toxicity increased by approximately 10 % in serum-deprived U87-MG cells. Table 3.3 demonstrates the percentage of dead cells when subjected to individual treatment with Taxol and TMZ.

Table 3.3: Cell viability results of the chemosensitivity assay using flow cytometry. Data values are mean \pm standard deviation, n = 3. *p < 0.05 was considered to be statistically significant for serum-deprived U87-MG cells when as compared to the control.

Chemotherapeutic Drugs	Percentage of dead cells (%)		
	Control	Hypoxic	Serum-deprived
Taxol	9.3 \pm 1.5	9 \pm 2.7	36.5 \pm 6.2*
TMZ	5.9 \pm 4.7	3.1 \pm 0.8	26.1 \pm 0.4*

Statistical analysis using Student's paired T-test indicated that there were no significant difference observed in the action of the chemotherapeutic drugs Taxol and TMZ on the U87-MG cells. However, individual data set comparison showed that the serum-deprived U87-MG cells had a significant dead cell percentage (*p < 0.05) as compared to the control cells treated individually with Taxol and TMZ respectively.

3.5 Cell cycle analysis

In addition, the U87-MG cells were subjected to cell cycle analysis under conditions of differentiation (control) and undifferentiation (hypoxia and serum deprivation). Cell cycle analysis was further performed on the differentiated and undifferentiated U87-MG cells treated with either Taxol or TMZ. With the experiments carried out, the control, hypoxic and serum-deprived U87-MG cells were analysed with the treated samples to serve as a reference. The results have been demonstrated in the form of histograms in fig. 3.13, 3.14 and 3.15, respectively, indicating different cell cycles phases. The gated population in P2 represents the cells in G1 phase, the gated population P3 (depression) indicates the percentage of cells in the S phase and the P4 gated population denotes the G2 phase of the cells.

3.5.1 Cell cycle analysis of the control, hypoxic and serum-deprived U87-MG cells.

Figure 3.13 demonstrates the different cell cycle phases of the control, hypoxic and serum-deprived U87-MG cells. U87-MG cells were subjected to cell cycle analysis under differentiated (control) and undifferentiated (hypoxia and serum deprivation) states. Histogram A represents the cell cycle phase of the control U87-MG cells (G1 - 72.3 %, S - 12.3 % and G2 - 14.5 %). Histogram B denotes the cell cycle phase of hypoxia-treated U87-MG cells (G1 - 68.5 %, S - 15.1 % and G2 - 15.5 %) and histogram C represents the cell cycle phase of serum-deprived U87-MG cells (G1 - 64.8 %, S - 19 % and G2 - 20.4 %).

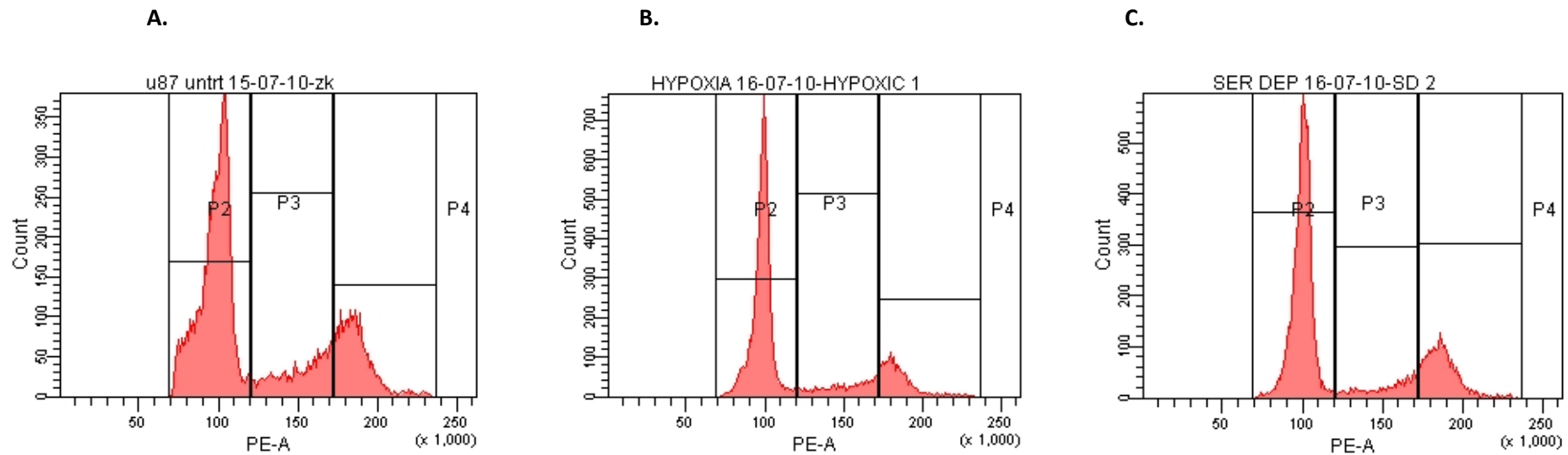


Figure 3.13: A typical example of cell cycle analysis of control, hypoxic and serum-deprived U87-MG cells. A. Control, B. Hypoxic and C. Serum-deprived. Gate P2 represents G1 phase, P3 (depression) indicates the S phase and P4 denotes the G2 phase of the cells. (Data obtained from three independent experiments, n = 3).

3.5.2 Cell cycle analysis of the U87-MG cells treated with Taxol.

Figure 3.14 represents cell cycle phases of U87-MG cells treated with Taxol. Control, hypoxic and serum-deprived U87-MG cells were subjected to treatment with Taxol and were further analysed for changes in their cell cycle phases. Histogram A represents the cell cycle phase of the control U87-MG cells treated with taxol (G1 – 33.7 %, S – 18.7 % and G2 – 46.4 %). Histogram B denotes the cell cycle phase of hypoxic U87-MG cells treated with taxol (G1 – 27.1 %, S – 14.6 % and G2 – 56.1 %) and histogram C represents the cell cycle phase of serum-deprived U87-MG cells (G1 – 58.6 %, S – 14.6 % and G2 – 25.8 %) when subjected to taxol treatment.

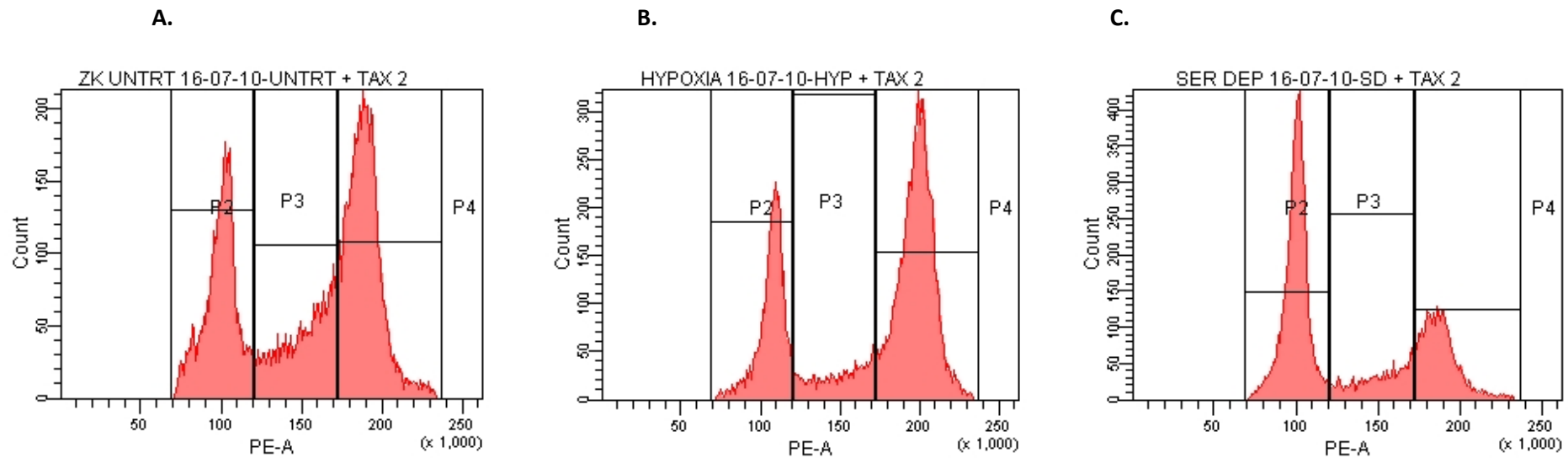


Figure 3.14: A typical example of cell cycle analysis of U87-MG cells treated with Taxol. A. Control cells treated with Taxol, B. Hypoxic cells treated with Taxol. C. Serum-deprived cells treated with Taxol. Gate P2 represents G1 phase, P3 (depression) indicates the S phase and P4 denotes the G2 phase of the cells. (Data obtained from three independent experiments, n = 3).

3.5.3 Cell cycle analysis of U87-MG cells treated with TMZ.

Figure 3.15 represents cell cycle phases of U87-MG cells treated with TMZ. Control, hypoxic and serum-deprived U87-MG cells were treated with TMZ and analysed for changes in their cell cycle phases. Histogram A represents the cell cycle phase of the control U87-MG cells treated with TMZ (G1 – 44.8 %, S – 23.7 % and G2 – 30.4 %). Histogram B denotes the cell cycle phase of hypoxic U87-MG cells treated with TMZ (G1 – 47.2 %, S – 28 % and G2 – 23.7 %) and histogram C represents the cell cycle phase of serum-deprived U87-MG cells (G1 – 59 %, S – 13.4 % and G2 – 25.9 %) when subjected to TMZ treatment.

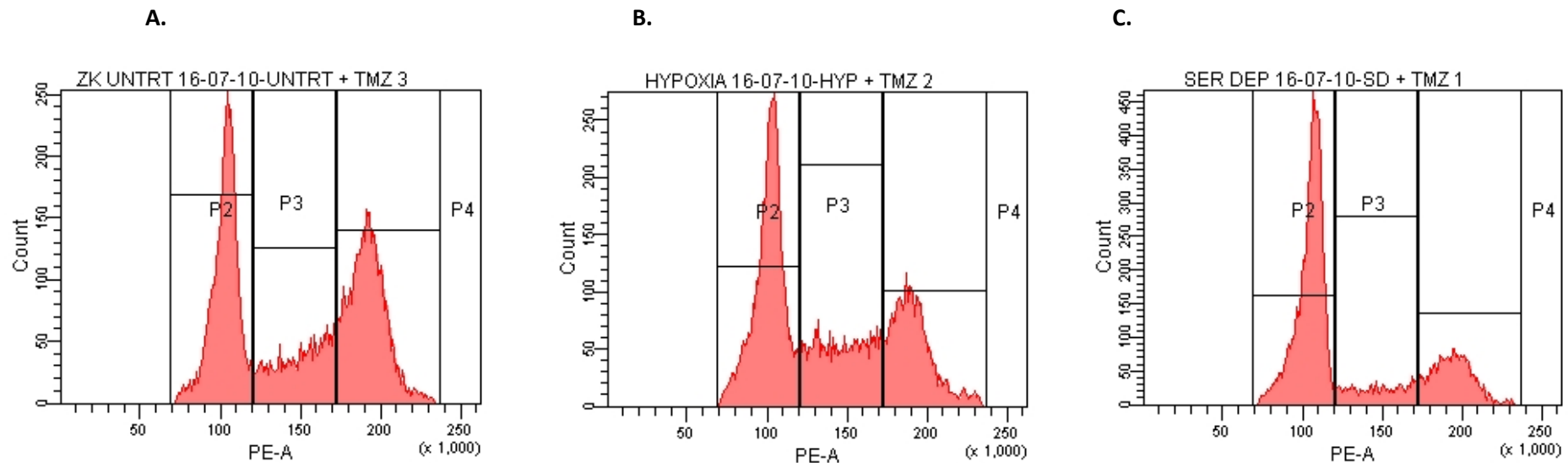


Figure 3.15: A typical example of cell cycle analysis of U87-MG cells treated with TMZ. A. Control, B. Hypoxic cells treated with TMZ and C. Serum-deprived cells treated with TMZ. Gate P2 represents G1 phase, P3 (depression) indicates the S phase and P4 denotes the G2 phase of the cells. (Data obtained from three independent experiments, n = 3).

The control, hypoxic and serum-deprived cells were subjected to cell cycle analysis before and after the treatment with Taxol and TMZ. Flow cytometric data displayed a differential percentage of cells residing in the G1, S and G2 phase, respectively. Table 3.4 shows the percentage of the U87-MG cells in various phases of cell cycle on account of the drug treatment and their state of differentiation.

Table 3.4: Percentages of differentiated and undifferentiated U87-MG cells in diverse phases of cell cycle and on treatment with cytotoxic drugs Taxol and TMZ as compared to the control. Data values are mean \pm standard deviation, n = 3. *p < 0.05 and **p < 0.001 were considered statistically significant for phases G1, S and G2.

U87-MG cells	Cell Cycle Phases (Percentage {%} of cells in the phase)		
	G1	S	G2
Control	72.3 \pm 0.3	12.3 \pm 1.6	14.5 \pm 1.6
Hypoxic	68.5 \pm 1.4*	15.1 \pm 2.6	15.5 \pm 2.2
Serum-deprived	64.8 \pm 3.1*	19.0 \pm 6.6**	20.4 \pm 3*
Control (Taxol)	33.7 \pm 2.3	18.7 \pm 2.9	46.4 \pm 1.6
Hypoxic (Taxol)	27.1 \pm 0.9*	14.6 \pm 5.3	56.1 \pm 5.8
Serum-deprived (Taxol)	58.6 \pm 3.7*	14.6 \pm 0.2*	25.8 \pm 4.1*
Control (TMZ)	44.8 \pm 5.9	23.7 \pm 4.1	30.4 \pm 10.2
Hypoxic (TMZ)	47.2 \pm 2.4	28 \pm 2.8	23.7 \pm 5.2
Serum-deprived (TMZ)	59 \pm 5.5*	13.4 \pm 1.8**	25.9 \pm 3.4

Figure 3.16 shows a graphical view of the control, hypoxic and serum-deprived cell proportion residing in different cell cycle phases. The results indicate that the cell cycle analysis of the control, hypoxic and serum-deprived cells did not show any significant changes in the cell cycle phases.

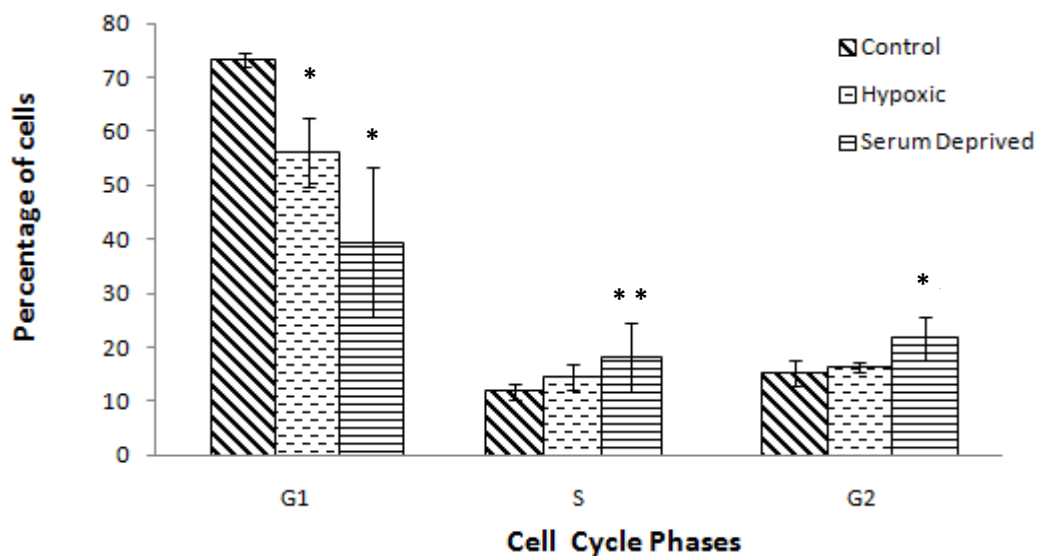


Figure 3.16: A typical example of cell cycle phases of control, hypoxic and serum-deprived U87-MG cells. G1 and G2 represent the gap phase and S denotes the phases of DNA synthesis. (Data values are mean \pm standard deviation (SD) from three independent experiments, $n = 3$). * $p < 0.05$ and ** $p < 0.001$ were considered statistically significant as compared to the control.

Student's paired T-test was performed for the different cell cycle phases of the control, hypoxic and serum-deprived U87-MG cells. It was observed that the G1 phases of the hypoxic and serum-deprived U87-MG cells was significantly different (* $p < 0.05$) as compared to the control cells. The S phase of the hypoxic cells was similar to the control, however, the serum-deprived cells showed a significant number of cells (** $p < 0.001$) residing in the respective phase. * $p < 0.05$ in the G2 phases of the serum-deprived cells indicated a statistical significance as compared to the control U87-MG cells.

Figure 3.17 represents the different cell cycle phases of the control, hypoxic and serum-deprived U87-MG cells treated with Taxol. The results display a similarity in the G1, S and G2 phases of the control and hypoxic U87-MG cells. The S phase of the serum -deprived cells was similar to that of the control and hypoxic U87-MG cells. An increase the G1 phase was observed in the serum-deprived cells (58.6 %), whereas, the percent of cells dropped significantly in the G2 phase (25.8 %).

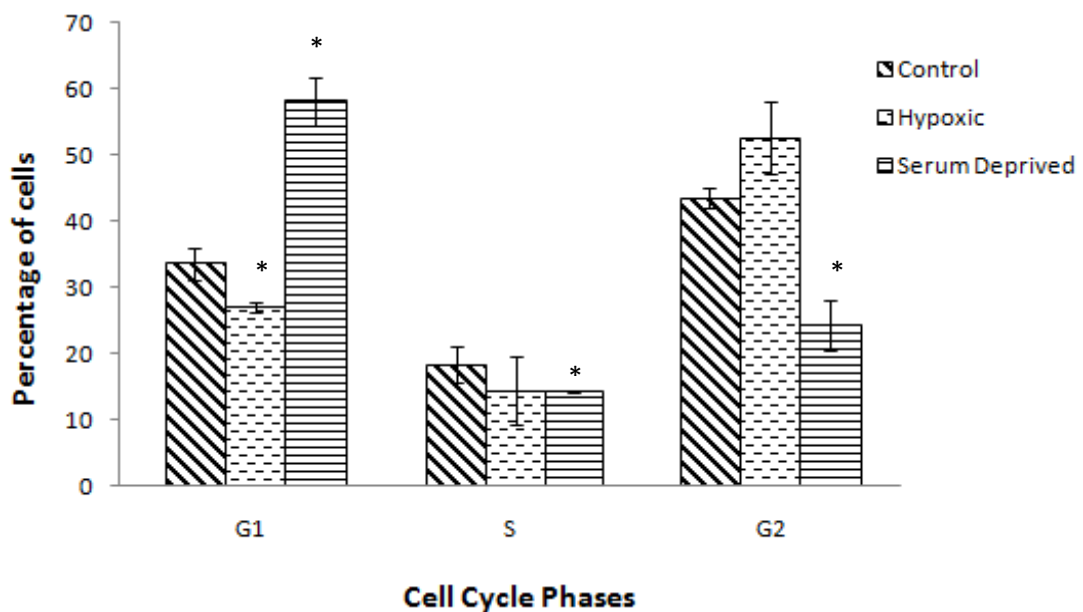


Figure 3.17: A typical example of cell cycle phases of control, hypoxic and serum-deprived U87-MG cells treated with Taxol. G1 and G2 represent the gap phase and S denotes the phases of DNA synthesis. (Data values are mean \pm standard deviation (SD) from three independent experiments, n = 3). *p < 0.05 was considered statistically significant for the hypoxic and serum-deprived cells as compared to the control U87-MG cell.

A significant difference (* p < 0.05) was observed in the G1 phase of the hypoxic and serum-deprived U87-MG cells on Taxol treatment. A similar difference (* p < 0.05) was observed in the S and G2 phases of the serum-deprived cells when subjected to taxol treatment. However, no changes were observed in the S and G2 phases of the hypoxic U87-MG cells as compared to the control when treated with Taxol.

Figure 3.18 demonstrates the percentage of TMZ-treated control, hypoxic and serum-deprived U87-MG cells in various cell cycle phases. The results show that the cell cycle phases of serum-deprived U87-MG cells treated with TMZ indicated a high number of cells residing in the G1 phase (59 %) as compared to the control and the hypoxic cells. A decrease in the number of serum-deprived U87-MG cells was found in the S phase of the cell cycle. No difference was observed in the cell cycle phases of the control and hypoxic U87-MG cells.

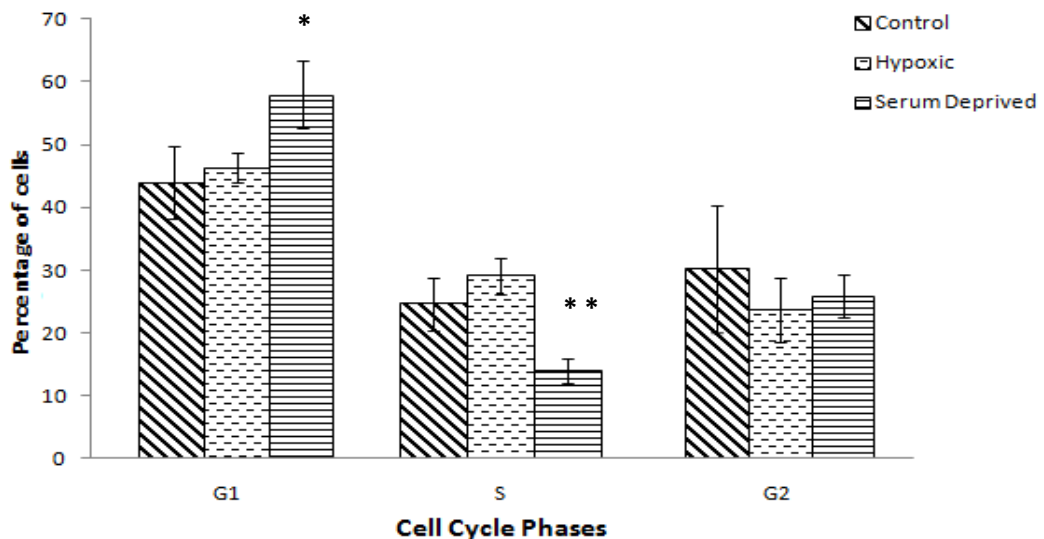


Figure 3.18: A typical example of cell cycle phases of control, hypoxic and serum-deprived U87-MG cells treated with TMZ. G1 and G2 represent the gap phase and S denotes the phases of DNA synthesis. (Data values are mean \pm standard deviation (SD) from three independent experiments, n = 3). *p < 0.05 and **p < 0.001 were considered statistically significant.

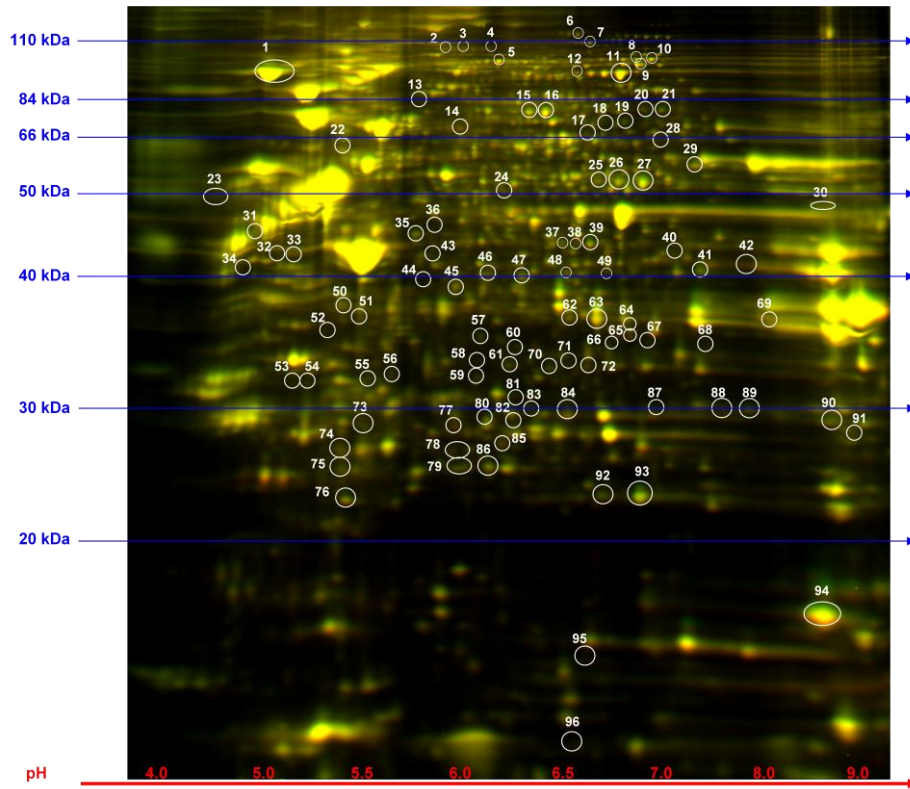
The results from Student's paired T-test showed that the G1 phase of the serum-deprived TMZ treated cells was significantly higher (* p < 0.05) as compared to the control TMZ treated cells. A higher significant difference (** p < 0.001) was observed in the S phase of the serum-deprived cells as compared to the control cells when subjected to TMZ. No statistical difference was observed in the G2 phases of the control, hypoxic and serum-deprived U87-MG cells on TMZ treatment.

3.6 Proteomic analysis

Proteomic analysis enabled monitoring the changes in the protein expression profile of the differentiated and undifferentiated U87-MG cells. The proteomic analysis was carried out by Applied Biomics (Hayward, CA). A complete study was carried out on the U87-MG (control/differentiated) cells, U87-MG hypoxic (undifferentiated) and U87-MG serum-deprived (undifferentiated) cells using the 2D-DIGE and MALDI-TOF. A total of 96 spots of proteins were identified by the 2D-DIGE analysis using the cut-off of fold ≥ 2 . The spots were selected using the De-Cyber analysis software and confirmed visually. The proteins identified can be observed as circled spots with an estimated grid of molecular weight (MW) and isoelectric points (pI) (Fig. 3.19).

Mass spectrophotometric analysis was performed using MALDI-TOF. For protein identification a total of 44 spots were chosen. Protein identification was based on peptide fingerprint mass mapping (using MS data) and peptide fragmentation mapping (using MS/MS data). MASCOT search engine was used to identify proteins from primary sequence databases, 37 of 44 spots were confidently identified as human proteins. "Protein ID" numbers correspond to the assigned numbers on the overlay gel images and are summarized in Table 3.5. Protein analysis identified more than one spots as the same protein. The reason could be attributed to the presence of different isoforms of the same protein due to post-translational modifications such as phosphorylation, methylation, degradation or cross-linkage within the proteins that alter the protein's MW and/or pI, causing the spots to shift. Publically available database Human protein research database (HPRD) was used to analyse the biological significance of the 44 identified proteins summarized in Table 3.6.

A. U87-MG Control and U87-MG-Hypoxic.



B. U87-MG Control and U87-MG-Serum-deprived.

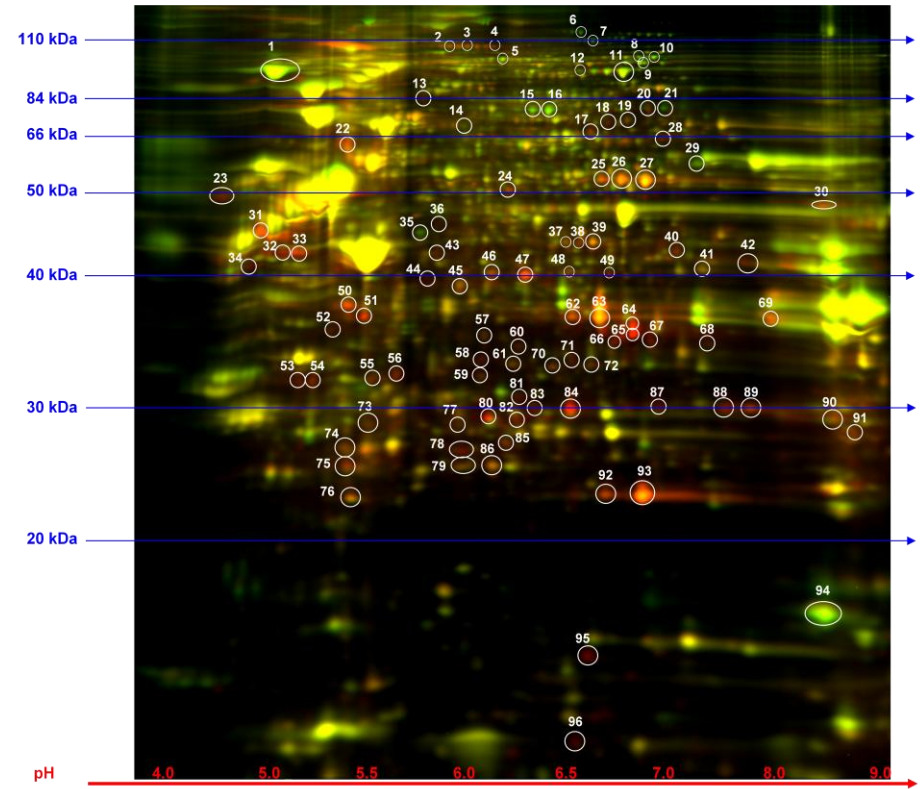


Figure 3.19: Representation of a typical 2D-DIGE protein expression profiles. A. U87-MG hypoxia-treated gel sample superimposed on the control. B. U87-MG serum-deprived gel sample overlaid on the control. Proteins observed as circled spots with an estimated grid of MW and pI. The red and green spots represent the up and down-regulated proteins, respectively. (Gel image demonstrates a single experiment performed on the U87-MG cells, n=1 due to cost).

Figure 3.19 represents the gel images obtained after performing 2D-DIGE experiment for protein expression profile. Figure 3.18(A) displays the image of U87-MG hypoxia-treated gel sample superimposed on the control and figure 3.18 (B) represents the U87-MG serum-deprived gel sample overlaid on the control. The scale overlaid on the gel images represents the protein pI and MW grid which aids in the identification of the proteins. The circled numbered spots represent a total of 96 spots suggested for protein identification by the Decyder analysis software. Red spots visualised on the gel images denoted the upregulated protein and the green dots indicate the proteins that has been down-regulated on account of hypoxia and serum deprivation, respectively.

3.6.1 Differential protein expression profiles obtained using Mass spectrophotometric analysis

A total number of 44 identified peptides were searched against the Mascot database. Proteins were categorized as up-regulated, down-regulated or differentially regulated based on induction of hypoxic and serum deprivation (micro-environmental changes /undifferentiated state) with reference to the U87-MG cells (control/ differentiated state) grown under normal cell culture conditions. The results shown in table 3.5 summarises the protein names, NCBI GI numbers, protein molecular weights, ion charges, peptide counts, protein scores, protein scores C. I. %, total ion scores and total ion C.I. % scores as generated by MASCOT. The fold change values of the individual protein expressions were measured as U87-MG-control v/s the U87-MG-hypoxic and U87-MG-control v/s the U87-MG-serum-deprived and are enlisted in the last two column of Table 3.5. The molecular class, molecular function and biological function of the proteins identified by mass spectrophotometry using Human Protein Research Database have been enlisted in Table 3.6.

Table 3.5: Differential protein expression profiles. (Data obtained from a single mass spectrophotometric analysis, n=1).

The selected peptides with ≥ 2 fold change were searched against MASCOT database for the corresponding proteins. Proteins were categorized according to their change in expression post treatment with hypoxia and serum deprivation U87-MG glioma cell line.

Top Ranked Protein Names	Accession No.	Protein MW	Protein PI	Peptide Counts	Protein Scores	Protein Scores C. I. %	Total Ion Scores	Total Ions C. I. %	U87-MG hypoxic / U87-MG	U87-MG Serum-deprived/ U87-MG
A. Up-regulated proteins										
Alpha 2 type VI collagen isoform 2C2 precursor	gi 115527062	108511.9	5.9	20	423	100	296	100	1.3	3.3
Heat shock protein 90kDa beta (Grp94)	gi 119618129	40939.0	4.4	9	384	100	327	100	1.0	4.1
Laminin A/C isoform 2	gi 5031875	65095.6	6.4	17	310	100	205	100	1.2	4.7
Laminin-binding protein	gi 34234	31773.9	4.8	10	582	100	504	100	2.0	11.8
Unnamed protein product	gi 158257566	45310.3	5.5	11	200	100	120	100	1.2	4.9
Vimentin	gi 5030431	41537.0	4.8	22	299	100	108	100	1.2	4.2
CLN2	gi 37182127	60420.1	5.9	5	228	100	210	100	1.0	3.5
Fructose-biphosphate aldolase A	gi 4557305	39395.3	8.3	17	519	100	348	100	1.8	3.9
Selenophosphate synthetase 1	gi 24797148	42882.7	5.6	11	203	100	125	100	1.3	3.4
Alpha-tubulin	gi 37492	50125.6	5.0	10	364	100	303	100	1.6	3.7
PGK1	gi 48145549	44574.1	8.3	16	532	100	368	100	1.0	7.5
Poly(rC) binding protein 3 isoform 1	gi 194306631	39440.3	8.2	2	238	100	233	100	1.4	3.6
Protein phosphatase 2, beta isoform	gi 4758952	35552.3	5.2	12	226	100	138	100	1.1	5.5
Coenzyme Q9 homolog	gi 40789233	35486.6	5.6	8	120	100	64	100	1.0	3.1
Capping protein (actin filament) muscle Z-line, beta, Chain A, Fidarestat bound to human aldose reductase	gi 119615295	29998.2	5.9	11	219	100	138	100	1.0	3.0
Glyceraldehyde-3-phosphate dehydrogenase	gi 13096112	35699.4	6.6	13	515	100	331	100	1.1	3.8
Uracil DNA glycosylase	gi 7669492	36030.4	8.6	9	337	100	244	100	1.2	12.3
	gi 35053	35470.1	8.2	12	348	100	245	100	1.2	6.5

Table 3.5 (Contd).

Top Ranked Protein Names	Accession No.	Proteins MW	Proteins PI	Peptide Counts	Protein Scores	Protein Scores C. I. %	Total Ion Scores	Total Ion C. I. %	U87-MG hypoxic / U87-MG	U87-MG Serum-deprived/ U87-MG
A. Up-regulated proteins										
Eukaryotic translation initiation factor 4E isoform 2	gi 194578909	28759.6	6.0	5	116	100	96	100	2.6	2.2
Triosephosphate isomerase 1	gi 17389815	26624.7	6.5	11	308	100	219	100	1.2	4.9
Phosphoglycerate mutase 1 (brain)	gi 4505753	28785.8	6.7	9	176	100	113	100	1.1	3.1
Phosphoglycerate mutase 1 (brain)	gi 38566176	28801.9	6.7	12	305	100	183	100	1.2	6.5
Similar to Chain , Heat-Shock Cognate 70kd Protein	gi 51095055	25582.3	7.0	3	128	100	116	100	1.1	4.3
H3L-like histone	gi 37654352	12096.7	10.6	3	85	100	70	100	1.4	7.3
B. Down-regulated proteins										
Heat shock protein 90kDa beta, member 1	gi 4507677	92411.3	4.8	22	826	100	614	100	-1.2	-2.7
ATP citrate lyase isoform 1	gi 38569421	120761.9	7.0	29	481	100	276	100	-1.0	-2.4
Moesin	gi 4505257	67777.8	6.1	31	700	100	428	100	-1.0	-2.9
Glutamine-fructose-6-phosphate transaminase 2	gi 12652545	76867.7	7.0	20	205	100	96	100	-1.3	-2.6
Phenylalanyl-tRNA synthetase, alpha subunit	gi 4758340	57527.5	7.3	12	181	100	113	100	-1.0	-2.8
C. Differentially regulated proteins										
Transformation upregulated nuclear protein	gi 460789	51040.4	5.1	10	164	100	98	100	-1.2	3.9
Nicotinamide phosphoribosyltransferase precursor	gi 5031977	55486.6	6.7	20	410	100	258	100	-1.2	3.4
Vimentin variant 3	gi 167887751	49623.1	5.2	28	876	100	581	100	-1.0	6.3
Casein kinase II alpha 1 subunit isoform a	gi 4503095	45114.8	7.3	12	185	100	111	100	-1.1	5.3
SEC13-like 1 (S. cerevisiae), isoform CRA_b	gi 119584482	37521.1	5.3	10	284	100	221	100	-1.1	4.7
Tubulin, beta 2C	gi 23958133	49808.0	4.8	11	225	100	152	100	-1.1	5.1

Table 3.5 (Contd).

Top Ranked Protein Names	Accession No.	Proteins MW	Proteins PI	Peptide Counts	Protein Scores	Protein Scores C. I. %	Total Ion Scores	Total Ion C. I. %	U87-MG hypoxic / U87-MG	U87-MG Serum-deprived/ U87-MG
A. Differentially regulated proteins										
Chain A, crystal structure of human peroxisomal	gi 183448176	32718.4	6.4	8	197	100	124	100	-1.1	3.8
Glyceraldehyde-3-phosphate dehydrogenase	gi 31645	36031.4	8.3	11	341	100	236	100	-1.0	10.3
Glyceraldehyde-3-phosphate dehydrogenase	gi 7669492	36030.4	8.6	12	340	100	252	100	-1.1	6.7
Annexin A2, isoform CRA_c	gi 119597993	32428.6	5.9	17	481	100	318	100	-1.1	3.1
Cathepsin B	gi 741376	17143.0	5.4	6	272	100	217	100	-1.0	3.5
Chain A, Human Aldose Reductase Mutant L301m	gi 171848769	35848.4	6.5	12	138	100	54	100	-1.0	3.6
Manganese-containing superoxide dismutase	gi 30841309	23658.0	6.9	10	353	100	251	100	-1.4	4.2
Chain A, structural and kinetic study of the differences between human and E.coli manganese superoxide dismutase	gi 194708956	21858.0	6.4	12	397	100	248	100	-1.3	5.3

Table 3.6: Molecular class, molecular function and biological function of proteins identified by mass spectrophotometry using Human Protein Research Database (HPRD). (Data obtained by single HPRD analysis, n=1).

The 44 identified proteins were further subjected to human protein research database to describe the details of their molecular classes, molecular and biological functions.

Proteins	Molecular classes	Molecular Functions	Biological functions
A. Up-regulated proteins			
Alpha 2 type VI collagen isoform 2C2 precursor	Matrix protein	Extracellular matrix structural constituent	Cell growth and/or maintenance
Heat shock protein 90kDa beta (Grp94), Laminin A/C isoform 2 Laminin-binding protein	Chaperone Structural protein Transcription regulatory protein	Chaperone activity Structural molecule activity Transcription regulator activity	Cell communication; signal transduction Cell growth and/or maintenance, strongly expressed in malignant gliomas Regulation of nucleobase, nucleoside, nucleotide and nucleic acid metabolism, Stem & glial cell differentiation.
Unnamed protein product Vimentin	Heat shock protein Cytoskeletal protein	Heat shock protein activity Cell communication ; Signal transduction	Protein metabolism Cell growth and/or maintenance
CLN2 Fructose-biphosphate aldolase A	Enzyme: Hydrolase Enzyme: Lyase	Metabolism ; Energy pathways Lyase activity	Metabolism ; Energy pathways Metabolism ; Energy pathways
Selenophosphate synthetase 1 Alpha-tubulin	Enzyme: Synthase Cytoskeletal protein	ATP binding Structural constituent of cytoskeleton	Metabolism ; Energy pathways Cell growth and/or maintenance
PGK1	Enzyme: Phosphotransferase	Catalytic activity	Metabolism ; Energy pathways
Poly(rC) binding protein 3 isoform 1	RNA binding protein	RNA binding	Regulation of nucleobase, nucleoside, nucleotide and nucleic acid metabolism
Protein phosphatase 2, beta isoform	Serine/threonine phosphatase	Protein serine/threonine phosphatase activity	Cell communication ; Signal transduction
Coenzyme Q9 homolog Capping protein muscle Z-line, beta.	Unclassified Structural protein	Molecular function unknown Structural molecule activity	Biological process unknown Cell growth and/or maintenance

Table 3.6 (Contd)

Proteins	Molecular classes	Molecular Functions	Biological functions
A. Up-regulated proteins			
Chain A, Fidarestat bound to human aldose reductase	Enzyme: Oxidoreductase	Oxidoreductase activity	Metabolism ; Energy pathways
Glyceraldehyde-3-phosphate dehydrogenase	Enzyme: Dehydrogenase	Catalytic activity	Metabolism ; Energy pathways
Uracil DNA glycosylase	DNA binding protein	DNA binding	DNA repair
Eukaryotic translation initiation factor 4E isoform 2	Translation regulatory protein	Translation regulator activity	Protein metabolism
Triosephosphate isomerase 1	Enzyme: Isomerase	Isomerase activity	Metabolism ; Energy pathways
Phosphoglycerate mutase 1 (brain)	Enzyme: Mutase	Catalytic activity	Metabolism ; Energy pathways
Phosphoglycerate mutase 1 (brain)	Enzyme: Mutase	Catalytic activity	Metabolism ; Energy pathways
Similar to Chain , Heat-Shock Cognate 70kd Protein	Chaperone	Chaperone activity	Protein Metabolism
H3L-like histone	DNA binding protein	DNA binding	Regulation of nucleobase, nucleoside, nucleotide, and nucleic acid metabolism
B. Down-regulated proteins			
Heat shock protein 90kDa beta, member 1	Chaperone	Chaperone activity	Cell communication; signal transduction
ATP citrate lyase isoform 1	ATPase	ATPase activity	Metabolism ; Energy pathways
Moesin	Cytoskeletal protein	Structural constituent of cytoskeleton	Cell growth and/or maintenance
Glutamine-fructose-6-phosphate transaminase 2	Enzyme: Aminotransferase	Transaminase activity	Metabolism ; Energy pathways
Phenylalanyl-tRNA synthetase, alpha subunit	Enzyme: Ligase	Ligase activity	Protein metabolism
C. Differentially regulated proteins			
Transformation upregulated nuclear protein	Ribonucleoprotein	Ribonucleoprotein	Regulation of nucleobase, nucleoside, nucleotide and nucleic acid metabolism
Nicotinamide phosphoribosyltransferase precursor	Cytokine	Transferase activity	Anti-apoptosis
Vimentin variant 3	Cytoskeletal protein	Structural constituent of cytoskeleton	Cell growth and/or maintenance
Casein kinase II alpha 1 subunit isoform a	Serine/threonine kinase	Protein serine/threonine kinase activity	Signal transduction/Protein Modification
SEC13-like 1 (<i>S. cerevisiae</i>), isoform CRA_b	Chaperone	Chaperone activity	Protein metabolism
Tubulin, beta 2C	Enzyme: Hydratase	Catalytic activity	Metabolism ; Energy pathways

Table 3.6 (Contd)

Proteins	Molecular classes	Molecular Functions	Biological functions
A. Differentially regulated proteins			
Chain A, crystal structure of human peroxisomal	Enzyme: Hydratase	Catalytic activity	Metabolism ; Energy pathways
Glyceraldehyde-3-phosphate dehydrogenase	Enzyme : Dehydrogenase	Catalytic activity	Metabolism; Energy pathways
Glyceraldehyde-3-phosphate dehydrogenase	Enzyme : Dehydrogenase	Catalytic activity	Metabolism; Energy pathways
Annexin A2, isoform CRA_c	Calcium binding protein	Calcium ion binding	Signal transduction/Cell communication
Cathepsin B	Cysteine protease	Cysteine-type peptidase activity	Protein metabolism; Apoptosis
Chain A, Human Aldose Reductase Mutant L301m	Enzyme:Oxidoreductase	Oxidoreducataase activity	Metabolism ; Energy pathways
Manganese-containing superoxide dismutase	Enzyme: Superoxide dismutase	Superoxide dismutase activity	Cell proliferation ; Anti-apoptosis ; Cell growth and/or maintenance in metabolism
Chain A, structural and kinetic study of the differences between human and E.coli manganese superoxide dismutase	Enzyme: Superoxide dismutase	Superoxide dismutase activity	Cell proliferation ; Anti-apoptosis ; Cell growth and/or maintenance

Figure 3.20 shows the functional distribution of the identified proteins plotted against the percentage of proteins related to the designated function. Based on the biological function identified using HPRD, the percentage of proteins was plotted against the designated function. The results show that the majority of the proteins identified were observed to be related to energy pathways (31.8 %), cell growth and maintenance (20.5 %).

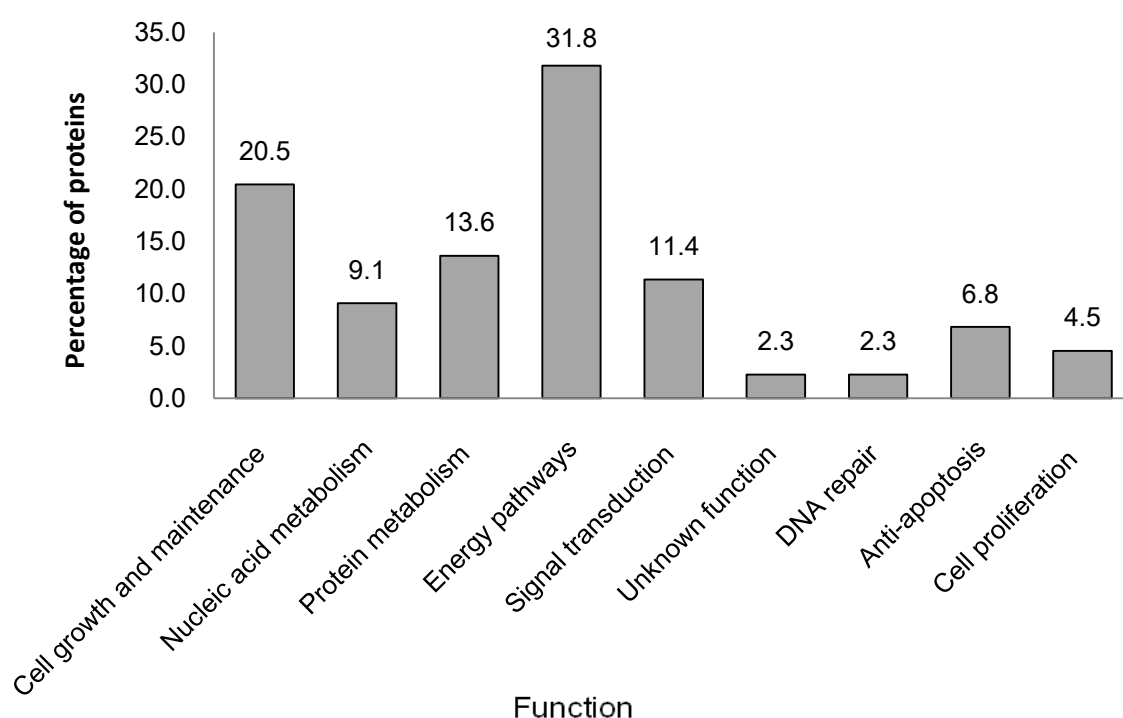


Figure 3.20: Functional distribution histograms of the identified proteins using HPRD database. (n=1 and $p < 0$). The x-axis represents the biological function and the Y - axis represents the percentage of proteins carrying out the respective functions.

Note that the majority of the proteins identified were related to the function of cell growth and maintenance and protein metabolism pathways.

3.6.2 Bioinformatic analysis of the proteomic data

The Ingenuity Pathways Analysis (IPA) (Ingenuity® Systems) is a software that enables researchers to model, analyse and understand the complexity of the composite biological and chemical systems. In the present study, IPA was used to identify the molecular functions and pathways which correlate with the proteins identified by mass spectrophotometry after the treatment of hypoxia and serum deprivation as compared to the control. The Ingenuity pathway analysis programme uses a knowledge base derived from the literature to relate gene products with each other based on their interaction and function and also links directly to the supporting references. Ingenuity allows a flexible search between multiple levels of biology with an ease to understand specific relationships between genes, molecular and cellular processes and diseases. The bio functions are grouped into three major categories:

- i. Disease and disorders
- ii. Molecular and cellular functions.
- iii. Physiological System Development and Function (Canonical pathways are grouped in metabolic pathways and signalling pathways).

Functional pathways and networks most significant to the data set were identified from the IPA library of canonical pathways. Two parameters were taken into consideration for the identification of the most significant pathways. Firstly, the ratio of the number of proteins that map to the pathway divided by the total number of proteins that map to the canonical pathways. Secondly, Fisher's exact test was used to calculate a p-value determining the probability that the association between the

proteins in the dataset and the canonical pathway is explained by chance alone (Table 3.7). Each of these networks was ranked by a score based on negative log of p-value. These scores ranked different networks based on its statistical significance.

The results in figure 3.20 show the top bio functions such as i) Disease and disorders ii) Molecular and cellular functions and iii) Physiological System Development and Function and iv) Canonical pathways related to the identified proteins. The biomarker analysis was carried out by applying filters specific to human species with respect to cancer provided a list of 17 specific proteins as potential biomarkers. The results demonstrated in table 3.8 include the name, location and fold change in the expression of the proteins observed in answer to micro-environmental changes (undifferentiated state).

Table 3.7: Top bio functions as generated by IPA. (Data obtained by considering negative log value of p, n=3).

Values are based on the negative log of p-value computed using a right tailed Fisher's exact test.

Top Bio Functions		
Diseases and Disorders		p-value
1	Cancer	$2.00 \times 10^{-9} - 4.61 \times 10^{-2}$
2	Gastrointestinal Disease	$2.00 \times 10^{-9} - 4.61 \times 10^{-2}$
3	Skeletal and Muscular Disorders	$1.15 \times 10^{-6} - 3.03 \times 10^{-2}$
4	Genetic Disorder	$5.62 \times 10^{-6} - 4.61 \times 10^{-2}$
5	Neurological Disease	$5.62 \times 10^{-6} - 2.49 \times 10^{-2}$
Molecular and Cellular Functions		
1	Cell Cycle	$4.18 \times 10^{-4} - 4.90 \times 10^{-2}$
2	Carbohydrate Metabolism	$7.51 \times 10^{-4} - 1.63 \times 10^{-2}$
3	Cell Death	$2.45 \times 10^{-3} - 4.90 \times 10^{-2}$
4	Cellular Assembly and Organisation	$2.05 \times 10^{-3} - 3.42 \times 10^{-2}$
5	Cellular Compromise	$2.05 \times 10^{-3} - 1.02 \times 10^{-2}$
Physiological System Development and Functions		
1	Cell Mediated-Immune Response	$2.05 \times 10^{-3} - 2.05 \times 10^{-3}$
2	Haematopoiesis	$2.05 \times 10^{-3} - 2.05 \times 10^{-3}$
3	Tumour Morphology	$2.05 \times 10^{-3} - 2.05 \times 10^{-3}$
4	Connective Tissue Development & Function	$4.09 \times 10^{-3} - 3.42 \times 10^{-2}$
5	Immune Cell Trafficking	$8.16 \times 10^{-3} - 8.16 \times 10^{-3}$
Top Canonical Pathways		
1	Glycolysis/Gluconeogenesis	9.73×10^{-7}
2	14-3-3-mediated Signalling	1.44×10^{-3}
3	Fructose and Mannose Metabolism	4.85×10^{-3}
4	Breast Cancer Regulation by Stathmin1	6.23×10^{-3}
5	Inositol Metabolism	1.02×10^{-2}

Figure 3.21 shows the graph obtained by the functional network analysis by IPA software. The data in graph A shows the number of proteins associated with the respective diseases and disorders. Graph B represents the molecular and cellular functions of the identified proteins. Graph C shows the proteins associated with the Physiological System Development and Functions and graph D represents the canonical pathways related to the identified proteins.

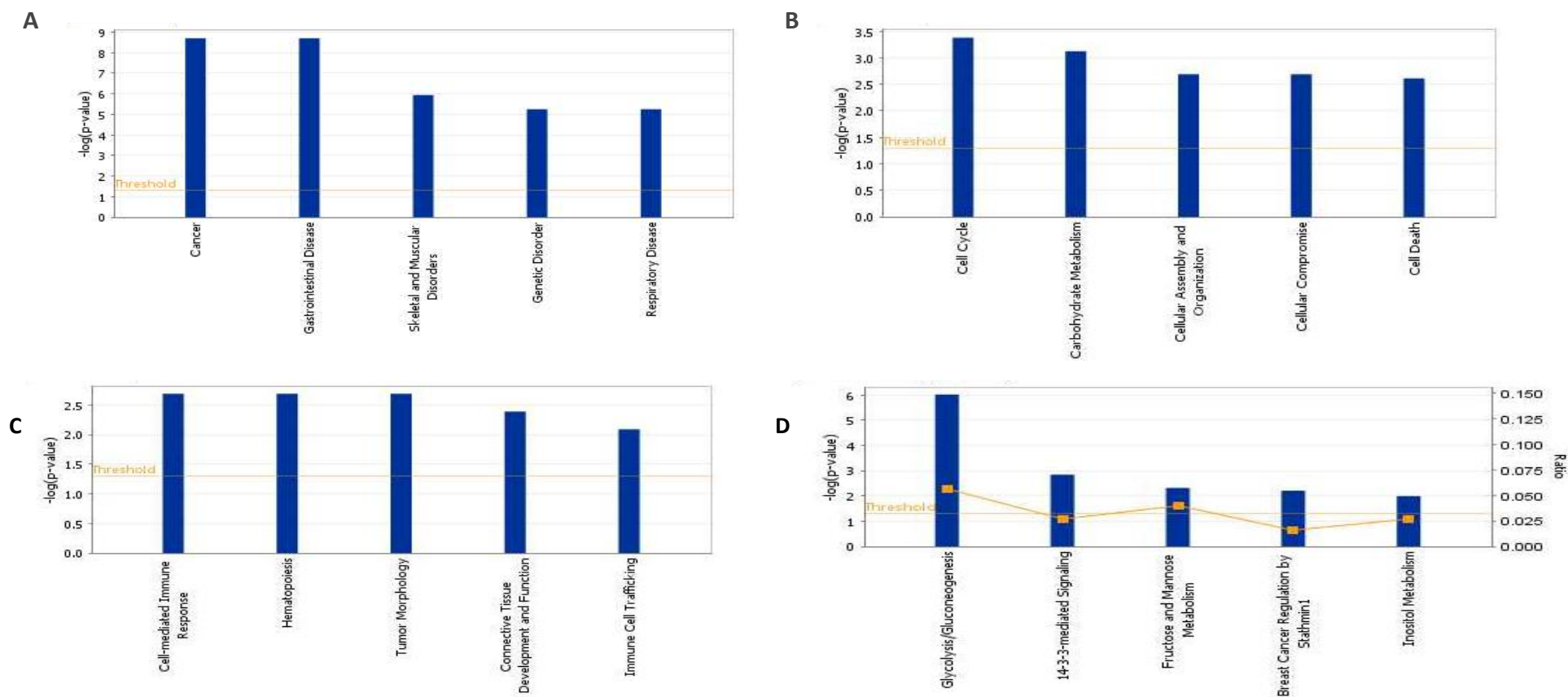


Figure 3.21: Functional network analysis by IPA. Top 5 (A) Diseases and disorders, (B) Molecular and cellular functions, (C) Physiological System Development and Functions and (D) Canonical pathways ($n = 1$, $p < 0$).

Table 3.8: shows the 17 potential biomarkers in cancer from the protein dataset using IPA analysis (n = 1).

Summarised in the table 3.8 are the potential markers identified in cancer. The majority of the markers are localised in the cytoplasm of the cells. The fold change in the protein expression level signifies its subsequent up and down-regulation on induction of micro-environmental changes. Majority of the proteins displayed an upregulated expression profile on induction of hypoxia and serum deprivation. These proteins were further subjected to biomarker analysis to study their significance cancer pathways.

Proteins	Locations	Fold changes
Aldolase A, fructose-biphosphate	Cytoplasm	1.780
ATP citrate lyase	Cytoplasm	1.000
Annexin A2	Plasma Membrane	-1.120
Casein kinase 2, alpha 1 polypeptide	Cytoplasm	-1.070
Collagen, type VI, alpha 2	Extracellular Space	1.260
Eukaryotic translation initiation factor 4E	Cytoplasm	2.560
Glyceraldehyde-3-phosphate dehydrogenase	Cytoplasm	1.240
Heat shock 70kDa protein 8	Cytoplasm	1.240
Heat shock protein 90kDa beta (Grp94),	Cytoplasm	-1.200
Heterogeneous nuclear ribonucleoprotein	Nucleus	-1.160
Nicotinamide phosphoribosyltransferase	Extracellular Space	-1.180
Phosphoglycerate kinase 1	Cytoplasm	1.040
Triosephosphate isomerase 1	Cytoplasm	1.210
Tubulin, alpha 1a	Cytoplasm	1.560
Tubulin, beta 2C	Cytoplasm	-1.090
Superoxide dismutase 2, mitochondrial	Cytoplasm	-1.420
Vimentin	Cytoplasm	1.180

The analysis of the proteins from the database did not generate any specific pathway through the IPA software. However, on applying a filter specific to human species and cancer generated a network involving 11 proteins from the dataset. The network was thereafter overlaid with a set of ingenuity biomarkers in order to identify potential biomarkers for the identification of glioma stem cells. The network displayed in Fig. 3.21 directs study to explore vimentin (Vim), heterogeneous nuclear riboprotein K (HNRNPK) and eukaryotic translation initiation factor 4e (EIF4e) as potential biomarkers for the identification of stem cells. The coloured ellipses within the cell denote the proteins involved in the network and their localisation within the cell. Large ellipses outside the cell represent the type of cancer linked to the expression of the respective protein.

Figure 3.22 shows the self – designed network created using IPA knowledge database. The coloured ellipses within the cell denote the proteins involved in the network and their localisation within the cell. Large ellipses outside the cell represent the type of cancer linked to the respective protein.

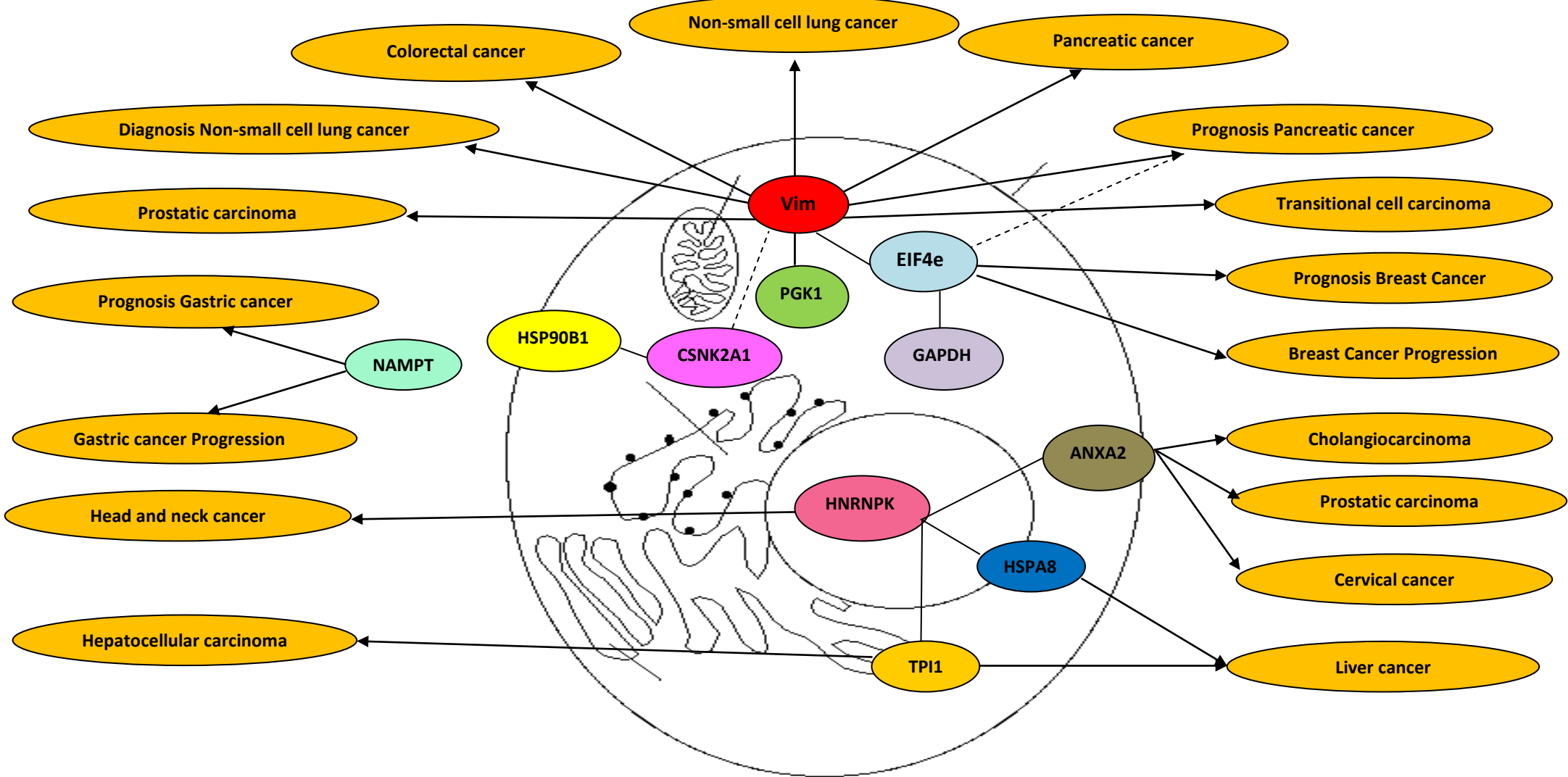


Figure 3.22; Network generated by IPA path designer overlaid with cancer biomarkers from ingenuity knowledge database.

Chapter 4

Discussion

Stem cells are considered to be the most primordial cells in the human body that impart plasticity to the organ system (Sabetrasekh *et al.*, 2006). The characteristic features which interests researchers in exploring stem cells are their self-renewal potential and the ability to proliferate into diverse cell types (Singh *et al.*, 2003). Stem cells have been extensively explored for their use in the field of developmental medicine, repair, gene therapy and transplant communities (Sabetrasekh *et al.*, 2006). Despite its therapeutic potential, tumour initiating stem cells (CSCs) have been known to trigger cancer. CSCs comprise of a small sub-group of cells within a tumour and are essential to its growth. The origin of CSCs still remains unclear leaving an open end justification that on acquiring a mutation or change in their DNA instructions could disturb their self-renewal control. In addition, the immediate progeny of stem cells (progenitors) due to genetic damage could regain the power of self-renewal instead of developing into mature cells. Overall, the resistive potential of CSCs towards chemotherapeutic agents and their ability to form tumours have given rise for a need to identify and understand the mechanisms of resistance. In addition, it is very important to predict the outcome and response to cancer treatment (Woodward and Sulman, 2008). Discrimination of CSCs by means of a biomarker can facilitate early diagnosis and help in reducing cancer-related mortality. Similar to other cancers, glioma is thought to be a disease of accumulated genetic alterations arising from transformed neural stem cells (Kitange *et al.*, 2001; Singh *et al.*, 2003).

Previous work carried out in our laboratory studied the expression profile of multi-drug resistance genes and proteins in cancerous and stem cells (Lu, PhD thesis, 2008). This study focused on the characterisation of CD133⁺ glioma stem-like cells with respect to the expressions of multi-drug resistance *mdr1* and *bcl-2* (Lu, PhD thesis, 2008). A high level of MDR-related molecules such as P-gp and Bcl-2 support the significant chemoresistance of CD133⁺ glioma and normal cells compared to the corresponding CD133⁻ cells. The study by Lu (2008) also indicated that the multi-drug resistance potential of CD133⁺ stem-like normal astrocytes was higher than the CD133⁺ glioma stem-like cells. Enrichment of CD133⁺ cells derived from the astrocytoma/oligodendroglioma (GOS-3) cells in serum deprivation indicate that CSCs could be enhanced by introducing micro-environmental changes (Lu, 2008).

The present study focused on investigating the stem cell-like characteristics in the differentiated and undifferentiated glioma cells. Considering equal evidence in support of CD133⁺ and CD133⁻ to generate tumours, the aim was to find a selective marker to define glioma stem cells and allow their distinction from NSCs. The novel approach of this study lies in assessing the expression profiles of two markers Oct4-A and BMP2 in glioma with respect to a well established undifferentiated stem cell marker CD133. Maintenance of an undifferentiated state is a key feature of stem cells, therefore monitoring the divergence in the differentiated and undifferentiated states in brain tumour cell lines would provide an insight regarding the altered regulatory mechanisms which leads to tumour formation, progression and chemoresistance. Evaluating stemness signatures in the differentiated and undifferentiated cells have been further explored by testing the chemo-resistive potential and cell cycle phases of

these cells. Finally, proteomic analysis carried out provides a dataset of proteins that have been altered in the process of differentiation of the U87-MG cells.

Preliminary experiments assess the levels of protein CD133, Oct4-A and BMP2 in different grades of glioma cell lines (1321-N1, GOS-3 and U87-MG). Genomic analysis carried out using qRT-PCR indicated an absence of the *CD133* gene in all the three grades of glioma cell lines. A minimal level of *Oct4-A* expression was observed in all the three cell lines with a slightly higher expression level noticed in the GOS-3 glioma cell line. The expression of the *BMP2* gene remained restricted to only U87-MG cells. The statistical analysis performed using Student's one sample T-test did not indicate any significant difference in the expression of candidate genes within the glioma cell lines. However, the minimal level of expression of *Oct4-A* and *BMP2* was still taken into consideration due to limited marker protein expression by the stem cells.

The analysis carried out using the flow cytometer and immunofluorescent studies, indicated an absence of CD133 and BMP2 protein in the three tested glioma cell lines. The GOS-3 cell line showed the highest level of Oct4-A protein (84.3 %), followed by 1321-N1 (75.6 %) and U87-MG (72.7 %). The results showed a significance difference observed in the expression of Oct4-A protein (* $p < 0.05$) in the GOS-3 and U87-MG cells as compared to the 1321-N1 cells. This analysis contributed to the study of the protein expression profiles in the differentiated glioma cells. Based on the literature search and evidence of finding CD133 cells in U87-MG cell lines (Wong *et al.*, 2009), further work was carried out on cell differentiation, chemosensitivity, cell cycle analysis and proteomics using U87-MG cells.

U87-MG cells were subjected to two different micro-environmental changes in order to enhance their state of undifferentiation and enrich its stemness. Glioma cells when subjected to hypoxia showed an elevated expression of CD133 protein with an increase in self-renewal potential and inhibition of their differentiation (Soeda *et al.*, 2009). In addition, the cells located in the intra-tumoral areas augmented with hypoxia elicit CD133 surface protein along with an expression of DNA repair protein O6-methylguanine-DNA-methyltransferase (MGMT) (Pistollato *et al.*, 2010). Hypoxia regulates stem cell phenotype with subsequent induction of specific tumour stem cell-related genes (Seidal *et al.*, 2010). Therefore, cells residing in the hypoxic environment could be characterised with noticeable stem cell features and further examined for chemoresistance. U87-MG cells were subjected to 100 % nitrogen atmosphere for 30 min in order to induce hypoxia and were analysed after 24 hrs of incubation for the expression of stem cell-related proteins CD133, Oct4-A and BMP2. After incubation, the cells attained a spherical morphology when observed under a light microscope (x 20 magnification). Oct4-A protein level was significantly (* $p < 0.05$) induced by 14 % due to hypoxia with a basal expression of CD133 (2.3 %) protein in the hypoxic U87-MG cells. An *in vivo* model in adult mouse previously demonstrated that the germ line-specific transcription factor Oct4 is sufficient to generate pluripotent stem cells from NSCs (Kim *et al.*, 2009). Furthermore, the existence of Oct4 protein in lung cancer plays a crucial role in maintaining pluripotency and supports the chemoresistive potential of lung cancer derived CD133⁺ cells (Chen *et al.*, 2008). An elevated expression of Oct4-A protein along with a marginal expression of CD133⁺ stem-like cells could therefore indicate a development of stem cell-like characteristics in the undifferentiated hypoxic U87-MG cells as compared to the control. However, the results do indicate the existence of stem cells on the basis of Oct4-A expression.

Cancer cells adjust to the serum-deprived environment and display a down-regulation of genes associated with neural mature markers with a subsequent up-regulation of genes which are related to primitive NSC markers (Kang *et al.*, 2006). In addition to high drug resistance and an enhanced proliferative potential, these dedifferentiated cells also exhibit important proliferation signalling proteins, primitive neural lineage-related proteins, cancer genes, and transporter genes which may contribute towards cancer and its aggressiveness (Kang *et al.*, 2006). Another attempt to induce undifferentiation in U87-MG cells was carried out by induction of serum deprivation supplemented with growth factors hEGF and bFGF (Stem Cell Sciences, UK). A quantitative measurement of the candidate proteins showed a significant (* $p < 0.05$) decrease in the Oct4-A protein level by 26.7 % as compared to the control cells. Similar to the control U87-MG cells, serum-deprived cells did not exhibit the expression of CD133 and BMP2 proteins. Flow cytometric results were further confirmed by immunofluorescent studies. Although, microscopic observation showed a neurospheric morphology indicating a state of undifferentiation, a down-regulation of Oct4-A and the absence of CD133 protein indicated an absence of stemness characteristics in the serum-deprived cells. Inconclusive results have been drawn from the use of chemotherapy targeted against cancer proliferation and reoccurrence. By virtue of different molecular mechanisms such as cell cycle kinetics, DNA replication and repair mechanisms, asynchronous DNA synthesis, anti-apoptotic proteins and transporter proteins, stem cells resist the effect of potent chemotherapeutic agents (Wicha *et al.*, 2006). In addition to MDR, multi-drug associated proteins (MRP) offer defence against xenobiotics and endogenous toxic metabolites, leukotriene-mediated inflammatory responses, as well as protection from the toxic effect of oxidative stress (Shervington and Lu, 2008; Bakos and Homolya, 2007). Effective chemotherapeutic drugs such as

Taxol and TMZ were used to check the chemosensitivity of differentiated and undifferentiated U87-MG cells. Taxol mediates a strong cytotoxic and anti-proliferative activity in malignant glioma cell lines (Roth *et al.*, 1998) whereas, CD133⁺ stem-like cells have been found to be resistant towards Taxol (Dey *et al.*, 2010). On treatment with TMZ, glioma cells undergo G2/M arrest and die due to autophagy (Kanzawa *et al.*, 2003; Zeng *et al.*, 2007). However, CD133⁺ cells in glioma withstand the toxic effect of TMZ by involving cell cycle regulating proteins CHK1/CHK2 (Hambardzumyan *et al.*, 2006). The cytotoxic effect of Taxol remained unchanged for the control and hypoxic U87-MG cells, by killing approximately 9 % of cells from the entire population. A significant (* $p < 0.05$) fourfold increase in cytotoxicity was observed in serum-deprived U87-MG cells accounting for 36 % of cell death. On the other hand, TMZ displayed an overall weak cytotoxic effect on the U87-MG cells. As compared to the control cells (6 %), the percent of cell death was reduced to 3 % in the hypoxia-treated cells. However, the number of dead cells increased to more than threefold (26 %, * $p < 0.05$) on serum deprivation. Cellular differentiation showed that Taxol is a better chemotherapeutic drug compared to TMZ. Since, previous data from our lab have demonstrated the multi-drug resistance ability of CD133⁺ cells with the co-expression of anti-apoptosis related molecules such as P-gp and Bcl2 (Lu, 2008), the chemoresistance of the hypoxic U87-MG cells could, therefore, be attributed to the existence of a subset of CD133⁺ cells. Hence, the overall effectiveness of the cytotoxic drugs was more noticeable in the U87-MG cells deprived of serum which displayed neurospherical morphology but did not exhibit any stem cell-related properties.

Chemotherapeutic drugs limit cancer growth by blocking one or more stages of cell cycle. The serum-deprived U87-MG cells showed a significant (* $p < 0.05$) difference in the G1, S and G2 phase of the cell cycles as compared to the control. A similar (* $p < 0.05$) change in the cell cycle phase was observed when the serum-deprived cells were treated with taxol. A prominent G2/M arrest in the cell cycle phase of control (46.4 %) and hypoxic (56.1 %) cells was observed when treated with Taxol. TMZ induced a G1 phase arrest in the U87-MG cells line, where the maximum arrest was observed in the serum-deprived cells (59 %, * $p < 0.05$) followed by a similar response in the hypoxic (47.2 %) and control cells (44.8 %). The S-phase of the serum-deprived was highly and significantly (* $p < 0.001$) affected on account of TMZ treatment.

While Taxol was more effective in blocking the G2/M phase of hypoxia-treated U87-MG cells, serum-deprived cells showed a prominent block of the G1 phase irrespective of the treatment with Taxol and TMZ. The present data suggest that though TMZ induced a G1 phase arrest in the control, hypoxic and serum-deprived cells, Taxol was equally capable of arresting the serum-deprived cells in the G1 phase. The probable reason for cell-killing by Taxol could be the induction of apoptosis by internucleosomal DNA fragmentation (Sui *et al.*, 2004). This finding could be investigated further to study the sensitisation of serum-deprived cells towards Taxol by considering the mitochondrial pathway mediated apoptosis (Goyeneche *et al.*, 2006).

The proteomic approach in this study helps to organize the alteration in the tumour related protein levels and identify new therapeutic targets and biomarkers correlated to cancer (Zhang *et al.*, 2010). In the present study, proteomics was used to monitor the changes at the cellular protein level in the differentiated and undifferentiated U87-MG cells and to define selective biomarkers for the identification of glioma stem cells.

The experiments involved 2D-DIGE for the separation of proteins which favours minimal inter-gel variation and MALDI-TOF for protein identification. Approximately, 96 protein spots listed by 2D-DIGE were found to be differentially expressed, out of which 44 spots were selected for identification (These 44 spots were highly up, down or differentially regulated as compared to the others. All of the spots could not be identified due to limited consumable money allotted). The up-regulated spots showing a 2.0 fold increase, the down-regulated spots showing a 1.0 fold decrease and the differentially regulated spots with a 4.5 fold increase were selected for protein identification using MALDI-TOF. All the 44 spots were identified with a high confidence level of 100 %, 37 of 44 spots were confidently identified as human proteins. Based on the biological function of the proteins, they were grouped into 9 categories: metabolism and energy pathways (n = 14), cell growth and maintenance (n = 9), protein metabolism (n = 6), signal transduction (n = 5), nucleic acid metabolism (n = 4), anti-apoptosis (n = 3), cell proliferation (n = 2), DNA repair (n = 1) and unknown (n = 1). (n = number of proteins related to the respective function).

Up-regulated proteins

On induction of hypoxia and serum-deprivation, 24 proteins were found to be up-regulated. The majority of the up-regulated proteins (n = 9) participated in metabolism and energy pathways. Amongst them, protein CLN2 is a cyclin involved in cell cycle regulation promoting G1 to S phase transition. Fructose-biphosphate aldolase A is an enzyme involved in glycolysis abundantly expressed in oligodendroglioma (Park *et al.*, 2008). ATP binding enzyme Selenophosphate synthetase 1 affects cell viability upon ionizing radiation through modulation of p53 activity (Chung *et al.*, 2006). Phosphoglycerate kinase 1 (PGK1) is a glycolytic enzyme

catalyzing the conversion of 1, 3-diphosphoglycerate to 3-phosphoglycerate. In contrast, fidarestat is a human aldose reductase (hAR) inhibitor which catalyzes the reduction of different compounds such as aldehydes, xenobiotic aldehydes, ketones and trioses with nicotinamide adenine dinucleotide phosphate (NADPH) as a cofactor. It blocks glucose metabolism in cancer cells (Fournier *et al.*, 2009). Glyceraldehyde-3-phosphate dehydrogenase (GAPDH) is a glycolytic enzyme over expressed in many tumours and induced by hypoxia in normal and malignant cells (Said *et al.*, 2007). Another glycolytic enzyme Triosephosphate isomerase 1 (TPI1) serves as an essential factor for the production of energy for cells. A variant of Triosephosphate isomerase 1 has also been detected in late passages of glioblastoma cells using proteomic analysis (Khalil and Madhamshetty, 2006). Two different forms of the glycolytic enzyme phosphoglycerate mutase 1 (PGM1) were observed on treatment with hypoxia and serum deprivation. In tumour cell lines PGM1 is known to regulate the balance between glycolysis and another ATP-producing pathway, glutaminolysis (Engel *et al.*, 2004).

The proteins related to cell growth and maintenance (n = 5) include Alpha 2 type VI collagen isoform 2C2 precursor, Laminin A/C isoform 2, Vimentin, Alpha-tubulin and Capping protein muscle Z-line (actin-filament), beta. Alpha 2 type VI collagen isoform 2C2 precursor basically functions as a cell binding protein whereas the Laminin isoform 2 is abundantly expressed in gliomas promoting integrin mediated glioma cell migration and glioma invasion (Kawataki *et al.*, 2007). Vimentin is the major subunit protein of the intermediate filaments involved with the intracellular transport of proteins between the nucleus and plasma membrane. It was found to be present in high levels in the non-invasive and non-infiltrative tumours and appeared to be a

discriminative marker for clustering infiltrative and/or invasive meningiomas versus non-invasive meningiomas (Bouamrani *et al.*, 2010). A 3.5 fold up-regulation of vimentin may indicate the aggressiveness of glioma cells when shifted towards an undifferentiated state. The expression of cytoskeletal protein alpha tubulin in its nitrated form has been extensively found in a progressive neoplasm indicating advancement in the tumour grade (Fiore *et al.*, 2006). The capping protein muscle Z-line up-regulation marks the onset of cellular assembly in the undifferentiated U87-MG cells (Cooper and Sept, 2008).

Proteins involved in cell communication and signal transduction include Heat shock protein 90kDa beta (Hsp90 β) and Protein phosphatase 2, beta isoform. Hsp90 β is a molecular chaperone stabilizing Akt (serine/threonine protein kinase) and oncogenic forms of mutant epidermal growth factor receptor, both of which favour the growth of a variety of cancers including gliomas (Basso *et al.*, 2002 and Lavictore *et al.*, 2003). Protein phosphatase 2, beta isoform is implicated in the negative control of cell growth and division. In addition Poly(rC) binding protein 3 isoform 1 and H3L-like histones were reported as proteins regulating the nucleobase, nucleoside, nucleotide, together with nucleic acid metabolism. Poly(rC) binding protein 3 isoform 1 functions as a cytosolic iron chaperone in the delivery of iron to ferritin (Shi *et al.*, 2008). H3L-like histones are basic nuclear proteins maintaining the nucleosome structure of the chromosomal fiber. Hsp70 is an anti-apoptotic protein found to be elevated in various types of cancer. Stress conditions up-regulate Hsp70 levels through transcriptional activation, preferential translation and mRNA stabilization and restrains apoptosis by inhibiting aggregation of cell proteins (Lindquist *et al.*, 1988 and Calderwood *et al.*, 2005). EIF4e isoform 2 is involved in enhancing translational

efficiency, splicing, mRNA stability, and RNA nuclear export. EIF4e isoform 2 can function as an oncogene and its activation may be a key event in oncogenic transformation by phosphoinositide-3 kinase and Akt (Ruggero *et al.*, 2004). HPRD analysis revealed that an unknown protein product detected together with Hsp70 and Eif4e) isoform 2 undertake the function of protein metabolism. Furthermore, DNA repair protein Uracil DNA glycosylase (UDG) functions to suppress the GC-to-AT transition mutations (Caradonna and Muller-Weeks, 2001).

An up-regulation in the expression of the stem cell marker protein suggests a state of undifferentiation. In addition to CD133, stemness signature has been identified by an up-regulation of several marker proteins namely nestin, mushashi, Sox2, PTEN, Oct4 and BMPs (Bao *et al.*, 2006; Dasari *et al.*, 2010). The proteomic data disclosed different up-regulated proteins (n = 3), whose elevated expression was observed more under serum-deprived conditions. Laminin binding protein was up-regulated by a 9.8 fold in serum-deprived cells as compared to the hypoxic cells. Laminin promotes tumour angiogenesis by providing appropriate signals and structure required for endothelial cell attachment and proliferation (O'Brien *et al.*, 2001; Croft *et al.*, 2004). In glioma, laminins also regulate pathways which support growth, invasion, and resistance to chemotherapeutic drugs (Keivit *et al.*, 2010). The laminin receptor Integrin $\alpha 6\beta 1$ directly regulates their tumorigenic capacity, anchoring the adult neural stem cells to the niche vasculature (Corsini and Martin-Villalba 2010). The condition of serum deprivation would prepare U87-MG cells for increased proliferation and chemoresistance, a measured approach to acquiring stemness. *UNG* (gene coding UDG protein) expression is regulated by the cell cycle and its enhanced activity is observed in proliferating cells as compared to the non-proliferating cells (Nagelhus *et al.*, 1995;

Walsh *et al.*, 1995 and Aprelikova and Tomilin, 1982). A study carried out on the survival of embryonic rat hippocampal neurones suggests that depletion of UNG results in a DNA damage response, inducing p53-dependent apoptosis (Kruman *et al.*, 2004). By means of transcription-coupled repair (TCR) pathway, differentiated cells undertake the repair of transcribed genes (Nospikel and Hanawalt., 2004). Base - excision repair (BER) is one such mechanism involved in TCR maintaining genomic integrity in the brain initiated by UDGs (Le *et al.*, 2000). Under ischemic conditions uracil misincorporated DNA damage is compensated by an up-regulation of UNG and uracil-BER activity and holding up the genomic stability within brain (Kruman *et al.*, 2004). The increase in the level of UDG in hypoxia as well serum-deprived U87-MG cells from fold 1.2 - 6.5, signifies a DNA repair mechanism. This further indicates that the majority of the serum-deprived cells are residing in the phase of differentiation as compared to the hypoxic cells.

The dinucleotide poly phosphates (Ap₄A) rise in response to stress conditions contributes to cell proliferation, DNA repair and replication, vasotone regulation and neurotransmission (Baxi and Vishwanatha, 1995). In HeLa cells, it is found that UDG and GAPDH are an Ap₄A binding proteins targeting DNA repair/replication (Meyer-Siegler *et al.*, 1991). GAPDH is extensively expressed in tumours and during phases of cell cycle which require more energy. Cytosolic expression of GAPDH does not correspond to cell death. GAPDH displays other activities, such as uracil DNA glycosylase activity that mediates DNA repair and binding to transfer RNA and DNA (Sawa *et al.*, 1997).

A prominent over expression of GAPDH by 11.1 fold was observed in the serum-deprived cells as compared to the hypoxic U87-MG cells. The *in-vitro* analysis of GAPDH expression was not found to be induced or regulated under hypoxic conditions

(Said *et al.*, 2007). Serum-deprived cells showed a cytosolic GAPDH colocalised with stress fibres indicating a specialised function of GAPDH for its interaction with cytoskeletal elements, apart from the normal glycolytic function (Schmitz and Bereiter-Hahn, 2001). The use of GAPDH as a housekeeping should also be revisited due to differential expression pattern under conditions of hypoxia and serum deprivation compared to the control U87-MG cells.

In this study the overall several fold increases in the levels of the up-regulated proteins were more prominent in the serum-deprived cells as compared to the hypoxic cells. Serum-deprived cells exhibit an increased demand of energy production due to low glucose availability. The tendency of the serum-deprived cells to form neurospheres correlates with an enhanced expression of cytoskeletal proteins such as laminin A/C isoforms 2, vimentin, alpha tubulin and capping protein muscle Z-line beta contributing to the structural alteration in the undifferentiated U87-MG cells. The expressions of proteins related to heat shock response and DNA repair further prepare the dedifferentiating cells against stress conditions of serum starvation and low oxygen levels.

Down-regulated proteins

In the present study the proteomic analysis disclosed down-regulated proteins (n = 5) amongst which Hsp90 β was detected with a 1.5 fold decrease in the expression level. Metabolism and energy pathway related proteins included ATP citrate lyase (ACL) isoform 1 and Glutamine-fructose-6-phosphate transaminase 2 (GFPT2). ACL isoform 1 converts glucose-derived citrate into acetyl-CoA. ACL activity is an essential factor linking growth factor-induced increases in nutrient metabolism to the regulation of histone acetylation and gene expression (Wellen *et al.*, 2009). GFPT2 is the first

rate-limiting enzyme of the hexosamine biosynthesis pathway mainly expressed in the central nervous system. Sub-membranous cytoskeletal protein moesin function in cell-cell recognition, signalling and for cell movement. Enzyme phenylalanyl-tRNA synthetase, alpha subunit, performing a ligase activity is involved in protein metabolism.

Down-regulation of ACL indicates a progress in the state of differentiation in the glucose dependent cells (Hatzivassiliou *et al.*, 2005). Thus, it is perceptible to notice a 1.4 fold decrease in the expression of ACL in serum-deprived cells as compared to ischemic cells which are non-glycolytic having less dependency on ACL activity. As observed in pancreatic cancer, reduction in the level of moesin could result in increased migration, invasion and metastasis promoting cellular translocation of β -catenin, and re-distribution and organization of the cytoskeleton (Abiatari *et al.*, 2010). In addition to anaplastic carcinoma, moesin could also function as a phenotypic marker for undifferentiated glioma cells. Phenylalanyl-tRNA synthetase is expressed in a tumour-selective and cell cycle stage- and differentiation-dependent manner (NCBI). A marked decrease in the expression level, therefore, denotes a possible shift towards the state of undifferentiation and tumour progression.

Differentially expressed proteins

The proteomic analysis in this study have also shown differentially expressed proteins (n = 15) including five proteins related to metabolism and energy pathways. Two isoforms of GAPDH were increased by fold 9.3 and 5.6, respectively, in the serum-deprived cells as compared to the hypoxic sample. Tubulin, beta 2C forms the major

constituent of the microtubules. Its molecular functions include guanosine triphosphate (GTP) and unfolded protein binding and regulating GTPase activity. Chain A, crystal structure of human peroxisomal delta 3, 5, delta 2, 4-dienoyl Co-A isomerase carries out isomerisation of 3-trans, 5-cis-dienoyl-CoA to 2-trans, 4-trans-dienoyl-CoA. In addition to protein binding and isomerase activity, it is also involved in fatty acid-beta oxidation and generation of precursor metabolites and energy. Another molecule related to metabolism and energy pathways is Chain A, Human Aldose Reductase Mutant L301m complexed with sorbinil which performs the oxidoreductase activity.

Vimentin variant 3 showed a 5.3 fold increase in its expression level in the serum-deprived U87-MG cells, responsible for the function of cell growth and maintenance. Casein kinase II alpha 1 (CSNK2A1) subunit isoform A is a serine/threonine protein kinase that phosphorylates acidic proteins such as casein. Casein kinases are known to have a regulatory function in cell proliferation, cell differentiation and apoptosis. In addition to phosphorylation of various key intracellular signalling proteins involved in tumour suppression (protein 53; p53-tumour suppressor protein and phosphatase and tensin homolog; PTEN- tumour suppressor gene) and tumorigenesis (myc - oncogene, jun - oncogene, nuclear factor kappa-light-chain-enhancer of activated B cells; NF-kappaB - DNA transcription control). CSNK2A1 is also considered to influence Wnt signalling via beta-catenin phosphorylation and the PI 3-K signalling pathway via Akt phosphorylation. Annexin A2, isoform CRA_c is a protein regulating cell growth and signal transduction pathways. In addition to protein modification, Annexin A2 is considered to play a role in eliciting heat shock response. Transformation up regulated nuclear protein is a conserved RNA-binding protein involved in various processes of

gene expression including chromatin remodelling, transcription, mRNA splicing, translation, and stability. This protein is important for cell migration and metastasis and also participates in cell cycle progression (Dejgaard *et al.*, 1994; Inoue *et al.*, 2007).

Protein metabolism-related proteins comprised of SEC13-like 1 (*S. cerevisiae*), isoform CRA_b and Cathepsin B. SEC13-like 1 (*S. cerevisiae*), isoform CRA_b is a part of endoplasmic reticulum and the nuclear pore complex and functions in protein transport. Cathepsin B (CSTB) gene is over expressed in a variety of cancer such as lung, prostate, colon, breast, and stomach (Hughes *et al.*, 1998). Analysis of cytosolic accumulated CSTB in mouse hepatocytes and rat hepatoma cells has implicated its contribution in TNFA-induced apoptosis (Guicciardi *et al.*, 2000). Nicotinamide phosphoribosyltransferase precursor (NAMPT) catalyses one step in the biosynthesis of nicotinamide adenine dinucleotide (Ramsey *et al.*, 2009). This anti-apoptotic protein promotes vascular smooth muscle cell maturation and inhibits neutrophil apoptosis. Two forms of manganese-containing superoxide dismutases involved in cell proliferation and maintenance were found to be up-regulated by 2.7 and 4.0 fold, respectively, in the serum-deprived cells. Manganese-containing superoxide dismutase binds to the superoxide by-products of oxidative phosphorylation and converts them to hydrogen peroxide and diatomic oxygen. It destroys biologically toxic radicals which are normally produced within the cells.

Differential expression indicated a down-regulation of proteins under hypoxic conditions (scale -1.0 to -1.4) and an apparent increase under serum-deprived conditions (scale 3.1 to 10.3). Since a total of 15 proteins have been identified as differentially regulated, it could be deduced that hypoxia and serum deprivation shift the cells towards an undifferentiated state via different approaches. While serum

withdrawal enhances the need for metabolism and cell growth related proteins, hypoxic cells express its subsequent down-regulation. A similar expression profile was observed for proteins involved in protein metabolism, signal transduction, anti-apoptosis and regulation of nucleotides.

The IPA compare analysis confirmed an identical protein expression profile in the hypoxia-treated cells and the serum-deprived cells with reference to the U87-MG control cells. The IPA software further helped in analysing the role of identified proteins in various diseases and disorders, top molecular and cellular functions, physiological system development and top canonical pathways. Treatment with hypoxia and serum deprivation modulated cancer at the top most level, indicating that the state of undifferentiation plays a crucial role in oncogenesis. The other disease and disorders included gastrointestinal disease, skeletal and muscular disorders, genetic disorder and neurological disease. The cellular and molecular functions affected include cell cycle, carbohydrate metabolism, cell death, cellular assembly, organisation and cellular compromise. In line with the experiments performed in the undifferentiation state of U87-MG cells, the proteins involved in altering the cell cycle phases could provide an insight into discriminating the regulatory mechanism of the differentiated and undifferentiated glioma cells. The identified proteins affected the physiological functions such as Cell mediated-immune response, Haematopoiesis, Tumour morphology, Connective tissue development and function and Immune cell trafficking. The records of canonical pathways displayed that glycolysis/gluconeogenesis, 14-3-3-mediated signalling, fructose and mannose metabolism, breast cancer regulation by stathmin1, inositol metabolism were the top

five pathways affected on induction of micro-environmental changes. A detailed investigation of above mentioned parameters with respect to the micro-environmental changes induced in glioma cell lines could probably provide evidence to the contribution of hypoxia and serum deprivation in maintaining stem-like cells and promoting tumour formation and relapse.

Biomarker analysis carried on the protein dataset by applying filters specific to human species and cancer, proposed a total of 17 proteins identified as potential biomarkers (Table 3.8). Furthermore, a functional protein association network for proteins that were differentially expressed due cellular undifferentiation was generated using IPA. The network was overlaid to an inbuilt biomarker library generated in the IPA knowledgebase. The network, thus, generated 11 proteins namely Vimentin, PGK1, EIF4e, GAPDH, CSNK2A1, Hsp90 β 1, HNRNPK, ANXA2, HspA8, TPI1 and NAMPT. The identification of these 11 proteins narrows down the research focus to explore in detail the expression profiles of these proteins in the undifferentiated U87-MG glioma cell line in order to define selective alternative marker/s for CSCs in addition to CD133. Vimentin is involved in a variety of cancers including prostatic carcinoma, efficacy and diagnosis of non-small lung and pancreatic cancer, colorectal cancer, transitional cell carcinoma and in the prognosis and progression of breast cancer (Katsumoto *et al.*, 1990). Vimentin is the major intermediate filament cytoskeletal protein playing an important role in cell movement and motility (Katsumoto *et al.*, 1990). It belongs to glioma specific extracellular matrix components and is implicated in both neo-vascularisation and invasion of malignant glial cells (Zhang *et al.*, 2006). Constitutive coexpression of vimentin with casein kinase in prostate cancer cell lines is linked with an invasive phenotype that can be reversed by reducing vimentin expression (Singh *et al.*, 2003). Hypoxic conditions have been known to cause redistribution of vimentin to

a more insoluble and extensive filamentous networks that could play a role in endothelial barrier stabilization. Redistribution of vimentin is mediated through altering the phosphorylation of the protein and its interaction with HSP27 (Liu *et al.*, 2010). However, growth factors such as bFGF have been found to control the cytoskeletal network by up-regulating vimentin under conditions of serum deprivation (Bramanti *et al.*, 2006). Proteomic analysis revealed that two different forms of vimentin were up-regulated by a magnitude of 3 - 5.3 fold in the serum-deprived cells as compared to the hypoxic U87-MG cells.

In addition, vimentin is linked directly to PGK1, CSNK2A1 and EIF4e. HIF1 α -regulated gene PGK1 was strongly up-regulated in non-stem glioma cells under hypoxia as compared to glioma stem cells (Keith and Simon, 2007). The expression profile observed in serum-deprived cells was 6.5 fold higher as compared to the hypoxia - treated cells indicating that the majority of the serum-deprived cells did not exhibit stem cell-related proteins. PGK1 can be adopted as a marker in future experiments for the isolation of differentiated glioma cells, thus, favouring isolation of the stem-like cells. CSNK2A1 is considered as immuno-histochemical astrocytic marker is responsible for processes such as cell proliferation, differentiation, apoptosis and tumour development (Kramerov *et al.*, 2006). An approximate 6.5 fold of CSNK2A1 in serum-deprived cells as compared to hypoxia, thus, demonstrates a more proliferative nature of serum-deprived cells. CSNK2A1 is also noted to be linked with the down-regulated expression of Hsp90 β 1 in the undifferentiated as compared to the control, signifying an alteration in the cell cycle phases and increased chemosensitivity of tumour cells (Liu *et al.*, 1999).

A direct connection of EIF4e was observed with vimentin and GAPDH. In addition to its implication in prognosis of pancreatic cancer and breast cancer progression, EIF4e activated Sox2 in glial cells at the transitional level conferring them with pluripotency and self-renewal properties (Ge *et al.*, 2010). EIF4e facilitates the synthesis of several powerful tumour angiogenic factors (FGF-2 and VEGF) by selectively enhancing their translation. Hypoxia increases EIF4e expression marking the transition of the vascular phase of cancer progression (Defatta *et al.*, 1999). By promoting cellular proliferation through Akt activation, EIF4e helps serum-deprived cells to escape from the apoptotic stimuli (Culjkovic *et al.*, 2008). EIF4e showed an identical expression in the hypoxic as well as serum-deprived cells, indicating that it serves as an oncogene promoting tumour progression under conditions of undifferentiation irrespective of the type of micro-environmental changes induced.

HNRNPK is a protein that shows multiple interactions with other proteins related to different types of cancers. HNRNPK is directly involved in head and neck cancer, through ANXA2 it is related to cholangiocarcinoma, prostatic and cervical cancer. TPI1 and HspA8 links HNRNPK to liver and hepatocellular carcinoma. This protein was found to be up-regulated by 5.1 fold in cells deprived of serum when compared to the hypoxic cells. In response to extra-cellular signals, HNRNPK directly regulates the rate of transcription and translation. An enhanced nuclear expression of HNRNPK was observed in fast proliferating cells with increased levels of tyrosine phosphorylation (Ostrowski and Bomsztyk, 2003). An elevated level of HNRNPK in serum free condition supplemented with growth factors may support the proliferation of cells; therefore, HNRNPK can be used as a differentiation marker.

Cells of different origin derived from diverse molecular mechanisms give rise to different types of CSCs. A recent study performed on 17 glioblastoma multiforme

(GBM) CSC lines displayed two different groups of CSC lines: Type I “proneural” signature genes that resemble foetal NSC (fNSC; CD133⁺ and the formation of neurospheres) and Type II “mesenchymal” transcriptional profile similar to adult NSC (aNSC; CD133⁻ and semi-adherent growth) (Lottaz *et al.*, 2010). GBM originates from CSCs that arise with preserved features of NSC via the process of undifferentiation (Lee *et al.*, 2006). Aligning the present proteomic studies to this research based on 24-gene signature indicated that the state of hypoxia and serum deprivation could inhibit Type I CSCs. The proteins identified within the dataset included BMP2 which should be present in Type II CSCs, ELF4 and HSPs which should be expressed in Type II CSCs. In the entire study BMP2 protein expression was not detected, the proteomic investigation implicated an up-regulation of ELF4e and Hsp90 β , supporting the hypothesis of Type I CSCs resembling fNSCs. Furthermore, Type II CSCs can be reprogrammed towards pluripotency by activation of Oct4 (Zheng *et al.*, 2008). The absence of Oct4-A protein in the dataset provided by the proteomics analysis could be attributed to the post translational modification or degradation. An abundant expression of Oct4-A protein detected in the control, hypoxic and serum-deprived U87-MG cells by flow cytometric analysis and immunofluorescent studies indicate micro-environmental changes can induce stem like cells. However, there exists a different molecular mechanism which contributes to tumorigenesis via CD133⁻.

Conclusion

In conclusion, the hypothesis that Oct4-A and BMP2 could be glioma stem cell markers did not prove to be correct. In this study observation of CD133 expression in hypoxic U87-MG cells through flow cytometric analysis indicated that CD133 could be used a marker for Type I stem cells or its progenitors which have acquired stem cell-like function due to an altered micro-environment. Undifferentiation conditions of serum deprivation did not display the expression of stem cell-related markers. However, the cells were found to be more chemosensitive as compared to the control and hypoxic cells. In addition, cell cycle analysis confirmed the chemotherapeutic potential of Taxol as compared to TMZ in inhibiting glioma cell proliferation. Furthermore, proteomic analysis provided an insight in the altered mechanism/s in the differentiated and undifferentiated cells as well as between the two different micro-environmental conditions used to attain the undifferentiated state (hypoxia and serum deprivation). The IPA analysis confirmed the participation of the majority of the proteins in altering the cell cycle phases that needs to be further investigated in order to understand the deregulated mechanism in NSCs and CSCs. Proteomic studies enlisted a few markers which could be selected to isolate CSCs from the bulk tumour mass using western blot technique. Proteins such as UDG, PGK1, HNRNPK and moesin can be used as markers to identify a group of differentiated cells in glioma. Vimentin, EIF4e, CSNK2A1 can be further investigated in downstream experiments to support proteomic analysis and to define their contribution in the initiation of brain tumours.

The present study suggests that Laminin binding protein associated with Integrin $\alpha6\beta1$ and BMP2 could be explored in future research and as a potential biomarker for the isolation of glioma stem cells.

It could be hypothesised that both hypoxia and serum deprivation support the process of cellular undifferentiation. However, hypoxic conditions result in rapid onset of CSC related properties. Serum deprivation, on the other hand, introduces a gradual change in the stemness related features of the undifferentiated glioma cells. Both these micro-environmental changes result in the derivation of Type I CSCs. Further work needs to focus on identification of Type II CSCs based on their transcriptional and proteome profiles. Therapeutics, therefore need to identify both these sub types of CSCs and eliminate them in order to cure glioma.

Future work (Molecular targets to study glioma stem cells)

Cancer stem cells divide symmetrically resulting in identical daughter cells conferring them with self-renewal properties and asymmetric division results in a stem cell and a progenitor (Clarkes *et al.*, 2006). However, recent data suggest that the description of asymmetric division within a cancer stem cell decides the cells fate by means of the segregation of the template DNA to the daughter cell (Pine *et al.*, 2010). In order to draw a conclusion, two prospects need to be confirmed as to whether tumours originate from existing stem cells which have self-renewal capacity but acquire epigenetic and genetic alterations or the progenitor cells may act as cancer stem cells on attainment of their self-renewal ability (Clarkes *et al.*, 2006). Both these probabilities could occur making it essential to confirm the role stem cells play in cancer. Moreover, resistance to drugs and therapeutic strategies have been associated with self-renewal properties of stem cells. A high expression of homeobox protein-A10 (HOXA10; stem cell progenitor marker) gene together with the co-expression of growth arrest and DNA-damage-inducible protein, Gamma (GADD45G; cell cycle checkpoint gene) is responsible for resistance towards TMZ and chemotherapy in

general (Murat *et al.*, 2008). An in depth study of the asymmetric division and discovery of such specific genes could help target CSCs and minimize drug resistance.

The detection of recurrence cancer stem cells (rCSCs) could also be evidence towards tumour relapse. Cell fusion is the mechanism through which rCSCs are generated yielding highly proliferative hybrid cells. The origination of rCSCs occurs during first line therapy resulting into a cell progeny that is highly malignant and resistant to first line therapy that has been shown to have an increased resistance to apoptosis (Dittmar *et al.*, 2009). It is believed that all tumour cells are fusogenic and their capacity to fuse remains unlimited, however, the grade of cell fusion differs amongst the tumour cell lines (Duelli and Lazebnik, 2003). Therefore, if fusion of a NSC with a tumour cell occurs there is a possibility that the resultant CSCs exhibit an enhanced proliferative potential with increased drug resistance. A study combining cancer cell division, drug-resistance, rCSCs and the stem cell niche could help identify true tumour-initiating cells. Furthermore, proteomic studies focusing on the cancer altered signalling pathways can provide a better understanding of glioma with regards to treatment.

Chapter 5

References

Abiatari I, Esposito I, Oliveira TD, Felix K, Xin H, Penzel R, Giese T, Friess H, & Kleeff J (2010). Moesin-dependent cytoskeleton remodelling is associated with an anaplastic phenotype of pancreatic cancer. *J Cell Mol Med* **14**, 1166-1179.

Adams J. (2008) The Proteome: Discovering the Structure and Function of Proteins. *Nat Edu.* **1**, 3 (An abstract).

An JH, Lee SY, Jeon JY, Cho KG, Kim SU, & Lee MA (2009). Identification of gliotropic factors that induce human stem cell migration to malignant tumor. *J Proteome Res* **8**, 2873-2881.

Aprelikova ON & Tomilin NV (1982). Activity of uracil-DNA glycosylase in different rat tissues and in regenerating rat liver. *FEBS Lett* **137**, 193-195.

Atlasi Y, Mowla SJ, Ziaee SA, Gokhale PJ, & Andrews PW (2008). OCT4 spliced variants are differentially expressed in human pluripotent and nonpluripotent cells. *Stem Cells* **26**, 3068-3074.

Bachoo RM, Maher EA, Ligon KL, Sharpless NE, Chan SS, You MJ, Tang Y, DeFrances J, Stover E, Weissleder R, Rowitch DH, Louis DN, & DePinho RA (2002). Epidermal growth factor receptor and Ink4a/Arf: convergent mechanisms governing terminal differentiation and transformation along the neural stem cell to astrocyte axis. *Cancer Cell* **1**, 269-277.

Bakos E & Homolya L (2007). Portrait of multifaceted transporter, the multidrug resistance-associated protein 1 (MRP1/ABCC1). *Pflugers Arch* **453**, 621-641.

Baltimore D (2001). Our genome unveiled. *Nature* **409**, 814-816.

Bao S, Wu Q, McLendon RE, Hao Y, Shi Q, Hjelmeland AB, Dewhirst MW, Bigner DD, & Rich JN (2006). Glioma stem cells promote radioresistance by preferential activation of the DNA damage response. *Nature* **444**, 756-760.

Basso AD, Solit DB, Chiosis G, Giri B, Tsihchlis P, & Rosen N (2002). Akt forms an intracellular complex with heat shock protein 90 (Hsp90) and Cdc37 and is destabilized by inhibitors of Hsp90 function. *J Biol Chem* **277**, 39858-39866.

Baxi MD & Vishwanatha JK (1995). Uracil DNA-glycosylase/glyceraldehyde-3-phosphate dehydrogenase is an Ap4A binding protein. *Biochemistry* **34**, 9700-9707.

Beier D, Hau P, Proescholdt M, Lohmeier A, Wischhusen J, Oefner PJ, Aigner L, Brawanski A, Bogdahn U, & Beier CP (2007). CD133(+) and CD133(-) glioblastoma-derived cancer stem cells show differential growth characteristics and molecular profiles. *Cancer Res* **67**, 4010-4015.

Bensmail H & Haoudi A (2003). Postgenomics: Proteomics and Bioinformatics in Cancer Research. *J Biomed Biotechnol* **4**, 217-230.

Bi CL, Fang JS, Chen FH, Wang YJ, & Wu J (2007). [Chemoresistance of CD133(+) tumor stem cells from human brain glioma]. *Zhong Nan Da Xue Xue Bao Yi Xue Ban* **32**, 568-573.

Bouamrani A, Ramus C, Gay E, Pelletier L, Cubizolles M, Brugiere S, Wion D, Berger F, & Issartel JP (2010). Increased phosphorylation of vimentin in noninfiltrative meningiomas. *PLoS One* **5**, e9238 (An abstract).

Boyer LA, Lee TI, Cole MF, Johnstone SE, Levine SS, Zucker JP, Guenther MG, Kumar RM, Murray HL, Jenner RG, Gifford DK, Melton DA, Jaenisch R, & Young RA (2005). Core transcriptional regulatory circuitry in human embryonic stem cells. *Cell* **122**, 947-956.

Bradford MM (1976). A rapid and sensitive method for the quantitation of microgram quantities of protein utilizing the principle of protein-dye binding. *Anal Biochem* **72**, 248-254.

Brahimi-Horn MC, Chiche J, & Pouyssegur J (2007). Hypoxia and cancer. *J Mol Med* **85**, 1301-1307.

Bramanti V, Bronzi D, Tomassoni D, Costa A, Raciti G, Avitabile M, Amenta F, & Avola R (2008). Growth factors and steroid mediated regulation of cytoskeletal protein expression in serum-deprived primary astrocyte cultures. *Neurochem Res* **33**, 2593-2600.

Calderwood SK, Theriault JR, & Gong J (2005). Message in a bottle: role of the 70-kDa heat shock protein family in anti-tumor immunity. *Eur J Immunol* **35**, 2518-2527.

Capper D, Gaiser T, Hartmann C, Habel A, Mueller W, Herold-Mende C, von DA, & Siegelin MD (2009). Stem cell-like glioma cells are resistant to TRAIL/Apo2L and exhibit down-regulation of caspase-8 by promoter methylation. *Acta Neuropathol* **117**, 445-456.

Caradonna S & Muller-Weeks S (2001). The nature of enzymes involved in uracil-DNA repair: isoform characteristics of proteins responsible for nuclear and mitochondrial genomic integrity. *Curr Protein Pept Sci* **2**, 335-347.

Cardone RA, Casavola V, & Reshkin SJ (2005). The role of disturbed pH dynamics and the Na⁺/H⁺ exchanger in metastasis. *Nat Rev Cancer* **5**, 786-795.

Chen YC, Hsu HS, Chen YW, Tsai TH, How CK, Wang CY, Hung SC, Chang YL, Tsai ML, Lee YY, Ku HH, & Chiou SH (2008). Oct-4 expression maintained cancer stem-like properties in lung cancer-derived CD133-positive cells. *PLoS One* **3**, e2637 (An abstract).

Chung HJ, Yoon SI, Shin SH, Koh YA, Lee SJ, Lee YS, & Bae S (2006). p53-Mediated enhancement of radiosensitivity by selenophosphate synthetase 1 overexpression. *J Cell Physiol* **209**, 131-141.

Clarke MF, Dick JE, Dirks PB, Eaves CJ, Jamieson CH, Jones DL, Visvader J, Weissman IL, & Wahl GM (2006). Cancer stem cells--perspectives on current status and future directions: AACR Workshop on cancer stem cells. *Cancer Res* **66**, 9339-9344.

Clement V, Dutoit V, Marino D, Dietrich PY, & Radovanovic I (2009). Limits of CD133 as a marker of glioma self-renewing cells. *Int J Cancer* **125**, 244-248.

Colinge J, Masselot A, Giron M, Dessingy T, & Magnin J (2003). OLAV: towards high-throughput tandem mass spectrometry data identification. *Proteomics* **3**, 1454-1463.

Cooper JA & Sept D (2008). New insights into mechanism and regulation of actin capping protein. *Int Rev Cell Mol Biol* **267**, 183-206.

Corsini NS & Martin-Villalba A (2010). Integrin alpha 6: anchors away for glioma stem cells. *Cell Stem Cell* **6**, 403-404.

Croft DR, Sahai E, Mavria G, Li S, Tsai J, Lee WM, Marshall CJ, & Olson MF (2004). Conditional ROCK activation in vivo induces tumor cell dissemination and angiogenesis. *Cancer Res* **64**, 8994-9001.

Culjkovic B, Tan K, Orolicki S, Amri A, Meloche S, & Borden KL (2008). The eIF4E RNA regulon promotes the Akt signaling pathway. *J Cell Biol* **181**, 51-63.

Dang C and Jayasena SD (1996). Oligonucleotide Inhibitors of Taq DNA polymerase Facilitate Detection of Low Copy Number Targets by PCR. *J Mol Biol.* **264**, 268-278.

Dasari VR, Kaur K, Velpula KK, Gujrati M, Fassett D, Klopfenstein JD, Dinh DH, & Rao JS (2010). Upregulation of PTEN in glioma cells by cord blood mesenchymal stem cells inhibits migration via downregulation of the PI3K/Akt pathway. *PLoS One* **5**, e10350 (An abstract).

DeFatta RJ, Turbat-Herrera EA, Li BD, Anderson W, & De BA (1999). Elevated expression of eIF4E in confined early breast cancer lesions: possible role of hypoxia. *Int J Cancer* **80**, 516-522.

Dejgaard K, Leffers H, Rasmussen HH, Madsen P, Kruse TA, Gesser B, Nielsen H, & Celis JE (1994). Identification, molecular cloning, expression and chromosome mapping of a family of transformation upregulated hnRNP-K proteins derived by alternative splicing. *J Mol Biol* **236**, 33-48.

Dey M, Ulasov IV, & Lesniak MS (2010). Virotherapy against malignant glioma stem cells. *Cancer Lett* **289**, 1-10.

Dieffenbach CW, Lowe TMJ, Dveksler GS (1993). General concepts for PCR primer design. *PCR Methods Appl* **3**, S30-S37.

Dittmar T, Nagler C, Schwitalla S, Reith G, Niggemann B, & Zanker KS (2009). Recurrence cancer stem cells--made by cell fusion? *Med Hypotheses* **73**, 542-547.

Duelli D & Lazebnik Y (2003). Cell fusion: a hidden enemy? *Cancer Cell* **3**, 445-448.

Duncan MW & Hunsucker SW (2005). Proteomics as a tool for clinically relevant biomarker discovery and validation. *Exp Biol Med (Maywood)* **230**, 808-817.

Engel M, Mazurek S, Eigenbrodt E, & Welter C (2004). Phosphoglycerate mutase-derived polypeptide inhibits glycolytic flux and induces cell growth arrest in tumor cell lines. *J Biol Chem* **279**, 35803-35812.

Fargeas CA, Corbeil D, & Huttner WB (2003). AC133 antigen, CD133, prominin-1, prominin-2, etc.: prominin family gene products in need of a rational nomenclature. *Stem Cells* **21**, 506-508.

Fenstermacher D (2005). Introduction to Bioinformatics. *JASIST* **56**, 440-446.

Fiore G, Di CC, Monti G, Amoresano A, Columbano L, Pucci P, Cioffi FA, Di CA, Palumbo A, & d'Ischia M (2006). Tubulin nitration in human gliomas. *Neurosci Lett* **394**, 57-62.

Fischer H, Taylor N, Allerstorfer S, Grusch M, Sonvilla G, Holzmann K, Setinek U, Elbling L, Cantonati H, Grasl-Kraupp B, Gauglhofer C, Marian B, Micksche M, & Berger W (2008). Fibroblast growth factor receptor-mediated signals contribute to the malignant phenotype of non-small cell lung cancer cells: therapeutic implications and synergism with epidermal growth factor receptor inhibition. *Mol Cancer Ther* **7**, 3408-3419.

Fournier B, Bendeif e, Guillot B, Podjarny A, Lecomte C, & Jelsch C (2009). Charge density and electrostatic interactions of fidarestat, an inhibitor of human aldose reductase. *J Am Chem Soc* **131**, 10929-10941.

Freshney, R (1987) Culture of Animal Cells: A Manual of Basic Technique. *Liss, Inc., New York*. pp 117.

Friedman HS, Kerby T, & Calvert H (2000). Temozolomide and treatment of malignant glioma. *Clin Cancer Res* **6**, 2585-2597.

Fruehauf JP, Brem H, Brem S, Sloan A, Barger G, Huang W, & Parker R (2006). In vitro drug response and molecular markers associated with drug resistance in malignant gliomas. *Clin Cancer Res* **12**, 4523-4532.

Fu J, Liu ZG, Liu XM, Chen FR, Shi HL, Pangjesse CS, Ng HK, & Chen ZP (2009). Glioblastoma stem cells resistant to temozolomide-induced autophagy. *Chin Med J (Engl)* **122**, 1255-1259.

Gage FH (2000). Mammalian neural stem cells. *Science* **287**, 1433-1438.

Garcia R, Franklin RA, & McCubrey JA (2006). EGF induces cell motility and multi-drug resistance gene expression in breast cancer cells. *Cell Cycle* **5**, 2820-2826.

Ge Y, Zhou F, Chen H, Cui C, Liu D, Li Q, Yang Z, Wu G, Sun S, Gu J, Wei Y, & Jiang J (2010). Sox2 is translationally activated by eukaryotic initiation factor 4E in human glioma-initiating cells. *Biochem Biophys Res Commun* **397**, 711-717.

Geer LY, Markey SP, Kowalak JA, Wagner L, Xu M, Maynard DM, Yang X, Shi W, & Bryant SH (2004). Open mass spectrometry search algorithm. *J Proteome Res* **3**, 958-964.

Gidekel S, Pizov G, Bergman Y, & Pikarsky E (2003). Oct-3/4 is a dose-dependent oncogenic fate determinant. *Cancer Cell* **4**, 361-370.

Globus JH & Kuhlenbeck H (1944). The subependymal cell plate (matrix) and its relationship to brain tumors of the ependymal type. *J Neuropathol Exp Neurol* **3**, 1-35.

Godovac-Zimmermann J, Soskic V, Poznanovic S, & Brianza F (1999). Functional proteomics of signal transduction by membrane receptors. *Electrophoresis* **20**, 952-961.

Gottesman MM & Pastan I (1993). Biochemistry of multidrug resistance mediated by the multidrug transporter. *Annu Rev Biochem* **62**, 385-427.

Goyeneche AA, Harmon JM, & Telleria CM (2006). Cell death induced by serum deprivation in luteal cells involves the intrinsic pathway of apoptosis. *Reproduction* **131**, 103-111.

Guicciardi ME, Deussing J, Miyoshi H, Bronk SF, Svingen PA, Peters C, Kaufmann SH, & Gores GJ (2000). Cathepsin B contributes to TNF-alpha-mediated hepatocyte apoptosis by promoting mitochondrial release of cytochrome c. *J Clin Invest* **106**, 1127-1137.

Gupta V, Su YS, Wang W, Kardosh A, Liebes LF, Hofman FM, Schonthal AH, & Chen TC (2006). Enhancement of glioblastoma cell killing by combination treatment with temozolomide and tamoxifen or hypericin. *Neurosurg Focus* **20**, E20 (An abstract).

Gygi SP, Rist B, Gerber SA, Turecek F, Gelb MH, & Aebersold R (1999). Quantitative analysis of complex protein mixtures using isotope-coded affinity tags. *Nat Biotechnol* **17**, 994-999.

Hambardzumyan D, Squatrito M, & Holland EC (2006). Radiation resistance and stem-like cells in brain tumors. *Cancer Cell* **10**, 454-456.

Hatzivassiliou G, Zhao F, Bauer DE, Andreadis C, Shaw AN, Dhanak D, Hingorani SR, Tuveson DA, & Thompson CB (2005). ATP citrate lyase inhibition can suppress tumor cell growth. *Cancer Cell* **8**, 311-321.

Heck AJ, Mummery C, Whetton A, Oh S, Lee B, Pera M, Lemischka I, & Krijgsveld J (2007). Proteome biology of stem cells. *Stem Cell Res* **1**, 7-8.

Heddleston JM, Li Z, McLendon RE, Hjelmeland AB, & Rich JN (2009). The hypoxic microenvironment maintains glioblastoma stem cells and promotes reprogramming towards a cancer stem cell phenotype. *Cell Cycle* **8**, 3274-3284.

Heese O, Disko A, Zirkel D, Westphal M, & Lamszus K (2005). Neural stem cell migration toward gliomas in vitro. *Neuro Oncol* **7**, 476-484.

Hughes SJ, Glover TW, Zhu XX, Kuick R, Thoraval D, Orringer MB, Beer DG, & Hanash S (1998). A novel amplicon at 8p22-23 results in overexpression of cathepsin B in esophageal adenocarcinoma. *Proc Natl Acad Sci U S A* **95**, 12410-12415.

Inoue A, Sawata SY, Taira K, & Wadhwa R (2007). Loss-of-function screening by randomized intracellular antibodies: identification of hnRNP-K as a potential target for metastasis. *Proc Natl Acad Sci U S A* **104**, 8983-8988.

Issaq HJ, Conrads TP, Janini GM, & Veenstra TD (2002). Methods for fractionation, separation and profiling of proteins and peptides. *Electrophoresis* **23**, 3048-3061.

Johannessen TC, Bjerkvig R, & Tysnes BB (2008). DNA repair and cancer stem-like cells -potential partners in glioma drug resistance? *Cancer Treat Rev* **34**, 558-567.

Kang SK, Park JB, & Cha SH (2006). Multipotent, dedifferentiated cancer stem-like cells from brain gliomas. *Stem Cells Dev* **15**, 423-435.

Kanzawa T, Bedwell J, Kondo Y, Kondo S, & Germano IM (2003). Inhibition of DNA repair for sensitizing resistant glioma cells to temozolomide. *J Neurosurg* **99**, 1047-1052.

Kanzawa T, Germano IM, Komata T, Ito H, Kondo Y, & Kondo S (2004). Role of autophagy in temozolomide-induced cytotoxicity for malignant glioma cells. *Cell Death Differ* **11**, 448-457.

Karp G (2009). Cancers. *Cell and Molecular Biology: Concepts and Experiments* **6**. 652-653.

Katsumoto T, Mitsushima A, & Kurimura T (1990). The role of the vimentin intermediate filaments in rat 3Y1 cells elucidated by immunoelectron microscopy and computer-graphic reconstruction. *Biol Cell* **68**, 139-146.

Kawataki T, Yamane T, Naganuma H, Rouselle P, Anduren I, Tryggvason K, & Patarroyo M (2007). Laminin isoforms and their integrin receptors in glioma cell migration and invasiveness: Evidence for a role of alpha5-laminin(s) and alpha3beta1 integrin. *Exp Cell Res* **313**, 3819-3831.

Keith B & Simon MC (2007). Hypoxia-inducible factors, stem cells, and cancer. *Cell* **129**, 465-472.

Kemper K, Sprick MR, de BM, Scopelliti A, Vermeulen L, Hoek M, Zeilstra J, Pals ST, Mehmet H, Stassi G, & Medema JP (2010). The AC133 epitope, but not the CD133 protein, is lost upon cancer stem cell differentiation. *Cancer Res* **70**, 719-729.

Khalil AA, & Madhamshetty J (2006). Proteome Analysis of Whole-cell Lysates of Human Glioblastoma Cells During Passages. *Res J Med Med Sci* **1**, 120-131.

Kievit FM, Florczyk SJ, Leung MC, Veisoh O, Park JO, Disis ML, & Zhang M (2010). Chitosan-alginate 3D scaffolds as a mimic of the glioma tumor microenvironment. *Biomaterials* **31**, 5903-5910.

Kim JB, Sebastiano V, Wu G, Arauzo-Bravo MJ, Sasse P, Gentile L, Ko K, Ruau D, Ehrich M, van den Boom D, Meyer J, Hubner K, Bernemann C, Ortmeier C, Zenke M, Fleischmann BK, Zaehres H, & Scholer HR (2009). Oct4-induced pluripotency in adult neural stem cells. *Cell* **136**, 411-419.

Kim TD (2000). PCR primer design: an inquiry-based introduction to bioinformatics on the World Wide Web. *Biochem Mol Bio Educ* **28**,274 -276.

Kitange GJ, Smith JS, & Jenkins RB (2001). Genetic alterations and chemotherapeutic response in human diffuse gliomas. *Expert Rev Anticancer Ther* **1**, 595-605.

Kleihues P, Cavenee, WK (2000). Pathology & genetics of tumours of the nervous system. IARC Press. Lyon, pp. 9-80.

Kondziolka D & Bilbao JM (1988). Mixed ependymoma-astrocytoma (subependymoma?) of the cerebral cortex. *Acta Neuropathol* **76**, 633-637.

Kosodo Y, Roper K, Haubensak W, Marzesco AM, Corbeil D, & Huttner WB (2004). Asymmetric distribution of the apical plasma membrane during neurogenic divisions of mammalian neuroepithelial cells. *EMBO J* **23**, 2314-2324.

Kramerov AA, Saghizadeh M, Pan H, Kabosova A, Montenarh M, Ahmed K, Penn JS, Chan CK, Hinton DR, Grant MB, & Ljubimov AV (2006). Expression of protein kinase CK2 in astroglial cells of normal and neovascularized retina. *Am J Pathol* **168**, 1722-1736.

Kruman II, Schwartz E, Kruman Y, Cutler RG, Zhu X, Greig NH, & Mattson MP (2004). Suppression of uracil-DNA glycosylase induces neuronal apoptosis. *J Biol Chem* **279**, 43952-43960.

Lavictoire SJ, Parolin DA, Klimowicz AC, Kelly JF, & Lorimer IA (2003). Interaction of Hsp90 with the nascent form of the mutant epidermal growth factor receptor EGFRvIII. *J Biol Chem* **278**, 5292-5299.

Le MN, Rossini A, Gasparetto M, Smith C, Brinkman RR, & Gentleman R (2007). Data quality assessment of ungated flow cytometry data in high throughput experiments. *Cytometry A* **71**, 393-403.

Le PF, Randrianarison V, Marot D, Cabannes J, Perricaudet M, Feunteun J, & Sarasin A (2000). BRCA1 and BRCA2 are necessary for the transcription-coupled repair of the oxidative 8-oxoguanine lesion in human cells. *Cancer Res* **60**, 5548-5552.

Lee J, Kim HK, Rho JY, Han YM, & Kim J (2006). The human OCT-4 isoforms differ in their ability to confer self-renewal. *J Biol Chem* **281**, 33554-33565.

Lee J, Kotliarova S, Kotliarov Y, Li A, Su Q, Donin NM, Pastorino S, Purow BW, Christopher N, Zhang W, Park JK, & Fine HA (2006). Tumor stem cells derived from glioblastomas cultured in bFGF and EGF more closely mirror the phenotype and genotype of primary tumors than do serum-cultured cell lines. *Cancer Cell* **9**, 391-403.

Lengner CJ, Camargo FD, Hochedlinger K, Welstead GG, Zaidi S, Gokhale S, Scholer HR, Tomilin A, & Jaenisch R (2007). Oct4 expression is not required for mouse somatic stem cell self-renewal. *Cell Stem Cell* **1**, 403-415.

Li Z, Wang H, Eyler CE, Hjelmeland AB, & Rich JN (2009). Turning cancer stem cells inside out: an exploration of glioma stem cell signaling pathways. *J Biol Chem* **284**, 16705-16709.

Liang YJ, Chen CY, Juang SJ, Lai LP, Shyu KG, Wang BW, Liu SY, & Leu JG (2010). Peroxisome proliferator-activated receptor delta agonists attenuated the C-reactive protein-induced pro-inflammation in cardiomyocytes and H9c2 cardiomyoblasts. *Eur J Pharmacol* **643**, 84-92.

Lindquist S & Craig EA (1988). The heat-shock proteins. *Annu Rev Genet* **22**, 631-677.

Liu G, Yuan X, Zeng Z, Tunici P, Ng H, Abdulkadir IR, Lu L, Irvin D, Black KL, & Yu JS (2006). Analysis of gene expression and chemoresistance of CD133+ cancer stem cells in glioblastoma. *Mol Cancer* **5**, 67 (An abstract).

Liu HG & Zhang XH (2009). How to search for specific markers of cancer stem cells. *Asian Pac J Cancer Prev* **10**, 177-180.

Liu Q, Nguyen DH, Dong Q, Shitaku P, Chung K, Liu OY, Tso JL, Liu JY, Konkankit V, Cloughesy TF, Mischel PS, Lane TF, Liau LM, Nelson SF, & Tso CL (2009). Molecular properties of CD133+ glioblastoma stem cells derived from treatment-refractory recurrent brain tumors. *J Neurooncol* **94**, 1-19.

Liu T, Guevara OE, Warburton RR, Hill NS, Gaestel M, & Kayyali US (2010). Regulation of vimentin intermediate filaments in endothelial cells by hypoxia. *Am J Physiol Cell Physiol* **299**, C363-C373.

Liu XL, Xiao B, Yu ZC, Guo JC, Zhao QC, Xu L, Shi YQ, & Fan DM (1999). Down-regulation of Hsp90 could change cell cycle distribution and increase drug sensitivity of tumor cells. *World J Gastroenterol* **5**, 199-208.

Long X, Olszewski M, Huang W, & Kletzel M (2005). Neural cell differentiation in vitro from adult human bone marrow mesenchymal stem cells. *Stem Cells Dev* **14**, 65-69.

Lottaz C, Beier D, Meyer K, Kumar P, Hermann A, Schwarz J, Junker M, Oefner PJ, Bogdahn U, Wischhusen J, Spang R, Storch A, & Beier CP (2010). Transcriptional profiles of CD133+ and C. *Cancer Res* **70**, 2030-2040.

Lu W, Lee HK, Cazacu S, Finniss S, Xiang C, Zenklusen J, Fine HA, Rennert J, Berens ME, Mikkelsen T, & Brodie C (2006). BMP2 is highly expressed in gliomas correlated with glioma patient survival and regulates the proliferation and migration of glioma cells. *Proc Amer Assoc Cancer Res* **47**, 5266 (An abstract).

Lu, C (2008) Expression profile of multidrug resistance genes and proteins in cancerous and stem cells. University of Central Lancashire PhD theses collection.

Maher EA, Furnari FB, Bachoo RM, Rowitch DH, Louis DN, Cavenee WK, & DePinho RA (2001). Malignant glioma: genetics and biology of a grave matter. *Genes Dev* **15**, 1311-1333.

Mann M, Hojrup P, & Roepstorff P (1993). Use of mass spectrometric molecular weight information to identify proteins in sequence databases. *Biol Mass Spectrom* **22**, 338-345.

Mansur NR, Meyer-Siegler K, Wurzer JC, & Sirover MA (1993). Cell cycle regulation of the glyceraldehyde-3-phosphate dehydrogenase/uracil DNA glycosylase gene in normal human cells. *Nucleic Acids Res* **21**, 993-998.

Marouga R, David S, & Hawkins E (2005). The development of the DIGE system: 2D fluorescence difference gel analysis technology. *Anal Bioanal Chem* **382**, 669-678.

McCord AM, Jamal M, Shankavaram UT, Lang FF, Camphausen K, & Tofilon PJ (2009). Physiologic oxygen concentration enhances the stem-like properties of CD133+ human glioblastoma cells in vitro. *Mol Cancer Res* **7**, 489-497.

Medzihradzky KF, Campbell JM, Baldwin MA, Fallick AM, Juhasz P, Vestal ML, & Burlingame AL (2000). The characteristics of peptide collision-induced dissociation

using a high-performance MALDI-TOF/TOF tandem mass spectrometer. *Anal Chem* **72**, 552-558.

Meyer-Siegler K, Mauro DJ, Seal G, Wurzer J, deRiel JK, & Sirover MA (1991). A human nuclear uracil DNA glycosylase is the 37-kDa subunit of glyceraldehyde-3-phosphate dehydrogenase. *Proc Natl Acad Sci U S A* **88**, 8460-8464.

Minden J (2007). Comparative proteomics and difference gel electrophoresis. *Biotechniques* **43**, 739, 741, 743.

Mohammed, K (2007). A study of gene expression in human normal and carcinogenic cell lines using qRT-PCR. *Theses Collection 572.865/MOH University of Central Lancashire theses collection*.

Nagelhus TA, Slupphaug G, Lindmo T, & Krokan HE (1995). Cell cycle regulation and subcellular localization of the major human uracil-DNA glycosylase. *Exp Cell Res* **220**, 292-297.

Nakano I, Saigusa K, & Kornblum HI (2008). BMPing off glioma stem cells. *Cancer Cell* **13**, 3-4.

Nichols J, Zevnik B, Anastassiadis K, Niwa H, Klewe-Nebenius D, Chambers I, Scholer H, & Smith A (1998). Formation of pluripotent stem cells in the mammalian embryo depends on the POU transcription factor Oct4. *Cell* **95**, 379-391.

Nobuyoshi S, Ryoji Y, Koichiro O, Osamu N, Nobuyuki S, & Katsuyuki K (2006). Local Recurrence of Metastatic Brain Tumor after Surgery. *Jpn J Cancer Clin* **51**, 933-937.

Nospikel T & Hanawalt PC (2002). DNA repair in terminally differentiated cells. *DNA Repair (Amst)* **1**, 59-75.

O'Brien LE, Jou TS, Pollack AL, Zhang Q, Hansen SH, Yurchenco P, & Mostov KE (2001). Rac1 orientates epithelial apical polarity through effects on basolateral laminin assembly. *Nat Cell Biol* **3**, 831-838.

Ostrowski J & Bomsztyk K (2003). Nuclear shift of hnRNP K protein in neoplasms and other states of enhanced cell proliferation. *Br J Cancer* **89**, 1493-1501.

Pappin DJ, Hojrup P, & Bleasby AJ (1993). Rapid identification of proteins by peptide-mass fingerprinting. *Curr Biol* **3**, 327-332.

Park CK, Kim JH, Moon MJ, Jung JH, Lim SY, Park SH, Kim JH, Kim DG, Jung HW, Cho BK, & Paek SH (2008). Investigation of molecular factors associated with malignant transformation of oligodendroglioma by proteomic study of a single case of rapid tumor progression. *J Cancer Res Clin Oncol* **134**, 255-262.

Piccirillo SG & Vescovi AL (2006). Bone morphogenetic proteins regulate tumorigenicity in human glioblastoma stem cells. *Ernst Schering Found Symp Proc* **5**. 59-81.

Piccirillo SG, Reynolds BA, Zanetti N, Lamorte G, Binda E, Broggi G, Brem H, Olivi A, Dimeco F, & Vescovi AL (2006). Bone morphogenetic proteins inhibit the tumorigenic potential of human brain tumour-initiating cells. *Nature* **444**, 761-765.

Pine SR, Ryan BM, Varticovski L, Robles AI, & Harris CC (2010). Microenvironmental modulation of asymmetric cell division in human lung cancer cells. *Proc Natl Acad Sci U S A* **107**, 2195-2200.

Pistollato F, Abbadi S, Rampazzo E, Persano L, Della PA, Frasson C, Sarto E, Scienza R, D'Avella D, & Basso G (2010). Intratumoral hypoxic gradient drives stem cells distribution and MGMT expression in glioblastoma. *Stem Cells* **28**, 851-862.

Pomeroy SL, Tamayo P, Gaasenbeek M, Sturla LM, Angelo M, McLaughlin ME, Kim JYH, Goumnerova LC, Black PM, Lau C, Allen JC, Zagzag D, Olson JM, Curran T, Wetmore C, Biegel JA, Poggio T, Mukherjee S, Rifkin R, Califano A, Stolovitzky G, Louis DN, Mesirov JP, Lander ES, & Golub TR (2002). Prediction of central nervous system embryonal tumour outcome based on gene expression. *Nature* **415**, 436-442.

Pouyssegur J, Dayan F, & Mazure NM (2006). Hypoxia signalling in cancer and approaches to enforce tumour regression. *Nature* **441**, 437-443.

Rajan P, Panchision DM, Newell LF, & McKay RD (2003). BMPs signal alternately through a SMAD or FRAP-STAT pathway to regulate fate choice in CNS stem cells. *J Cell Biol* **161**, 911-921.

Rajaraman R, Guernsey DL, Rajaraman MM, & Rajaraman SR (2006). Stem cells, senescence, neosis and self-renewal in cancer. *Cancer Cell Int* **6**, 25 (An abstract).

Ramsey KM, Yoshino J, Brace CS, Abrassart D, Kobayashi Y, Marcheva B, Hong HK, Chong JL, Buhr ED, Lee C, Takahashi JS, Imai S, & Bass J (2009). Circadian clock feedback cycle through NAMPT-mediated NAD⁺ biosynthesis. *Science* **324**, 651-654.

Reshkin SJ, Bellizzi A, Albarani V, Guerra L, Tommasino M, Paradiso A, & Casavola V (2000). Phosphoinositide 3-kinase is involved in the tumor-specific activation of human breast cancer cell Na⁽⁺⁾/H⁽⁺⁾ exchange, motility, and invasion induced by serum deprivation. *J Biol Chem* **275**, 5361-5369.

Reya T, Morrison SJ, Clarke MF, & Weissman IL (2001). Stem cells, cancer, and cancer stem cells. *Nature* **414**, 105-111.

Rios I, Alvarez-Rodriguez R, Marti E, & Pons S (2004). Bmp2 antagonizes sonic hedgehog-mediated proliferation of cerebellar granule neurones through Smad5 signalling. *Development* **131**, 3159-3168.

Ropolo M, Daga A, Griffero F, Foresta M, Casartelli G, Zunino A, Poggi A, Cappelli E, Zona G, Spaziante R, Corte G, & Frosina G (2009). Comparative analysis of DNA repair in stem and nonstem glioma cell cultures. *Mol Cancer Res* **7**, 383-392.

Roth W, Wagenknecht B, Grimm C, Dichgans J, & Weller M (1998). Taxol-mediated augmentation of CD95 ligand-induced apoptosis of human malignant glioma cells: association with bcl-2 phosphorylation but neither activation of p53 nor G2/M cell cycle arrest. *Br J Cancer* **77**, 404-411.

Ruggero D, Montanaro L, Ma L, Xu W, Londei P, Cordon-Cardo C, & Pandolfi PP (2004). The translation factor eIF-4E promotes tumor formation and cooperates with c-Myc in lymphomagenesis. *Nat Med* **10**, 484-486.

Sabetrasekh R, Teng YD, Ourednik J, Park K, & Snyder EY (2006). Current Views of the Embryonic and Neural Stem Cell. *Cell Replacement or Molecular Repair? Cell Therapy, Stem Cells, and Brain Repair* pp 1-3.

Said HM, Hagemann C, Stojic J, Schoemig B, Vince GH, Flentje M, Roosen K, & Vordermark D (2007). GAPDH is not regulated in human glioblastoma under hypoxic conditions. *BMC Mol Biol* **8**, 55 (An abstract).

Sawa A, Khan AA, Hester LD, & Snyder SH (1997). Glyceraldehyde-3-phosphate dehydrogenase: nuclear translocation participates in neuronal and nonneuronal cell death. *Proc Natl Acad Sci U S A* **94**, 11669-11674.

Schmitz HD & Bereiter-Hahn J (2002). Glyceraldehyde-3-phosphate dehydrogenase associates with actin filaments in serum-deprived NIH 3T3 cells only. *Cell Biol Int* **26**, 155-164.

Schwartz PH, Bryant PJ, Fuja TJ, Su H, O'Dowd DK, & Klassen H (2003). Isolation and characterization of neural progenitor cells from post-mortem human cortex. *J Neurosci Res* **74**, 838-851.

Seidel S, Garvalov BK, Wirta V, von SL, Schanzer A, Meletis K, Wolter M, Sommerlad D, Henze AT, Nister M, Reifenberger G, Lundeberg J, Frisen J, & Acker T (2010). A hypoxic niche regulates glioblastoma stem cells through hypoxia inducible factor 2 alpha. *Brain* **133**, 983-995.

Sell S (2006). Cancer stem cells and differentiation therapy. *Tumour Biol* **27**, 59-70.

Shervington A & Lu C (2008). Expression of multidrug resistance genes in normal and cancer stem cells. *Cancer Invest* **26**, 535-542.

Shi H, Bencze KZ, Stemmler TL, & Philpott CC (2008). A cytosolic iron chaperone that delivers iron to ferritin. *Science* **320**, 1207-1210.

Shinohara C, Muragaki Y, Maruyama T, Shimizu S, Tanaka M, Kubota Y, Oikawa M, Nakamura R, Iseki H, Kubo O, Takakura K, & Hori T (2008). Long-term prognostic assessment of 185 newly diagnosed gliomas: Grade III glioma showed prognosis comparable to that of Grade II glioma. *Jpn J Clin Oncol* **38**, 730-733.

Shmueli O, Horn-Saban S, Chalifa-Caspi V, Shmoish M, Ophir R, Benjamin-Rodrig H, Safran M, Domany E, Lancet D (2003). GeneNote: whole genome expression profiles in normal human tissues. *C R Biol.* **326**, 1067-1072.

Singh S, Sadacharan S, Su S, Belldegrun A, Persad S, & Singh G (2003). Overexpression of vimentin: role in the invasive phenotype in an androgen-independent model of prostate cancer. *Cancer Res* **63**, 2306-2311.

Singh SK, Clarke ID, Terasaki M, Bonn VE, Hawkins C, Squire J, & Dirks PB (2003). Identification of a cancer stem cell in human brain tumors. *Cancer Res* **63**, 5821-5828.

Soeda A, Park M, Lee D, Mintz A, Androutsellis-Theotokis A, McKay RD, Engh J, Iwama T, Kunisada T, Kassam AB, Pollack IF, & Park DM (2009). Hypoxia promotes expansion of the CD133-positive glioma stem cells through activation of HIF-1alpha. *Oncogene* **28**, 3949-3959.

Strojnik T, Rosland GV, Sakariassen PO, Kavalari R, & Lah T (2007). Neural stem cell markers, nestin and musashi proteins, in the progression of human glioma: correlation of nestin with prognosis of patient survival. *Surg Neurol* **68**, 133-143.

Sui M, Dziadyk JM, Zhu X, & Fan W (2004). Cell cycle-dependent antagonistic interactions between paclitaxel and gamma-radiation in combination therapy. *Clin Cancer Res* **10**, 4848-4857.

Sun Y, Kong W, Falk A, Hu J, Zhou L, Pollard S, & Smith A (2009). CD133 (Prominin) negative human neural stem cells are clonogenic and tripotent. *PLoS One* **4**, e5498 (An abstract).

Timms JF & Cramer R (2008). Difference gel electrophoresis. *Proteomics* **8**, 4886-4897.

Tseng SH, Bobola MS, Berger MS, & Silber JR (1999). Characterization of paclitaxel (Taxol) sensitivity in human glioma- and medulloblastoma-derived cell lines. *Neuro Oncol* **1**, 101-108.

Vestling MM & Fenselau C (1994). Polyvinylidene difluoride (PVDF): an interface for gel electrophoresis and matrix-assisted laser desorption/ionization mass spectrometry. *Biochem Soc Trans* **22**, 547-551.

Wallace RB, Shaffer J, Murphy RF, Bonner J, Hirose T, Itakura K (1979). Hybridization of synthetic oligodeoxyribonucleotides to phi chi 174 DNA: the effect of single base pair mismatch. *Nucleic Acids Res.* **6**, 3543-3555.

Walsh MJ, Shue G, Spidoni K, & Kapoor A (1995). E2F-1 and a cyclin-like DNA repair enzyme, uracil-DNA glycosylase, provide evidence for an autoregulatory mechanism for transcription. *J Biol Chem* **270**, 5289-5298.

Wang B, Li W, Meng X, & Zou F (2009). Hypoxia up-regulates vascular endothelial growth factor in U-87 MG cells: involvement of TRPC1. *Neurosci Lett* **459**, 132-136.

Wang J, Sakariassen PO, Tsinkalovsky O, Immervoll H, Boe SO, Svendsen A, Prestegarden L, Rosland G, Thorsen F, Stuhr L, Molven A, Bjerkvig R, & Enger PO (2008). CD133 negative glioma cells form tumors in nude rats and give rise to CD133 positive cells. *Int J Cancer* **122**, 761-768.

Wang X & Dai J (2010). Concise review: isoforms of OCT4 contribute to the confusing diversity in stem cell biology. *Stem Cells* **28**, 885-893.

Weil RJ (2006). Glioblastoma multiforme--treating a deadly tumor with both strands of RNA. *PLoS Med* **3**, e31 (An abstract).

Wellen KE, Hatzivassiliou G, Sachdeva UM, Bui TV, Cross JR, & Thompson CB (2009). ATP-citrate lyase links cellular metabolism to histone acetylation. *Science* **324**, 1076-1080.

Whetton AD, Williamson AJ, Krijgsveld J, Lee BH, Lemischka I, Oh S, Pera M, Mummery C, & Heck AJ (2008). The time is right: proteome biology of stem cells. *Cell Stem Cell* **2**, 215-217.

White J & Dalton S (2005). Cell cycle control of embryonic stem cells. *Stem Cell Rev* **1**, 131-138.

Whiteley GR (2006). Proteomic patterns for cancer diagnosis--promise and challenges. *Mol Biosyst* **2**, 358-363.

Wicha MS, Liu S, & Dontu G (2006). Cancer stem cells: an old idea--a paradigm shift. *Cancer Res* **66**, 1883-1890.

Wong A, Mitra S, & Gupta, P (2009). Targeting brain tumor stem cells using a bispecific antibody directed against CD133+ and EGFRvIII+. *J Clin Onco*. Abstract. **27**, 15S.

Woodward WA, & Sulman EP (2008). Cancer stem cells: markers or biomarkers? *Cancer Meta Rev* **27**, 459-470.

Yates JR, III, Carmack E, Hays L, Link AJ, & Eng JK (1999). Automated protein identification using microcolumn liquid chromatography-tandem mass spectrometry. *Methods Mol Biol* **112**, 553-569.

Yu SC, Ping YF, Yi L, Zhou ZH, Chen JH, Yao XH, Gao L, Wang JM, & Bian XW (2008). Isolation and characterization of cancer stem cells from a human glioblastoma cell line U87. *Cancer Lett* **265**, 124-134.

Zeng X & Kinsella TJ (2007). A novel role for DNA mismatch repair and the autophagic processing of chemotherapy drugs in human tumor cells. *Autophagy* **3**, 368-370.

Zeppernick F, Ahmadi R, Campos B, Dictus C, Helmke BM, Becker N, Lichter P, Unterberg A, Radlwimmer B, & Herold-Mende CC (2008). Stem cell marker CD133 affects clinical outcome in glioma patients. *Clin Cancer Res* **14**, 123-129.

Zhang MH, Lee JS, Kim HJ, Jin DI, Kim JI, Lee KJ, & Seo JS (2006). HSP90 protects apoptotic cleavage of vimentin in geldanamycin-induced apoptosis. *Mol Cell Biochem* **281**, 111-121.

Zhang Z, Zhang L, Hua Y, Jia X, Li J, Hu S, Peng X, Yang P, Sun M, Ma F, & Cai Z (2010). Comparative proteomic analysis of plasma membrane proteins between human osteosarcoma and normal osteoblastic cell lines. *BMC Cancer* **10**, 206 (An abstract).

Zheng H, Ying H, Yan H, Kimmelman AC, Hiller DJ, Chen AJ, Perry SR, Tonon G, Chu GC, Ding Z, Stommel JM, Dunn KL, Wiedemeyer R, You MJ, Brennan C, Wang YA, Ligon KL, Wong WH, Chin L, & dePinho RA (2008). p53 and Pten control neural and glioma stem/progenitor cell renewal and differentiation. *Nature* **455**, 1129-1133.

Zhou M, Zhao Y, Ding Y, Liu H, Liu Z, Fodstad O, Riker AI, Kamarajugadda S, Lu J, Owen LB, Ledoux SP, & Tan M (2010). Warburg effect in chemosensitivity: targeting lactate dehydrogenase-A re-sensitizes taxol-resistant cancer cells to taxol. *Mol Cancer* **9**, 33 (An abstract).

Web References

- http://www.allthingsstemcell.com/wpcontent/uploads/2009/09/p53_cancer_cell_formation-copy2.png
- http://drugdiscoveryopinion.com/images/cancer_stem_cells.jpg
- <http://www.biotec.tu-dresden.de/research/corbeil/>
- <http://njms.umdnj.edu/gsbs/stemcell/scofthemonth/esc/2.jpg>
- <http://rulai.cshl.edu/TRED/GRN/Oct.html>
- <http://www.mmf.umn.edu/initiatives/wh/2009/Spring/funding.cfm>
- <http://cureglioma.info/>
- <http://course1.winona.edu/sberg/308s10/Lec-note/CytoskeletonA.html>
- <http://www.genecards.org/>
- <http://www.ncbi.nlm.nih.gov/>
- http://frodo.wi.mit.edu/cgibin/primer3/primer3_www.cgi.

Appendix

List of publications in process

Khan Z, Shervington L, & Shervington A (2011). Is CD133 the appropriate stem cell marker for glioma? *Methods of cancer diagnosis therapy and prognosis. Brain* **8** (In press).

Khan Z, Shervington L, Munje C & Shervington A (2011). The complexity of identifying cancer stem cell biomarkers. Submitted.

Abstracts/Conference proceedings

Khan Z, Shervington L, & Shervington A (2010). Enhancing stemness in brain tumour stem cells by inducing micro-environmental changes. Faculty of Science Scientific Proceedings **7**: UCLAN.

Khan Z, Chuzhanova N, & Shervington A (2009). Can stemness be related to CD133? Faculty of Science Scientific Proceedings **6**: UCLAN.

Thakkar D, Khan Z, Patel R, & Shervington A (2009) Can bioinformatics predict novel transcription factors regulating telomerase in gliomas? EACR, London.